SPATIALLY AVERAGED MULTI-SCALE MODELS FOR CHEMICAL REACTORS

Saikat Chakraborty and Vemuri Balakotaiah*

Department of Chemical Engineering, University of Houston, Houston, Texas 77204-4004, USA

*E-mail: bala@uh.edu

Advances in Chemical Engineering, vol. 30
ISSN 0065 2377
DOI 10.1016/S0065-2377(05)30004-4

Abstract

The classical homogeneous and catalytic reactor models such as CSTR, PFR, and two-phase models, make *a priori* assumptions on the length and time scales of diffusion, convection, and reaction and apply the conservation laws at the macroscopic level. This intuitive averaging leads to incorrect and often non-physical description of the small-scale mixing/diffusion effects, accumulation and reaction terms in the averaged form of the conservation laws. We consider the full convection–diffusion–reaction equations with homogeneous and catalytic reaction and spatially average them rigorously over small length/time scales using the Liapunov–Schmidt method. This results in low-dimensional averaged models defined in terms of multiple concentration and temperature modes (variables), each of which is representative of a physical scale of the system. These multi-mode models are markedly different from the classical reactor models and are hyperbolic for most cases of practical interest. While their solution requires a numerical effort that is comparable to that of the classical reactor models, they retain all the parameters and qualitative features of the full governing equations (within their region of convergence) and overcome the shortcomings of the classical models (such as dependence of effective transport coefficients on kinetics, inability to describe micromixing effects, infinite speed of propagation of signals even in convection dominated systems, etc). Examples are presented to illustrate and compare the predictions of the new averaged multi-mode models with those of the classical models.

I. Introduction

Modeling and analysis of chemical reactors is at the core of the chemical engineering discipline. It is one activity that is unique to our discipline and distinguishes it from other branches of engineering. One fundamental difference between the modeling of chemical reactors and non-reacting systems is that the

length and time scales associated with reacting flows can vary from the molecular scale to the macro or process scale. Depending on the level of detail included at various length and time scales, mathematical models that describe chemical reactors can vary in complexity as well as in the number of physico-chemical parameters. In addition, due to the strong coupling between the transport and reaction processes and the dependence of the kinetic and transport rates on the state variables, the model equations are highly nonlinear and are known to exhibit a variety of complex spatio-temporal patterns. For most cases of practical interest, even with the present day computational power, it is impractical to solve such detailed models and explore the different types of solutions that may exist in the multi-dimensional parameter spaces. Even in cases where detailed solutions can be obtained, the numerical results have to be coarse-grained to determine quantities (such as the average conversion or speed of a thermal front) that are of interest to the designer. Accurate low-dimensional models in terms of measurable variables (such as cup-mixing concentrations or temperatures) are desired for the purpose of design, control, and optimization of chemical processes.

The most common procedure in chemical reaction engineering to develop low-dimensional models of reactors is to make certain *a priori* assumptions on the length and time scales of reaction, diffusion and convection and apply the conservation laws at the meso or macroscales only. For example, the most famous and widely used chemical reactor model, namely that of the continuous-flow stirred-tank reactor (CSTR), is obtained by applying the species and energy balances at the macro (reactor) scale and consists of ordinary differential equations. This model ignores the physics at small length scales (and hence is independent of the transport properties such as the viscosity of the fluid or the diffusivities of the various species). The shortcomings of this model (such as its inability to predict micromixing effects on conversion and yield/selectivity of an intermediate product for the case of fast reactions) are well known. The same can be said of many other classical reactor models such as the plug-flow tubular reactor model, the axial dispersion model with Danckwerts boundary conditions, the two-phase catalytic reactor model, psuedohomogeneous models of multi-phase reactors, etc.

At the other extreme, it may be argued that the traditional low-dimensional models of reactors (such as the CSTR, PFR, etc.) should be abandoned in favor of the detailed models of these systems and numerical solution of the full convection–diffusion–reaction (CDR) equations using computational fluid dynamics (CFD). While this approach is certainly feasible (at least for single-phase systems) due to the recent availability of computational power and tools, it may be computationally prohibitive, especially for multi-phase systems with complex chemistry. It is also not practical when design, control and optimization of the reactor or the process is of main interest. The two main drawbacks/criticisms of this approach are: (i) It leads to discrete models of very high dimension that are difficult to incorporate into design and control schemes.

In addition, for highly nonlinear cases, the mesh size needed to avoid spurious solutions may be so small that this approach is not feasible. (ii) The CFD approach also uses averaged models (e.g., k–ε model for turbulent flows) with closure schemes that are not always justified and contain adjustable constants.

The main goal of this chapter is to demonstrate an intermediate approach and a systematic method of obtaining low-dimensional models of chemical reactors by spatial averaging of the full CDR equations. Our method of spatial averaging is rigorous and is based on the Liapunov–Schmidt (L–S) technique of classical bifurcation theory. Intuitively speaking, the L–S method of averaging is equivalent to Taylor expansion of a more detailed model in terms of one or more small parameters representing the ratio of length or time scales present in the detailed model. In such an expansion, the lowest (zeroth) order term (which ignores the physics at the small scales) is the simplified model (such as the ideal PFR or CSTR model), while the higher order corrections modify it by including the small but significant physical phenomena (such as local velocity gradients, molecular diffusion, finite rates of adsorption, reaction, etc.) present at various length and time scales.

Before we illustrate the new approach, we give a brief history of some important reactor models. We also outline the multi-scale nature of both homogeneous and catalytic reactors and present a brief review of prior efforts at describing the scale coupling using low-dimensional models. In Section II, we outline briefly the L–S procedure for spatial averaging of CDR equation. We illustrate the spatial-averaging procedure in Section III by considering some examples of non-reacting systems describing dispersion in tubes, packed beds and monoliths. In Sections IV and V we present low-dimensional averaged models for homogeneous, catalytic and coupled homogeneous and catalytic reactors, respectively. Examples illustrating the use of these models and a comparison of their predictions with the classical reactor models is also given in these sections. In Section VI, we discuss briefly the convergence and the region of validity of the low-dimensional models. Finally, in the last section, we outline some possible extensions of our approach to multi-phase reacting systems.

A. A Brief History of Chemical Reactor Models

The most widely used homogeneous reactor models are the three classical ideal reactor models, namely the plug-flow reactor (PFR) model, the CSTR model, and the batch reactor (BR) model. While the BR model and the PFR model (which are identical for constant density systems with time replaced by space time or dimensionless distance along the tube) have existed since the late eighteenth century, a conceptual leap came in the form of the CSTR model through the work of Bodenstein and Wolgast (1908). Unlike the PFR model, which assumes no gradients in the radial direction and no mixing in the axial direction, the CSTR model assumes complete mixing at all scales. For constant

density systems, the three classical homogeneous reactor models for the case of a single reaction of the form

$$\sum_{j=1}^{M} v_j A_j = 0$$

(where M is the number of species, $v_j > 0$ for products and $v_j < 0$ for reactants) are described by the following equations:

$$\text{PFR}: \quad \langle u_x \rangle \frac{\mathrm{d}\langle C_j \rangle}{\mathrm{d}x} = v_j R(\langle \mathbf{C} \rangle) \quad \text{with } \langle C_j \rangle = C_{j,\text{in}} \quad \text{at } x = 0 \tag{1}$$

$$\text{BR}: \quad \frac{\mathrm{d}\langle C_j \rangle}{\mathrm{d}t'} = v_j R(\langle \mathbf{C} \rangle) \quad \text{with } \langle C_j \rangle = C_{j,\text{in}} \quad \text{at } t' = 0 \tag{2}$$

$$\text{CSTR}: \quad \frac{\langle C_j \rangle - C_{j,\text{in}}}{\tau_\text{C}} = v_j R(\langle \mathbf{C} \rangle) \ (j = 1, 2, \ldots, M) \tag{3}$$

where $\langle C_j \rangle$ is the spatially (or cross-sectional) averaged reactant concentration of species A_j, $C_{j,\text{in}}$ is the mean inlet (or initial) concentration of the reactant, $R(\langle \mathbf{C} \rangle)$ the rate of the homogeneous reaction, x the distance coordinate along the length of the PFR, $\langle u_x \rangle$ the mean fluid velocity in the reactor in the axial direction, t' the time, and τ_C is the total residence time of the reactor. (*Remark*: No distinction is made between spatially averaged concentration, $\langle C \rangle$, and cup-mixing concentration, C_m, in these ideal one-mode reactor models.)

Irving Langmuir (1908) first replaced the assumption of no axial mixing of the PFR model with finite axial mixing and the accompanying Dirichlet boundary condition ($\langle C_j \rangle = C_{j,\text{in}}$ at $x = 0$) by a flux-type boundary condition

$$D_{\text{m},j} \frac{\mathrm{d}\langle C_j \rangle}{\mathrm{d}x} = \langle u_x \rangle [\langle C_j \rangle - C_{j,\text{in}}] \quad \text{at } x = 0 \tag{4}$$

where $D_{\text{m},j}$ is the molecular diffusivity of the species A_j. The above boundary condition was rediscovered several times later: first by Förster and Geib (1934), which was quoted and applied by Damköhler (1937); and then finally by Danckwerts (1953); and it has since then been known as "Danckwerts' boundary condition". In his paper, Langmuir dealt with both the limiting cases of "mixing nearly complete" and "only slight mixing".

Thirty years later, Gerhard Damköhler (1937) in his historic paper, summarized various reactor models and formulated the two-dimensional CDR model for tubular reactors in complete generality, allowing for finite mixing both in the radial and axial directions. In this paper, Damköhler used the flux-type boundary condition at the inlet and also replaced the assumption of plug flow with parabolic velocity profile, which is typical of laminar flow in tubes.

Förster and Geib (1934) first introduced the concept of residence time distribution (RTD) to study the problem of longitudinal dispersion in tubes. They also obtained the RTD curves for the axial dispersion model with Danckwerts boundary condition using the Laplace transform theory. Twenty years later, Danckwerts (1953), in his much celebrated paper, devised a generalized treatment of RTD and introduced the concepts of ''hold-back'' and ''segregation''. Following this, it was Zwietering (1959) who quantified the degrees of mixing with the ideas of ''complete segregation'' and ''maximum mixedness'' and brought forth the concept of *micromixing*, i.e. mixing caused by local diffusion, local velocity gradients and reaction at the small scales.

The study of mixing effects on chemical reactions has been an active area of research since the pioneering papers of Danckwerts (1958) and Zwietering (1959). The topic has become a part of classical Chemical Reaction Engineering and has been discussed in textbooks (Froment and Bischoff, 1990; Levenspiel, 1999; Westerterp *et al*., 1984) and review articles (Villermaux, 1991). Historically, this study has progressed in two parallel branches, based on the Lagrangian and Eulerian frameworks of description, respectively.

The mechanistic models based on the Lagrangian description were initiated by the studies of Danckwerts (1958) and Zwietering (1959), using the RTD theory and the ideas of ''complete segregation'' and ''maximum mixedness''. The two- and the three-environment models (Miyawaki *et al*., 1975; Ng and Rippin, 1965) that followed, described *micromixing* as an exchange between the environments of ''complete segregation'' and ''maximum mixedness''. Other mechanistic models that have been formulated in the last 40 years include the coalescence–redispersion model (Curl, 1963; Harada, 1962), the interaction by exchange with mean (IEM) model (Villermaux and Devillon, 1972), models that assume diffusion with chemical reaction in deforming fluid lamellae (Ottino *et al*., 1979), and the engulfment–deformation–diffusion (EDD) models (Baldyga and Bourne, 1984). Vatistas and Marconi (1992) extended the IEM model to address the issue of non-isothermal micromixing in exothermic reactions, Although many of these models were low-dimensional (and therefore are inexpensive to compute) and could relate the global to the local interactions quite effectively, they are phenomenological in nature and are derived based on a top-down approach involving simplifying assumptions on the different time and length scales of the system.

The Eulerian (bottom-up) approach is to start with the convective–diffusion equation and through Reynolds averaging, obtain time-smoothed transport equations that describe micromixing effectively. Several schemes have been proposed to close the two terms in the time-smoothed equations, namely, scalar turbulent flux in reactive mixing, and the mean reaction rate (Bourne and Toor, 1977; Brodkey and Lewalle, 1985; Dutta and Tarbell, 1989; Fox, 1992; Li and Toor, 1986). However, numerical solution of the three-dimensional transport equations for reacting flows using CFD codes are prohibitive in terms of the numerical effort required, especially for the case of multiple reactions with

fast/non-isothermal kinetics. As a result, in spite of the simplifying assumptions present, the century-old ideal classical reactor models [Eqs. (1)–(3)] are still the most popular choices among chemical engineering practitioners. The classical ideal reactor models, which are easy-to-solve ordinary differential or algebraic equations with no adjustable parameter, are particularly preferred to the full CDR models (which are partial differential equations in two or more independent variables) in case of multiple reactions with complex kinetics.

In contrast to the homogeneous reactor models, catalytic and multi-phase reactor models (using the interphase transfer coefficient concept) appeared only in the late 1950s and early 1960s. By this time, the concept of heat and mass transfer coefficients was widely accepted and used in the design and analysis of process equipment (mostly non-reacting systems such as absorbers, heat exchangers and separation columns). These transfer coefficient models were extended to reacting systems by just adding the reaction terms to appropriate balance equations for the phase. Wicke (1961) and Liu and Amundson (1962) developed and analyzed two-phase models of packed-bed catalytic reactors. Trambouze and Piret (1960) and Schmitz and Amundson (1963) developed and analyzed models of two-phase systems with heat and mass exchange and reaction in one of the phases. [Prior to these studies, mostly pseudohomogeneous models were used to describe packed-bed catalytic reactors. Also, while the concepts of effectiveness and enhancement factors (Hatta, 1932; Thiele, 1939; Zeldovich, 1939) were used much earlier in the 1930s and 1940s, the use of these in the design and analysis of multi-phase reactors occurred much later, i.e. in the late 1950s and early 1960s.] During the 1970s through 1990s, the literature on the modeling of homogeneous, catalytic, and multi-phase reactors has proliferated. More recently, CFD has also been applied in the modeling of bubble column and other single- and multi-phase reactors (Ranade, 2002).

B. Multi-scale Nature of Homogeneous and Catalytic Reactors

As stated earlier, chemical reactors are characterized by multiple length (or time) scales and these disparate scales are typically characterized by three representative ones, namely, micro (molecular), meso (catalyst particle or tube diameter) and macro (reactor or process) scales. Figures 1–4 show examples of simple to complex chemical reactors, in each of which scale separation exists.

Figure 1 shows the schematic of a tubular reactor, of radius a and length L, where $\alpha = a/L$ is the aspect ratio. Clearly, if $\alpha \gg 1$, or $\alpha \ll 1$, a physical length scale separation exists in the reactor. This length scale separation could also be interpreted in terms of time scales. For example, $\alpha \ll 1$ implies that the time scale for radial diffusion is much smaller than that of either convection and axial diffusion, and concentration gradients in the transverse direction are small compared to that in the axial direction.

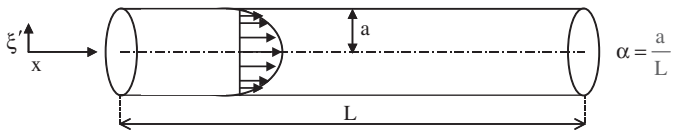

FIG. 1. Schematic diagram of a tubular reactor, showing the length scales in transverse and axial directions.

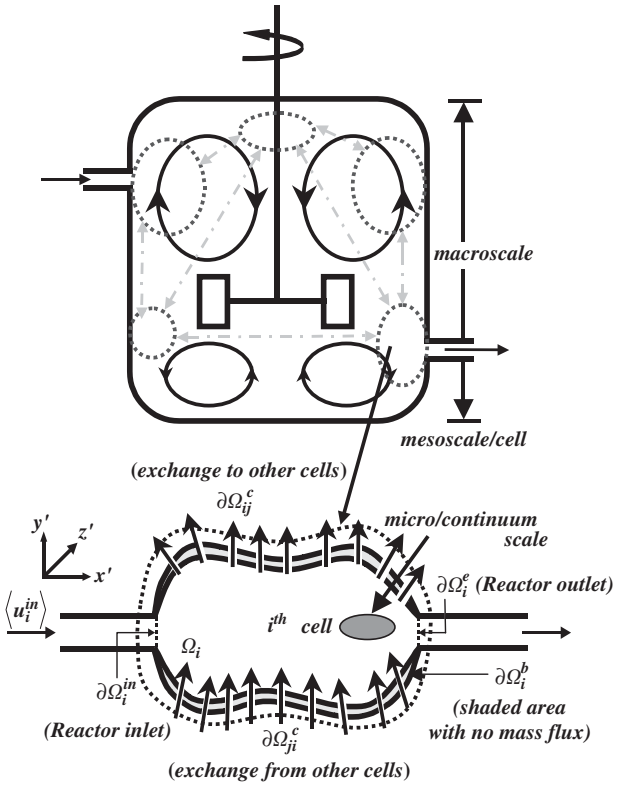

FIG. 2. Schematic diagram of a CSTR illustrating the macro-, meso-, and microscales and the scale-coupling (Bhattacharya *et al*., 2004).

The issue of multiple time scales is also present in the case of homogeneous tank reactors. As in Fig. 2, a tank reactor consists of several circulating flow loops which exchange material with each other and within which micromixing occurs at the continuum scale. Therefore, there are three physical length scales present in a tank reactor. The size of the reactor is the macroscale. The meso length scale could be anywhere from the size of a circulation loop to the size of an eddy (or cell). The continuum scale is the microscale. The time scales

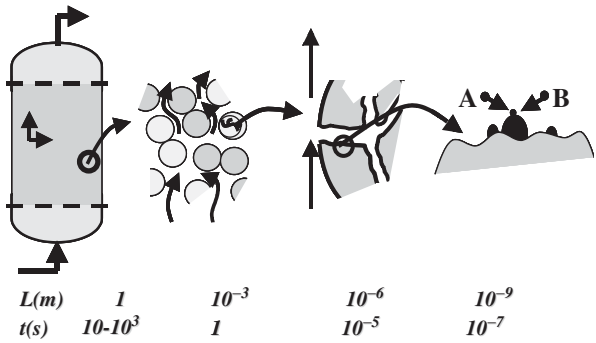

FIG. 3. Scale separation in a packed-bed reactor: L and t are the corresponding length and time scales in meters and seconds, respectively.

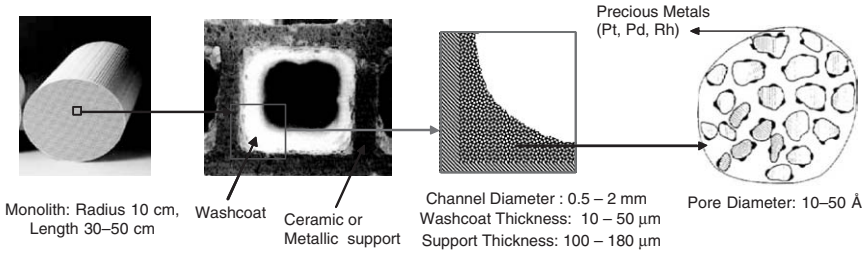

FIG. 4. Schematic diagram illustrating the different length scales in a catalytic monolith reactor.

associated with these three length scales are residence time of the reactor, circulation/macromixing time, and micromixing time, respectively.

More complex reactors, like packed-bed reactors or catalytic monoliths, consist of many physically separated scales, with complex nonlinear interactions between the processes occurring at these scales. Figure 3 illustrates scale separation in a packed-bed reactor. The four length (and time) scales present in the system are the reactor, catalyst particle, pore scale, and molecular scale. The typical orders of magnitude of these four length scales are as follows: reactor, 1 m; catalyst particle, 10^{-2} m (1 cm); macropore scale, 1 μm (10^{-6} m); micropore/molecular scale, 10 Å (10^{-9} m). The corresponding time scales also vary widely. While the residence time in the reactor varies between 1 and 1000 s, the intraparticle diffusion time is of the order of 0.1 s and is $\sim 10^{-5}$ s inside the pores. The time scale associated with molecular phenomenon like adsorption is typically less than a microsecond and could be as small as a nanosecond.

Figure 4 is a picture of another reactor with widely varying scales—a catalytic monolith. Like the tubular reactor, the monolith itself has two intrinsic length scales, the radius and the length, which are typically 10–20 cm and between 30 and 50 cm, respectively. The monolith cross-section has a honeycomb structure

consisting of 100–1000 channels, with washcoat and catalyst support. Typical channel width or hydraulic diameter is 0.5–2 mm, typical washcoat thickness is 10–50 μm, and support thickness is 100–180 μm, while the mean diameter of the pores present in the catalyst support is 10–100 Å. Thus, it could be seen that the reaction, which occurs inside the pores of the catalyst support, requires transport of reactants and products across length scales that vary from a few angstroms to meters.

In all of the above cases, a strong non-linear coupling exists between reaction and transport at micro- and mesoscales, and the reactor performance at the macroscale. As a result, the physics at small scales influences the reactor and hence the process performance significantly. As stated in the introduction, such small-scale effects could be quantified by numerically solving the full CDR equation from the macro down to the microscale. However, the solution of the CDR equation from the reactor (macro) scale down to the local diffusional (micro) scale using CFD is prohibitive in terms of numerical effort, and impractical for the purpose of reactor control and optimization. Our focus here is how to obtain accurate low-dimensional models of these multi-scale systems in terms of average (and measurable) variables.

C. Different Approaches to Multi-scale Averaging or Dimension Reduction

As stated in the introduction, dimension reduction of the governing partial differential equations describing reactors is necessary for the purpose of design, control, and optimization of chemical processes, and is typically achieved by three different approaches, as illustrated in Fig. 5.

The first approach is the discretization of the convection and the diffusion operators of the PDEs, which gives rise to a large (or very large) system of effective low-dimensional models. The order of these low-dimensional models depend on the minimum mesh size (or discretization interval) required to avoid spurious solutions. For example, the minimum number of mesh points (N_{xyz}) necessary to perform a direct numerical simulation (DNS) of convective–diffusion equation for non-reacting turbulent flow is given by (Baldyga and Bourne, 1999)

$$N_{xyz} \approx Re^{9/4} Sc^{3/2} \tag{5}$$

where Re and Sc are the Reynolds and turbulent Schmidt numbers, respectively. (For $Re = 10^4$ and $Sc = 10^3$, this leads to a N_{xyz} of 3×10^{13}, which is quite large.) For the case of laminar reacting flows in a tube of radius a and length L, the minimum number of mesh points required to solve the steady-state one-dimensional CDR problem has been shown (Dommeti and Balakotaiah, 2000)

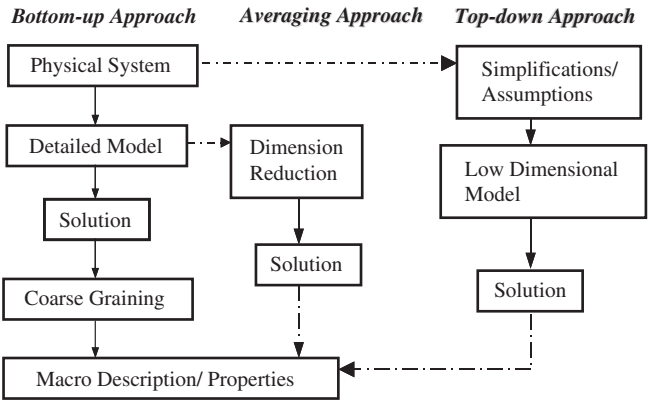

FIG. 5. Different approaches to dimension reduction.

to be

$$N_x = \sqrt{\frac{Pe^3}{24q}\left(q - 1 - \frac{2Da}{Pe} + \frac{2Da^2}{Pe^2}\right)} \tag{6}$$

where

$$q = \sqrt{1 + \frac{4Da}{Pe}} \tag{7}$$

Da is the Damköhler number, *Pe* the Peclet number based on the length of the reactor and is given by

$$Pe = \frac{L}{2a} ReSc$$

For very fast reactions i.e. $Da \gg 1$, criterion equation (6) gives the minimum number of mesh points required (to avoid spurious solutions) for a three-dimensional scalar CDR equation as

$$N_{xyz} = \left(\frac{\phi^3}{24}\right)^{3/2}$$

(where $\phi^2 = Pe\,Da$), which results in ODEs of very high order, especially for the case of diffusion-limited reactions, i.e. when ϕ^2 is large. For the case of non-isothermal kinetics, $\phi^2 = \phi_0^2 \exp[B]$, where ϕ_0^2 is the value based on the inlet/reference temperature and *B* is the Zeldovich number (dimensionless adiabatic temperature rise). Therefore, for a typical value of *B* of 20 (which is very common for partial oxidation and combustion reactions) and $\phi_0^2 = 1$, $N_{xyz} = 3 \times 10^{17}$ and the problem is rendered numerically unsolvable. Dynamical

systems of such high order cannot be easily incorporated in the existing control strategies. In such cases, low-dimensional models are a natural alternative.

The second approach is the one that chemical engineers have followed historically to develop low-dimensional models of reactors by making certain *a priori* assumptions on the length and time scales of reaction, diffusion, and convection and applying the conservation equations only at the macroscopic level. As stated earlier, the CSTR model is an example illustrating this "top-down approach" (Fig. 5). The assumptions made in developing such low-dimensional models are usually not justified since it involves comparison of the solutions obtained with more detailed (fundamental) models, which are not available. Because of the *a priori* assumptions, these models cannot explain many experimentally observed features that arise due to the coupling between transport processes and chemical reaction at the local scales. When the predictions of such ad-hoc models did not match with experimental results, the low-dimensional models were modified by expanding the degrees of freedom using concepts such as RTD, non-ideal flow and mixing, and introducing empirical constants such as effective dispersion coefficients (Danckwerts, 1958; Levenspiel, 1999; Zwietering, 1959). The shortcomings of this approach (such as the dependence of the effective dispersion coefficients on the kinetic parameters and inconsistencies such as infinite propagation speed of signals even in convection-dominated systems) are well known (Balakotaiah and Chang, 2003).

An alternative method of obtaining low-dimensional models is the bottom-up approach based on the averaging of the detailed models derived from the fundamental laws. Several different empirical as well as rigorous averaging techniques (with different terminology such as homogenization, dimension reduction, adiabatic elimination, multi-scale method, slaving principle, etc.) are used in different fields for obtaining low-dimensional models. For dynamical systems with scale separation, the Center Manifold theorem (Carr, 1981) has been used extensively in recent years to eliminate the slave (or fast decaying) modes and obtain low-dimensional models described by a few ordinary differential equations (Balakotaiah and Chang, 1995; Balakotaiah and Dommeti, 1999; Mercer and Roberts, 1990). While this is a powerful technique, a major limitation of this technique is that it can only describe the asymptotic behavior of a physical system close to a fixed point (such as a trivial solution).

This chapter presents spatially averaged chemical reactor models based on the L–S technique of classical bifurcation theory. This method is best suited for spatial averaging near a zero eigenvalue (corresponding to the vanishing of a small parameter representing the ratio of length or time scales in the system). For the case of CDR problems, local equilibrium exists in the limit when local diffusion is very fast as compared to convection and reaction [*Remark*: The convection time scale varies as $L/\langle u_x \rangle$, where L is the macro length scale and $\langle u_x \rangle$ is the average velocity in the axial direction. The reaction time scale varies as $C_R/R(C_R)$, where C_R is a reference concentration and $R(C_R)$ the reaction rate. The local diffusion time scale varies as ℓ^2/D_m, where ℓ is the meso or micro

length scale and D_m the molecular (or effective) diffusivity. When $\ell \to 0$, local diffusion becomes dominant as the other scales are independent of ℓ. Conversely, by choosing the appropriate length scale ℓ, the local diffusion can be made to be the dominant process and, hence, the spatial degrees of freedom associated with this length scale can be eliminated]. Dimension reduction of such systems using L–S technique consists in orthogonal projection of the CDR operator. The resultant low-dimensional models are described by multiple concentration and temperature variables, unlike the traditional low-dimensional models which are described by a single concentration and a single temperature variable. Each of these variables is representative of a physical scale of a system and is called a "mode", and the averaged models are called "multi-mode models". Moreover, spatial averaging by the L–S method retains all the parameters present in the full CDR equation. Therefore, within their region of validity, these low-dimensional models retain the complex spatio-temporal behaviors (multiple solutions, oscillations, micromixing effects, etc.) that are exhibited by the detailed model that are often missed by the traditional low-dimensional models.

II. Spatial Averaging of Convection–diffusion–reaction Models using the L–S Method

The L–S method is a well-known technique for eliminating the degrees of freedom near a zero eigenvalue. It has been used for analyzing the bifurcation behavior of a nonlinear operator near a zero eigenvalue (Balakotaiah *et al.*, 1984; Golubitsky and Schaeffer, 1984). Recently, this technique has been used for spatial averaging of CDR models provided a scale separation exists (Balakotaiah, 2004; Balakotaiah and Chakraborty, 2003; Balakotaiah and Chang, 2003; Chakraborty and Balakotaiah, 2002a, b, 2003, 2004). Here, we illustrate the main steps of this averaging procedure by considering a single partial differential equation of the CDR type and show how the local spatial degrees of freedom (present in the diffusion operator) may be eliminated by averaging. Application of the procedure for more general cases may be found in the cited references.

We consider a nonlinear partial differential equation of the form

$$F(c,p) \equiv \nabla^2 c - pf(x,y,z,t,c,p,\mathbf{p}^*) = 0 \tag{8}$$

where $c(x,y,z,t)$ is a concentration variable dependent on the local coordinates (x,y) as well as other independent variables z and t, ∇^2 is the diffusion (Laplacian) operator in the local coordinates x and y in a region Ω subject to either zero flux or periodic boundary conditions on the boundary $\partial\Omega$. The parameter p is assumed to be small and is the ratio of local diffusion time to

(global scale) convection time. f is a nonlinear operator that accounts for large scale mixing (diffusion) and convection effects as well as the source/sink terms due to reaction, adsorption, etc. It is assumed that f has a Taylor series expansion in terms of p and the parameters $\mathbf{p}^*$ appearing in f are of order unity.

We note that the diffusion operator with Neumann (or periodic) boundary conditions is symmetric and has a simple zero eigenvalue with a constant eigenfunction. Equivalently, the eigenvalue problem

$$\mathbb{L}\psi \equiv \nabla^2\psi = -\mu\psi \quad \text{in } \Omega \tag{9}$$

$$\nabla\psi \cdot \mathbf{n} = 0 \quad \text{on } \partial\Omega \tag{10}$$

is self-adjoint ($\mathbb{L}^* =$ adjoint operator $= \mathbb{L}$) with a zero eigenvalue $\mu_0 = 0$ and a constant eigenfunction $\psi_0(x, y) = 1$. Moreover, for $j \geqslant 1$, $\mu_j > 0$ and for all $j \geqslant 0$, the eigenfunctions $\psi_j(x, y)$ can be chosen to satisfy the orthogonality condition

$$\langle \psi_i, \psi_j \rangle = \frac{1}{A_\Omega} \int\int_\Omega \psi_i \psi_j \, \mathrm{d}x \, \mathrm{d}y = \delta_{ij} = \begin{cases} 0, & i \neq j \\ 1, & i = j \end{cases} \tag{11}$$

As shown below, these properties can be used to eliminate the spatial degrees of freedom in Eq. (8).

Averaging Eq. (8) over the domain Ω and use of divergence theorem gives

$$\langle f(x, y, z, t, c, p, \mathbf{p}^*), \psi_0 \rangle = 0 \tag{12}$$

(Here, the angle brackets stand for inner product or average over the domain Ω.) For obvious reasons, we shall refer to Eq. (12) as the averaged model. To write it in a more useful form, we express c as

$$c(x, y, z, t) = \langle c \rangle(z, t)\psi_0 + c'(x, y, z, t) \tag{13}$$

where

$$\langle c \rangle = \frac{1}{A_\Omega} \int\int_\Omega c(x, y, z, t) \, \mathrm{d}x \, \mathrm{d}y = \langle c, \psi_0 \rangle \tag{14}$$

is the spatially averaged concentration (over the domain Ω). It follows from Eq. (13) that

$$\langle c' \rangle = \langle c', \psi_0 \rangle = 0 \tag{15}$$

For obvious reasons, $c'(x, y, z, t)$ will be referred to as the local variation. The L–S procedure uses orthogonal complementary spaces in the domain to split c as given by Eq. (13). Similarly, in the codomain, Eq. (8) is satisfied iff

$$EF(\langle c \rangle\psi_0 + c') = 0 \tag{16}$$

$$(I - E)F(\langle c\rangle\psi_0 + c') = 0 \tag{17}$$

where E is the projection operator onto *range* $\mathbb{L}$. The complementary projection (onto ker $\mathbb{L}$) is given by

$$(I - E)F = \langle F, \psi_0\rangle\psi_0 \tag{18}$$

Then, Eq. (17) is identical to Eq. (12), which may be written as

$$\langle f(x, y, z, t, \langle c\rangle\psi_0 + c', p, \mathbf{p}^*), \psi_0\rangle = 0 \tag{19}$$

Simplification of Eq. (16) gives

$$\mathbb{L}c' = pf(x, y, z, t, \langle c\rangle\psi_0 + c', p, \mathbf{p}^*) - p\langle f(x, y, z, t, \langle c\rangle\psi_0 + c', p, \mathbf{p}^*), \psi_0\rangle\psi_0 \tag{20}$$

We refer to this as the local equation. Since $\mathbb{L} : \textit{range}\ \mathbb{L} \to \textit{range}\ \mathbb{L}$ is invertible, it follows from the implicit function theorem that the local equation [Eq. (20)] with the constraint given by Eq. (15) can be solved uniquely for c' in terms of $\langle c\rangle$. Substitution of this in Eq. (19) gives the reduced or averaged model.

The local equation may be solved perturbatively for c'. Writing

$$c' = \sum_{i=1}^{\infty} p^i c_i \tag{21}$$

we get

$$\mathbb{L}c_1 = f(\langle c\rangle\psi_0, 0, \mathbf{p}^*) - \langle f(\langle c\rangle\psi_0, 0, \mathbf{p}^*), \psi_0\rangle\psi_0; \quad \langle c_1\rangle = 0 \tag{22}$$

$$\begin{aligned}\mathbb{L}c_2 = {} & D_c f(\langle c\rangle\psi_0, 0, \mathbf{p}^*) \cdot c_1 + D_p f(\langle c\rangle\psi_0, 0, \mathbf{p}^*) \\ & - \langle D_c f(\langle c\rangle\psi_0, 0, \mathbf{p}^*) \cdot c_1 - D_p f(\langle c\rangle\psi_0, 0, \mathbf{p}^*), \psi_0\rangle\psi_0 = 0; \quad \langle c_2\rangle = 0\end{aligned}$$

etc. Taylor series expansion of Eq. (19) gives

$$\begin{aligned}&\langle f(\langle c\rangle\psi_0, 0, \mathbf{p}^*), \psi_0\rangle + \langle D_c f(\langle c\rangle\psi_0, 0, \mathbf{p}^*) \cdot c', \psi_0\rangle + p\langle D_p f(\langle c\rangle\psi_0, 0, \mathbf{p}^*), \psi_0\rangle \\ &\quad + \tfrac{1}{2!}\langle D^2_{cc} f(\langle c\rangle\psi_0, 0, \mathbf{p}^*) \cdot (c', c'), \psi_0\rangle + p\langle D^2_{cp} f(\langle c\rangle\psi_0, 0, \mathbf{p}^*) \cdot c', \psi_0\rangle \\ &\quad + \tfrac{1}{2!}p^2\langle D^2_{pp} f(\langle c\rangle\psi_0, 0, \mathbf{p}^*), \psi_0\rangle + \cdots = 0\end{aligned} \tag{23}$$

[For simplicity of notation, we have written $f(x, y, z, t, \langle c\rangle\psi_0, 0, \mathbf{p}^*)$ as $f(\langle c\rangle\psi_0, 0, \mathbf{p}^*)$.] Thus, the averaged model to order p^2 is given by

$$\begin{aligned}&\langle f(\langle c\rangle\psi_0, 0, \mathbf{p}^*), \psi_0\rangle + p\langle D_c f(\langle c\rangle\psi_0, 0, \mathbf{p}^*) \cdot c_1, \psi_0\rangle + p\langle D_p f(\langle c\rangle\psi_0, 0, \mathbf{p}^*), \psi_0\rangle \\ &\quad + \tfrac{p^2}{2!}\langle D^2_{cc} f(\langle c\rangle\psi_0, 0, \mathbf{p}^* \cdot (c_1, c_1), \psi_0\rangle + p^2\langle D^2_{cp} f(\langle c\rangle\psi_0, 0, \mathbf{p}^*) \cdot c_1, \psi_0\rangle \\ &\quad + p^2\langle D_c f(\langle c\rangle\psi_0, 0, \mathbf{p}^*) \cdot c_2, \psi_0\rangle + \tfrac{1}{2!}p^2\langle D^2_{pp} f(\langle c\rangle\psi_0, 0, \mathbf{p}^*), \psi_0\rangle + \cdots = 0\end{aligned} \tag{24}$$

Here, $D_c f$, $D_p f$, $D^2_{cc} f$, $D^2_{cp} f$ are the Fréchet derivatives of the nonlinear operator f and $D^2_{cc} f \cdot (c_i, c_j)$, is a symmetric bilinear form.

The following observations may be made from the structure of the averaged model given by Eq. (24): (i) The (zeroth-order) first term is the averaged model to the lowest order and can be obtained by setting $c' = 0$ and $p = 0$ in Eq. (19). (ii) The second and third terms represent the order-p corrections. The second term arises due to elimination of local spatial degrees of freedom. (In physical terms, this is the combined effect of the interaction of local diffusion, velocity gradients, and convection/reaction.) The third term is due to order-p effect that is already present in the function f of the original model. (iii) If the Taylor expansion of f in powers of p has terms up to order p^q ($q \geqslant 0$), then the averaged model has to be derived to order p^q so that all the physical phenomena present at different scales in the original detailed model are also represented in the averaged model. If this is not the case, then some of the physical phenomena represented in the original model are not important and can be ignored. (iv) When Eq. (24) is truncated at order p^q ($q \geqslant 1$), the truncation error arises from two sources, the first being the truncation of the Taylor series of the averaged equation (19), the second being the truncation error of the perturbation expansion (21) of the local equation. As we show in the following sections, the first truncation error may be zero in some practical cases (e.g. linear kinetics, wall reaction case, or solutal dispersion problems in which f is linear in c) and the averaged equation may be closed exactly, i.e. higher order Fréchet derivatives are zero and the Taylor expansion of f terminates at some finite order (usually after the linear and quadratic terms in most applications). In such cases, the only error is due to the truncation of the solution of the local equation.

It should be noted that while in principle, it is possible to obtain a single averaged equation in terms of $\langle c \rangle$ by elimination of c' (to some desired order in p), this equation may not be explicit in $\langle c \rangle$. In addition, this may not be useful or what is desired in applications. For example, in chemical reactors, it is not the spatially averaged concentration ($\langle c \rangle$) that is measured experimentally but the so-called "cup-mixing" or velocity-weighted concentration defined by

$$c_m = \langle c(x, y, z, t) g(x, y), \psi_0 \rangle \tag{25}$$

where $g(x, y)$ (with $\langle g \rangle = \langle g, \psi_0 \rangle = 1$) is the local velocity profile, The relationship between c_m and $\langle c \rangle$ may be obtained from Eq. (13) as

$$c_m(z, t) = \langle c \rangle(z, t) + \langle g(x, y) c', \psi_0 \rangle = \langle c \rangle(z, t) + p \langle g(x, y) c_1, \psi_0 \rangle + O(p^2) \tag{26}$$

Now, the averaged model to order p is defined in terms of c_m and $\langle c \rangle$ by the global equation (19) and the local equation (26). The local equation can be extended to any desired order in p by using higher order approximations of c'. This form of the reduced model, expressed in terms of two concentration variables, will be referred to as the "two-mode model", and is convenient for physical interpretation of various limiting cases as well as to extend the range of

validity of the local equation and hence the averaged model by a procedure called *regularization*.

The above averaging procedure described for Neumann boundary conditions may be extended to general flux boundary conditions of the form

$$\nabla c \cdot \mathbf{n} + pDa\, r_{\mathrm{w}}(c) = 0 \quad \text{on } \partial\Omega \tag{27}$$

where Da is a (reactor scale) Damköhler number (which is of order unity) and $r_{\mathrm{w}}(c)$ is some nonlinear function describing reaction or adsorption at the wall. When $p \to 0$, the local gradients vanish and the leading-order operator remains the same. Thus, the splitting given by Eq. (13) is again valid. However, for this case, the averaged equation as well as the local equation may contain extra terms that appear due to the inhomogeneous boundary condition at the wall. In addition, since the wall reaction term is evaluated at a different concentration (c_{w} or c_{s}) than c_{m} or $\langle c \rangle$, the resulting model may contain three concentration variables or three modes. These multi-mode models couple the local and global equations in terms of physically meaningful and measurable concentrations.

This spatial averaging theory could also be extended to the non-isothermal reacting flows to perform spatial averaging of coupled species and energy balances. This has been discussed in detail by Chakraborty and Balakotaiah (2004). It should also be pointed out that the above averaging theory is applicable to discrete interacting units, which is called L–S averaging in finite dimensions. In this case, Eq. (8) is modified to

$$\mathbf{A}\mathbf{c} + p\mathbf{f}(\mathbf{c}, p, \mathbf{p}^*) = 0 \tag{28}$$

where $\mathbf{c}$ is a concentration vector ($\mathbf{c} \in \mathbb{R}^n$) and $\mathbf{A}$ is an $n \times n$ interaction or exchange matrix. Due to mass conservation, $\mathbf{A}$ is singular (with columns summing to zero) and is symmetric (or can be made symmetric with a proper choice of the inner product in $\mathbb{R}^n$). For such cases, Eqs. (19) and (20) are valid (with $\mathbb{L}$ replaced by $\mathbf{A}$) and the averaged model is an algebraic equation for the average concentration $\langle \mathbf{c} \rangle$.

III. Spatially Averaged Models for Describing Dispersion Effects in Tubes and Packed Beds

In this section, we illustrate the spatial averaging procedure by considering several simple examples of non-reacting systems that describe dispersion effects in tubes, packed beds, and monoliths.

A. A Hyperbolic Averaged Model for Describing Dispersion Effects in Tubes/Capillaries

As our first application, we consider the classical Taylor–Aris problem (Aris, 1956; Taylor, 1953) that illustrates dispersion due to transverse velocity gradients and molecular diffusion in laminar flow tubular reactors. In the traditional reaction engineering literature, dispersion effects are described by the axial dispersion model with Danckwerts boundary conditions (Froment and Bischoff, 1990; Levenspiel, 1999; Wen and Fan, 1975). Here, we show that the inconsistencies associated with the traditional parabolic form of the dispersion model can be removed by expressing the averaged model in a hyperbolic form. We also analyze the hyperbolic model and show that it has a much larger range of validity than the standard parabolic model.

The dispersion of a non-reactive solute in a circular tube of constant cross-section in which the flow is laminar is described by the convective–diffusion equation

$$\frac{\partial C}{\partial t'} + 2\langle u_x\rangle\left(1 - \frac{\xi'^2}{a^2}\right)\frac{\partial C}{\partial x} = \frac{D_m}{\xi'}\frac{\partial}{\partial \xi'}\left(\xi'\frac{\partial C}{\partial \xi'}\right) + D_m\frac{\partial^2 C}{\partial x^2}, \quad 0 < \xi' < a, \quad x > 0, \quad t' > 0 \tag{29}$$

with the following boundary and initial conditions:

$$\frac{\partial C}{\partial \xi'} = 0 \quad \text{at } \xi' = 0, a \tag{30}$$

$$\text{IC}: \quad C(x, \xi', 0) = f(x, \xi') \tag{31}$$

$$\text{BC}: \quad C(0, \xi', t') = g(\xi', t') \tag{32}$$

Here, $\langle u_x\rangle$ is the average velocity in the pipe, a the radius, and D_m the molecular diffusivity of the species. [*Remark*: In writing the boundary condition at $x = 0$, we have assumed that $L/a \gg 1$. If this is not the case, it can be modified to include the diffusive flux. Also, when L/a is of order unity, we need boundary conditions at the inlet ($x = 0$) as well as exit ($x = L$).] Defining dimensionless variables

$$z = \frac{x}{L}, \quad t = \frac{\langle u_x\rangle t'}{L}, \quad \xi = \frac{\xi'}{a}, \quad p = \frac{a^2\langle u_x\rangle}{LD_m}, \quad Pe_r = \frac{a\langle u_x\rangle}{D_m} \tag{33}$$

we can write Eqs. (29) and (30) as

$$\mathbb{L}C \equiv \frac{1}{\xi}\frac{\partial}{\partial\xi}\left(\xi\frac{\partial C}{\partial\xi}\right) = p\left[\frac{\partial C}{\partial t} + 2(1-\xi^2)\frac{\partial C}{\partial z} - \frac{p}{Pe_r^2}\frac{\partial^2 C}{\partial z^2}\right], \quad \frac{\partial C}{\partial\xi} = 0 \text{ at } \xi = 0, 1 \tag{34}$$

Here, p is the local (transverse) Peclet number, which is the ratio of transverse diffusion time to the convection time. Pe_r is the radial Peclet number (ratio of transverse diffusion time to a convection time based on pipe radius). We assume that $p \ll 1$ while Pe_r is of order unity. (*Remark*: The parameter $Pe_r^2/p = \langle u_x\rangle L/D_m$ is also known as the axial Peclet number. Also note that for any finite Pe_r or tube diameter, the axial Peclet number tends to infinity as p tends to zero.) When such scale separation exists, we can average the governing equation over the transverse length scale using the L–S technique and obtain averaged model in terms of axial length and time scales.

We note that the transverse operator $\mathbb{L}$ is symmetric with respect to the inner product

$$(v, w) = \int_0^1 2\xi v(\xi)w(\xi)\,\mathrm{d}\xi \tag{35}$$

It has a zero eigenvalue with normalized eigenfunction of unity. We define the mixing-cup (velocity weighted) and spatial average concentrations by

$$C_m = \int_0^1 4\xi(1-\xi^2)C(\xi, z, t)\,\mathrm{d}\xi \tag{36}$$

$$\langle C\rangle = \int_0^1 2\xi C(\xi, z, t)\,\mathrm{d}\xi \tag{37}$$

Transverse averaging of Eq. (34) gives

$$\frac{\partial\langle C\rangle}{\partial t} + \frac{\partial C_m}{\partial z} - \frac{p}{Pe_r^2}\frac{\partial^2\langle C\rangle}{\partial z^2} = 0 \tag{38}$$

We note that when $p = 0$, $\langle C\rangle = C_m$ and substitution of this into Eq. (38) gives the leading (or zeroth) order evolution equation for the averaged concentration:

$$\frac{\partial\langle C\rangle}{\partial t} + \frac{\partial\langle C\rangle}{\partial z} = 0 \tag{39}$$

(*Remark*: This zeroth-order model is the ideal plug-flow model.) To obtain the averaged equation to order p, we write

$$C(\xi, z, t) = \langle C\rangle(z, t) + C'(\xi, z, t), \quad C' \in \ker L \tag{40}$$

and solve for the slave variable $C'(\xi, z, t)$ in terms of $\langle C\rangle(z, t)$ using the procedure outlined above. To leading order, we have

$$C'(\xi, z, t) = -p\,\frac{\partial\langle C\rangle}{\partial z}\left[\frac{1}{12} - \frac{\xi^2}{4} + \frac{\xi^4}{8}\right] + O(p^2) \tag{41}$$

Substitution of the Eq. (40) and transverse averaging (after multiplying by the velocity profile) gives the local equation relating C_{m} and $\langle C\rangle$:

$$C_{\mathrm{m}} - \langle C\rangle = -\frac{p}{48}\,\frac{\partial\langle C\rangle}{\partial z} + O(p^2) = -\frac{p}{48}\,\frac{\partial C_{\mathrm{m}}}{\partial z} + O(p^2) \tag{42}$$

This local equation (when written in dimensional form) defines a characteristic transfer time between the slowly evolving mode C_{m} and the slave mode $C_{\mathrm{m}} - \langle C\rangle$. Thus, the averaged model to order p is given by

$$\frac{\partial\langle C\rangle}{\partial t} + \frac{\partial C_{\mathrm{m}}}{\partial z} - \frac{p}{Pe_{\mathrm{r}}^2}\,\frac{\partial^2\langle C\rangle}{\partial z^2} = 0 \tag{43}$$

$$C_{\mathrm{m}} - \langle C\rangle = -\frac{p}{48}\,\frac{\partial C_{\mathrm{m}}}{\partial z} \tag{44}$$

For obvious reasons, we shall refer to Eq. (43) as the global equation while Eq. (44) that couples the local and global scales as the local equation. Although we can leave the reduced model in this two-mode form, in this special case, we can combine the two equations to obtain a single equation either for C_{m} or $\langle C\rangle$. In this specific example, the model is linear in the concentration and hence both C_{m} and $\langle C\rangle$ satisfy the same equation (as they are linearly related). Since the cup-mixing concentration (which is often measured in experiments) is more relevant in applications, we write the reduced model in terms of C_{m}:

$$\frac{\partial C_{\mathrm{m}}}{\partial t} + \frac{\partial C_{\mathrm{m}}}{\partial z} + \frac{p}{48}\,\frac{\partial^2 C_{\mathrm{m}}}{\partial z\partial t} - \frac{p}{Pe_{\mathrm{r}}^2}\,\frac{\partial^2 C_{\mathrm{m}}}{\partial z^2} + O(p^2) = 0 \tag{45}$$

We note that this averaged model is hyperbolic. The third term in Eq. (45) represents the Taylor dispersion term (due to velocity gradients and transverse molecular diffusion) while the last term is the Aris-correction term (representing the influence of axial molecular diffusion). In dimensional form, the reduced model may be written as

$$\frac{\partial C_{\mathrm{m}}}{\partial t'} + \langle u_x\rangle\,\frac{\partial C_{\mathrm{m}}}{\partial x} + \langle u_x\rangle t_{\mathrm{D}}\,\frac{\partial^2 C_{\mathrm{m}}}{\partial x\partial t'} - D_{\mathrm{m}}\,\frac{\partial^2 C_{\mathrm{m}}}{\partial x^2} = 0, \quad t' \gg t_{\mathrm{D}},\ x \gg \ell_{\mathrm{D}} \tag{46}$$

where the local diffusion or mixing time is defined by

$$t_{\mathrm{D}} = \frac{a^2}{48 D_{\mathrm{m}}} \tag{47}$$

The corresponding local length scale is given by $\ell_{\mathrm{D}} = \langle u_x \rangle t_{\mathrm{D}}$ while the diffusivity may be written as $D_{\mathrm{eff}} = \langle u_x \rangle^2 t_{\mathrm{D}}$. When axial molecular diffusion is neglected (or equivalently, in the limit of $Pe_{\mathrm{r}} \to \infty$) Eq. (46) simplifies to

$$\frac{\partial C_{\mathrm{m}}}{\partial t'} + \langle u_x \rangle \frac{\partial C_{\mathrm{m}}}{\partial x} + \langle u_x \rangle t_{\mathrm{D}} \frac{\partial^2 C_{\mathrm{m}}}{\partial x \partial t'} = 0 \tag{48}$$

In his famous paper, Taylor (1953) used the leading-order approximation

$$\frac{\partial C_{\mathrm{m}}}{\partial t'} = -\langle u_x \rangle \frac{\partial C_{\mathrm{m}}}{\partial x} \tag{49}$$

to express the mixed derivative term as a dispersion term and simplified Eq. (48) to

$$\frac{\partial C_{\mathrm{m}}}{\partial t'} + \langle u_x \rangle \frac{\partial C_{\mathrm{m}}}{\partial x} = D_{\mathrm{eff}} \frac{\partial^2 C_{\mathrm{m}}}{\partial x^2}, \quad D_{\mathrm{eff}} = \langle u_x \rangle^2 t_{\mathrm{D}} \tag{50}$$

In the literature, D_{eff} is also known as the Taylor dispersion coefficient. However, the approximation used by Taylor transforms a hyperbolic equation into a parabolic equation. In the chemical engineering literature, this approximation is made worse by the further requirement of an artificial boundary condition at the exit of the tube. During the last 50 years, the parabolic model with Danckwerts' boundary conditions is used extensively to describe dispersion effects in chemical reactors. We show here that the hyperbolic form of the model is more accurate, retains the proper physics, can describe dispersion effects more accurately than the parabolic model and is valid in a much larger domain of the physical parameter space. [*Remark*: A good analogy between the parabolic and hyperbolic models is the approximation of the function e^{-x} for small positive x by $f_{\mathrm{p}}(x) = 1 - x$ and $f_{\mathrm{h}}(x) = 1/(1 + x)$. Both approximations have the same accuracy for $x \to 0$ but the first approximation breaks down qualitatively for $x > 1$ while the second approximation is valid qualitatively for all positive x. The second (Pade) approximation is a regularized version of the first function. This regularization is closely connected with how we write the local equation. Although the local equation is an infinite series in powers of p, we can truncate it (often at the first term) and rewrite it so that it is qualitatively valid for all positive values of p. This regularization is discussed in Section VI.]

When the Taylor approximation is used in Eq. (46) the averaged model is again parabolic but now the effective dispersion coefficient is given by

$$D_{\mathrm{eff}} = \langle u_x \rangle^2 t_{\mathrm{D}} + D_{\mathrm{m}} = \frac{a^2 \langle u_x \rangle^2}{48 D_{\mathrm{m}}} + D_{\mathrm{m}} \tag{51}$$

This result was first derived by Aris (1956) using the method of moments. While the resulting model now includes both the effects (axial molecular diffusion and dispersion caused by transerverse velocity gradients and molecular diffusion) it has the same deficiency as the Taylor model, i.e. converting a hyperbolic model into a parabolic equation.

We note that when $D_m \ll \langle u_x \rangle^2 t_D$, or equivalently, the radial Peclet number $Pe_r \gg 6.93$, axial diffusion can be neglected. The local Peclet number p, which is equal to Pe_r times the aspect ratio (a/L), can be small even when $Pe_r \gg 6.93$, provided the aspect ratio is sufficiently small. Thus, the conditions $Pe_r \gg 6.93$ and $p \ll 1$ are usually satisfied in most tubular reactors. In such cases, it is more appropriate to use the leading-order approximation to modify the small axial dispersion term to a mixed derivative term and write the averaged model as

$$\frac{\partial C_m}{\partial t'} + \langle u_x \rangle \frac{\partial C_m}{\partial x} + \langle u_x \rangle \hat{t}_D \frac{\partial^2 C_m}{\partial x \partial t'} = 0, \quad \hat{t}_D = t_D + \frac{D_m}{\langle u_x \rangle^2} = \frac{a^2}{48 D_m} + \frac{D_m}{\langle u_x \rangle^2} \tag{52}$$

Now, the averaged hyperbolic model, Eq. (52), defines a characteristic initial-value problem (Cauchy problem). To complete the model, we need to specify C_m only along the characteristic curves $x' = 0$ and $t' = 0$. Thus, the initial and boundary conditions for the averaged model are obtained by taking the mixing-cup averages of Eqs. (31) and (32):

$$C_m(x, t' = 0) = \int_0^1 4\xi(1 - \xi^2) f(x, R\xi)\, d\xi \equiv f_m(x) \tag{53}$$

$$C_m(x = 0, t') = \int_0^1 4\xi(1 - \xi^2) g(R\xi, t')\, d\xi \equiv g_m(t') \tag{54}$$

When the assumption $Pe_r \gg 6.93$ is not valid, it is better to leave the averaged model in the more general hyperbolic form given by Eqs. (45) or (46) with boundary and initial conditions given by Eqs. (53)–(54). The important point to be made is the wave forms of the averaged model [either Eqs. (46) or (52)] have much larger domain of validity than the parabolic form as shown below. (*Remark*: The hyperbolic model is also much easier to solve numerically compared to the parabolic model.)

The L–S method can be used to derive the averaged model to higher orders in p but we will not be pursue it here (see Section VI). In fact, since our averaged model at order p is also regularized, higher order approximations are not necessary to see the qualitative behavior for all positive values of p.

Before closing this section, we compare the hyperbolic model derived here with the wave model of Westerterp *et al.* (1995). For the classical Taylor problem (without axial dispersion), the model of Westerterp *et al.* may be written in the present notation as

$$\frac{\partial\langle C\rangle}{\partial t}+\frac{\partial\langle C\rangle}{\partial z}+\frac{\partial J}{\partial z}=0 \tag{55}$$

$$J+\frac{p}{15}\frac{\partial J}{\partial t}+\frac{p}{12}\frac{\partial J}{\partial z}=-\frac{p}{48}\frac{\partial\langle C\rangle}{\partial z} \tag{56}$$

where J is the dimensionless flux (the flux normalized by $\langle u_x\rangle C_{\mathrm{R}}$, C_{R} being a reference concentration). The following observations may be made about this model: (i) The second and third terms on the l.h.s. of Eq. (56) are $O(p^2)$ terms. Hence, this model is parabolic at order p and is not different from the classical Taylor model (at this order). In contrast, the model derived by the L–S method is hyperbolic at order p. (ii) The model is not expressed in terms of measurable quantities such as the cup-mixing concentration. (iii) The steady-state version of the model predicts that there is dispersion even in the case of constant (and time invariant) inlet conditions. The dispersion coefficient predicted by the steady-state version of this model is quite different from the transient value. This dispersion is spurious and arises due to the choice of the concentration variable $\langle C\rangle$ since integration of the full PDE model (without the axial dispersion term) over the tube cross-section shows that the cup-mixing concentration remains constant with axial position. (iv) The model predicts that there are two waves moving in the axial direction, whereas in the physical problem there is only one wave.

1. Comparison of Solutions of Parabolic and Hyperbolic Models

We now present the solution of the hyperbolic model defined by Eqs. (52) and (53)–(54) and compare the solution to that of the classical parabolic model with Danckwerts boundary conditions. We use the axial length and convective time scales to non-dimensionalize the variables and write the hyperbolic model in the following form:

$$\frac{\partial C_{\mathrm{m}}}{\partial t}+\frac{\partial C_{\mathrm{m}}}{\partial z}+\eta\frac{\partial^2 C_{\mathrm{m}}}{\partial z\partial t}=0,\quad t\gg\eta,\ z\gg\eta \tag{57}$$

$$C_{\mathrm{m}}(z,t=0)=f(z) \tag{58}$$

$$C_{\mathrm{m}}(z=0,t)=g(t) \tag{59}$$

where η is now the effective local Peclet number (or the dimensionless local mixing time) defined by

$$\eta=\frac{\langle u_x\rangle\hat{t}_{\mathrm{D}}}{L}=\frac{a^2\langle u_x\rangle}{48LD_{\mathrm{m}}}+\frac{D_{\mathrm{m}}}{\langle u_x\rangle L}=p\left[\frac{1}{48}+\frac{1}{Pe_{\mathrm{r}}^2}\right] \tag{60}$$

and is the ratio of effective transverse diffusion time to the convection time.

The exit concentration $C_m(z=1,t)$ for the case of a unit impulse (Delta function) input ($f(z)=0,\ g(t)=\delta(t)$) is known as the dispersion (or RTD) curve. For the hyperbolic model, this can be found either by Laplace transformation or from the general solution of the model [see Balakotaiah and Chang (2003), for a general analytical solution of Eqs. (57)–(59)]. It is easily seen that the Laplace transform of the dispersion curve is given by

$$\widehat{E}(s) = \mathrm{Exp}\left\{-\frac{s}{1+s\eta}\right\} \tag{61}$$

while the dispersion curve is given by

$$E_h(t) = C_m(1,t) = \mathrm{Exp}\left(-\frac{(1+t)}{\eta}\right)\left[\delta(t) + \frac{1}{\eta\sqrt{t}}\, I_1\left(\frac{2\sqrt{t}}{\eta}\right)\right] \tag{62}$$

We note that the second central moment (or the dimensionless variance) of the dispersion curve is given by

$$\sigma^2 = 2\eta \tag{63}$$

Thus, for $\eta \to 0$, the variance approaches zero and the behavior approaches that of plug flow. For η small and $t \gg 1$, Eq. (62) may be simplified to

$$E_h(t) \approx \frac{1}{\sqrt{4\pi\eta t^{3/2}}}\,\mathrm{Exp}\left\{-\frac{(1-\sqrt{t})^2}{\eta}\right\} \tag{64}$$

Hence, the dispersion curve has a peak at $t=1$ and is slightly asymmetrical (but the deviation from the Gaussian curve is small). As η increases to 0.5, it can be shown by analyzing Eq. (62) that the peak moves to $t=0$ and for any $\eta>0.5$, the peak remains at $t=0$. For any $\eta>0.5$, the dispersion curve has a slow decaying (long) tail and the variance can exceed unity. Figure 6 shows the dispersion curves for different values of η. [*Note*: For simplicity, the delta function of magnitude $\mathrm{Exp}(-1/\eta)$ at $t=0$ is not shown in the figure.]

We now compare the solution of the hyperbolic model with that of the parabolic model used widely in the literature to describe dispersion in tubular reactors. The parabolic model with Danckwerts boundary conditions (in dimensionless form) is given by

$$\frac{\partial C}{\partial t} + \frac{\partial C}{\partial z} = \frac{1}{Pe}\,\frac{\partial^2 C}{\partial z^2}, \quad 0<z<1, \ \ t>0 \tag{65}$$

$$\frac{1}{Pe}\,\frac{\partial C}{\partial z} - C = g(t) \quad \text{at } z=0 \tag{66}$$

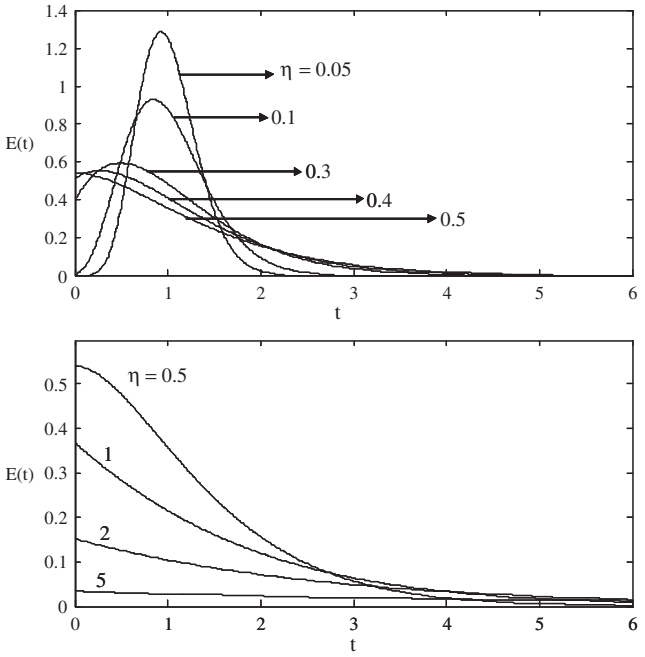

FIG. 6. Dispersion curves predicted by the hyperbolic model [Eq. (57)] for various values of the effective local Peclet number, η.

$$\frac{\partial C}{\partial z} = 0 \quad \text{at } z = 1 \tag{67}$$

$$C(z, t = 0) = f(z) \tag{68}$$

where Pe is the axial Peclet number. For the parabolic model (with $f(z) = 0$ and $g(t) = \delta(t)$), the dispersion curve is given by

$$E_p(t) = C(z = 1, t) = \frac{2}{Pe} \sum_{n=1}^{\infty} \text{Exp}\left\{ \frac{Pe}{2} - \frac{Pe^2 + 4\lambda_n}{4Pe} t \right\} \frac{\sqrt{\lambda_n}\, \sin \sqrt{\lambda_n}(Pe^2 + 4\lambda_n)}{(Pe^2 + 4Pe + 4\lambda_n)} \tag{69}$$

where

$$\cot \sqrt{\lambda_n} = \frac{\sqrt{\lambda_n}}{Pe} - \frac{Pe}{4\sqrt{\lambda_n}}, \quad n = 1, 2, \ldots \tag{70}$$

The dimensionless variance can be found more easily from the Laplace

transform and is given by

$$\sigma^2 = \frac{2}{Pe} - \frac{2}{Pe^2}(1 - e^{-Pe}) \tag{71}$$

We note that the variance for the parabolic model is always bounded between zero (for $Pe \to \infty$ or plug flow) and unity ($Pe \to 0$ or ideal CSTR behavior). Thus, the parabolic model can only describe dispersion behavior that lies between these two extremes. In contrast, the hyperbolic model can describe the same behavior when η varies between 0 and 0.5 as well as the bypassing, stagnant region or solute retaining behavior (with long tails as in segregated laminar flow) when $\eta > 0.5$. For very small η, the dispersion curves predicted by the two models are very close to each other but the hyperbolic model predicts an asymmetric curve with a slightly higher peak than the parabolic model. In addition, the parabolic model predicts upstream diffusion and infinite propagation speed. Both these non-physical phenomena are not present in the hyperbolic model which retains the qualitative behavior of the full model for all values of η. Thus, we conclude that the hyperbolic model describes dispersion effects better than the parabolic model and is valid over a wider range of the physical parameter space.

We also present solutions of the full hyperbolic model

$$\frac{\partial C_{\mathrm{m}}}{\partial t} + \frac{\partial C_{\mathrm{m}}}{\partial z} + \eta \frac{\partial^2 C_{\mathrm{m}}}{\partial z \partial t} - \lambda\eta \frac{\partial^2 C_{\mathrm{m}}}{\partial z^2} = 0, \quad \lambda = \frac{48}{Pe_{\mathrm{r}}^2} \tag{72}$$

for the case of a unit impulse input. The Laplace transform of the dispersion curve is now given by

$$\widehat{E}(s) = \mathrm{Exp}\left\{\frac{1 + s\eta - \sqrt{s^2\eta^2 + 2s\eta(1 + 2\lambda) + 1}}{2\eta\lambda}\right\} \tag{73}$$

from which we can obtain the second central moment (variance) as

$$\sigma^2 = 2\hat{\eta}; \quad \hat{\eta} = \eta(1 + \lambda) \tag{74}$$

This shows again that when λ is small (or equivalently, $Pe_{\mathrm{r}} \gg 1$), we can combine the small axial dispersion term with the mixed derivative term and simplify the general hyperbolic model [Eq. (72)] to the simpler model [Eq. (57)]. However, for λ values of order unity or larger, this cannot be justified. The inverse transform of Eq. (73) can be found by integrating around the branch points but we will not pursue it here. Instead, we show in Figs. 7 and 8 the numerically determined dispersion curves for $\eta = 0.1, 1$ and various values of λ. As can be expected, the qualitative behavior of the full hyperbolic model [Eq. (72)] is similar to that of the simpler case of $\lambda = 0$. Only for $\lambda \geqslant 1$, the peak value changes and shifts to lower times.

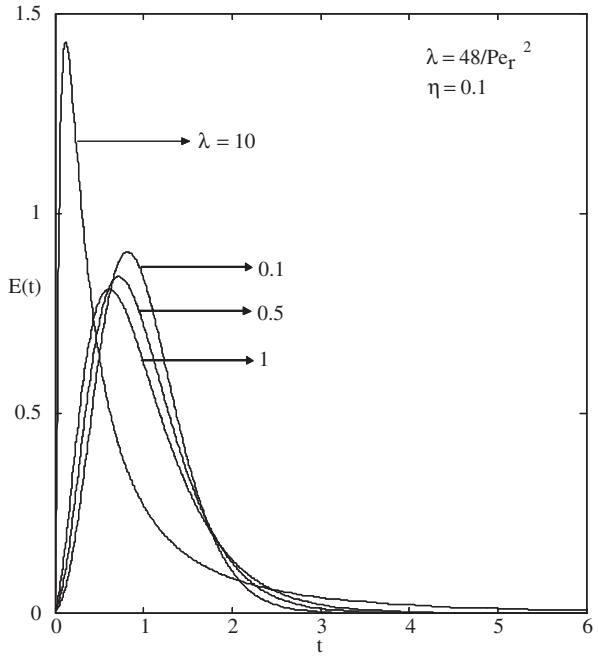

FIG. 7. Dispersion curves predicted by the full hyperbolic model [Eq. (72)] for $\eta = 0.1$.

2. Hyperbolic Model for Describing Dispersion Effects in Turbulent flow in a Tube

The hyperbolic model given by Eq. (48) is also applicable for describing dispersion in turbulent flow in a tube. In this case, we replace the local diffusion/mixing time t_D by the effective local (turbulent) mixing time t_{mix}, which can be calculated using the Reynolds-averaged convective–diffusion model, and is given by Eq. (164) and β_1 could be obtained by using an universal velocity profile (as shown in the following section) as given in Eq. (165). For the case of turbulent flow with $L/a \gg 1$, axial diffusion effects can be ignored and the hyperbolic model becomes even more appropriate compared to the laminar flow case.

3. Hyperbolic Model for Describing Dispersion Effects in Packed Beds

The traditional parabolic model with Danckwerts' boundary conditions is also used in the literature to describe dispersion effects in packed beds (and porous media). However, unlike the case of capillaries and straight tubes, the flow field in packed beds is more complex and is three-dimensional. However, for many cases of interest, the average velocity in the transverse directions is zero. In such cases, dispersion in the flow direction can be described by the

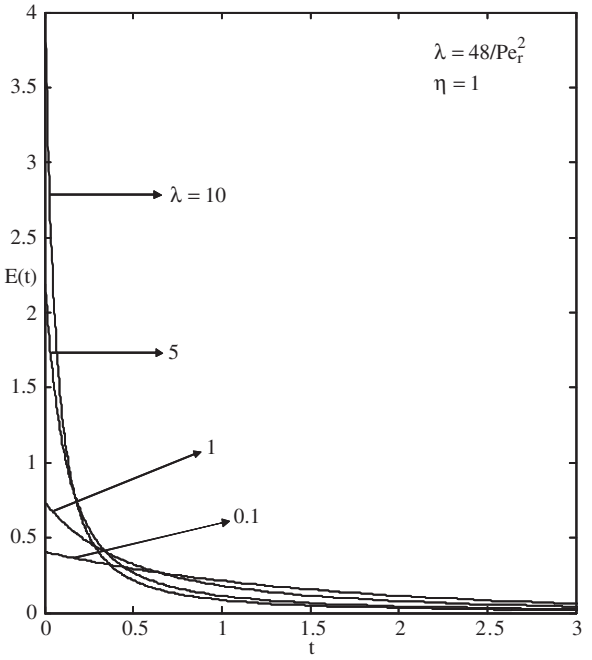

FIG. 8. Dispersion curves predicted by the full hyperbolic model [Eq. (72)] for $\eta = 1$.

hyperbolic model. For the case of isotropic beds with no mean flow in the transverse directions, the hyperbolic model may be expressed as

$$\varepsilon \frac{\partial C_{\mathrm{m}}}{\partial t'} + \langle u_x \rangle \frac{\partial C_{\mathrm{m}}}{\partial x} + \langle u_x \rangle t_D \frac{\partial^2 C_{\mathrm{m}}}{\partial x \partial t'} = \varepsilon D_{\mathrm{T}} \nabla_{\mathrm{T}}^2 C_{\mathrm{m}} \tag{75}$$

where ε is the bed porosity (assumed to be constant), $\langle u_x \rangle$ the velocity in the mean flow direction, and ∇_{T}^2 is the Laplacian operator in transverse coordinates (radial and azimuthal). Here, the local mixing time (t_D) and the transverse dispersion coefficient (D_{T}) may be expressed as

$$D_{\mathrm{T}} = D_{\mathrm{m}} + \alpha_{\mathrm{T}} \langle u_x \rangle d \tag{76}$$

$$t_D = \varepsilon \frac{D_{\mathrm{m}}}{\langle u_x \rangle^2} + \alpha_X \frac{d}{\langle u_x \rangle} \tag{77}$$

where d is the particle diameter and the numerical coefficients α_X and α_{T} depend on the structure of the bed. For the case of a randomly packed bed of spherical particles, typical values are $\alpha_{\mathrm{T}} = 0.1$ and $\alpha_X = 0.5$. The molecular contribution to dispersion, represented by the first term in the above expressions, can be neglected except at very small values of the local Peclet number ($\langle u_x \rangle d / D_{\mathrm{m}}$).

We do not pursue the solution of this new packed-bed dispersion model but note that it can be used to explain Hiby's (1962) experimental result, for which the traditional parabolic model cannot provide a good explanation.

B. Multi-mode Hyperbolic Averaged Models for Describing Dispersion Effects in Chromatographs

We now extend the averaging method to derive hyperbolic models to describe dispersion effects in chromatographs. We consider the case of a single solute being adsorbed on the wall of a tube in which the flow is laminar. Assuming Langmuir adsorption and neglecting axial molecular diffusion ($Pe_r \gg 1$), the governing partial differential equations (assuming azimuthal symmetry) may be written as

$$\frac{\partial C_A}{\partial t'} + 2\langle u_x\rangle\left(1 - \frac{\xi'^2}{a^2}\right)\frac{\partial C_A}{\partial x} = \frac{D_m}{\xi'}\frac{\partial}{\partial \xi'}\left(\xi'\frac{\partial C_A}{\partial \xi'}\right), \quad 0 < \xi' < a,\ x > 0 \tag{78}$$

$$-D_m\frac{\partial C_A}{\partial \xi'}(\xi' = a, z, t) = k_a C_{Aw} C_s - k_d C_{As}, \quad \frac{\partial C_A}{\partial \xi'}(\xi' = 0, z, t) = 0 \tag{79}$$

$$\frac{\partial C_{As}}{\partial t'} = k_a C_{Aw} C_s - k_d C_{As} \tag{80}$$

$$C_{Aw} = C_A(\xi' = a, z, t), \quad C_s + C_{As} = C_0 \tag{81}$$

with appropriate inlet and initial conditions. Here, k_a and k_d are the adsorption and desorption rate constants and C_{Aw} is the solute concentration at the wall and the other symbols have their usual meaning. Scaling the solute concentration using some reference inlet concentration (C_{A0}), adsorbed concentration by the total concentration of sites $C_0(\theta = C_{As}/C_0)$, time, radial, and axial coordinates as in the Taylor problem (using convection time, tube radius and length, respectively) and defining dimensionless parameters

$$\Gamma = \frac{2}{a}\frac{C_0}{C_{A0}}, \quad K = \frac{k_a C_{A0}}{k_d}, \quad Da_I = \frac{a^2 k_a C_{A0}}{D_m} \tag{82}$$

the dimensionless model equations may be written as

$$\mathbb{L}C \equiv \frac{1}{\xi}\frac{\partial}{\partial \xi}\left(\xi\frac{\partial C}{\partial \xi}\right) = p\left[\frac{\partial C}{\partial t} + 2(1 - \xi^2)\frac{\partial C}{\partial z}\right] \tag{83}$$

$$\frac{\partial C}{\partial \xi} = 0 \quad \text{at } \xi = 0 \tag{84}$$

$$\frac{1}{Da_{\mathrm{I}}}\frac{\partial C}{\partial \xi}(\xi=1,z,t)=-\frac{\Gamma}{2}\left[C_{\mathrm{w}}(1-\theta)-\frac{\theta}{K}\right],\quad C_{\mathrm{w}}=C(\xi=1,z,t) \tag{85}$$

$$\frac{\Gamma}{Da_{\mathrm{I}}}\frac{\partial \theta}{\partial t}=\left[C_{\mathrm{w}}(1-\theta)-\frac{\theta}{K}\right] \tag{86}$$

with initial and inlet conditions

$$C(\xi,z,t=0)=C_0(\xi,z) \tag{87}$$

$$\theta(z,t=0)=\theta_0(z) \tag{88}$$

$$C(\xi,z=0,t)=C_{\mathrm{in}}(\xi,t) \tag{89}$$

Here, $C(\xi,z,t)$ is the scaled solute concentration in the fluid phase, C_{w} the solute concentration at the wall, θ the normalized adsorbed concentration ($0\leqslant\theta\leqslant1$), K the adsorption equilibrium constant, p the transverse Peclet number, Γ represents the adsorption capacity (ratio of adsorption sites per unit tube volume to the reference solute concentration), and Da_{I} is the local Damköhler number (ratio of transverse diffusion time to the characteristic adsorption time). We shall assume that $p\ll1$ while Γ and Da_{I} are order-one parameters. (In physical terms, this implies that transverse molecular diffusion and adsorption processes are much faster compared to the convection.)

Transverse averaging of the above model using the procedure outlined in Section II gives the following averaged model to order p:

$$\frac{\partial\langle C\rangle}{\partial t}+\frac{\partial C_{\mathrm{m}}}{\partial z}+\Gamma\frac{\partial\theta}{\partial t}=0 \tag{90}$$

$$p\frac{\partial\theta}{\partial t}=Da_{\mathrm{I}}\left[C_{\mathrm{w}}(1-\theta)-\frac{\theta}{K}\right] \tag{91}$$

$$C_{\mathrm{w}}-\langle C\rangle=\frac{p}{8}\frac{\partial\langle C\rangle}{\partial t}+\frac{p}{6}\frac{\partial\langle C\rangle}{\partial z} \tag{92}$$

$$C_{\mathrm{m}}-\langle C\rangle=-\frac{p}{24}\frac{\partial\langle C\rangle}{\partial t}-\frac{p}{16}\frac{\partial\langle C\rangle}{\partial z} \tag{93}$$

$$\langle C\rangle(z,t=0)=\langle C_0(\xi,z)\rangle,\quad \theta(z,t=0)=\theta_0(z),\quad C_{\mathrm{m}}(z=0,t)=C_{\mathrm{m,in}}(t) \tag{94}$$

The averaged model is a *four-mode model*, the four modes (or variables) being the fluid-phase cup-mixing concentration (C_{m}), the fluid-phase average concentration ($\langle C\rangle$), the solute concentration at the wall (C_{w}), and the adsorbed

concentration (θ). [*Note*: Since the initial and boundary conditions for the averaged model are obtained in the same manner as in the Taylor problem by taking transverse averages of Eqs. (87) and (89), we do not consider them any further.] We now consider various limiting cases of this model.

For the case of $p = 0$ (which corresponds to adsorption, desorption, and transverse diffusion time scales going to zero), we have

$$C_{\mathrm{m}} = C_{\mathrm{w}} = \langle C \rangle, \quad \theta = \frac{K\langle C \rangle}{1 + K\langle C \rangle} \tag{95}$$

and the above model reduces to the widely used zeroth-order hyperbolic model (with no dispersion) (Rhee *et al.*, 1986):

$$\frac{\partial \langle C \rangle}{\partial t} + \frac{\partial \langle C \rangle}{\partial z} + \Gamma \frac{\partial \theta}{\partial t} = 0 \tag{96}$$

The first non-trivial case we consider is that of linear adsorption and desorption. For this case, we have $\theta \ll 1$ and the model becomes linear. For small p, we can use the leading-order approximation to further simplify the model by eliminating the variables C_{w} and $\langle C \rangle$ and write it in terms of C_{m}:

$$\frac{\partial C_{\mathrm{m}}}{\partial t} + \frac{1}{(1+\gamma)} \frac{\partial C_{\mathrm{m}}}{\partial z} + p\Lambda \frac{\partial^2 C_{\mathrm{m}}}{\partial z \partial t} = 0 \tag{97}$$

$$\Lambda = \frac{1}{48} \frac{1 + 6\gamma + 11\gamma^2}{(1+\gamma)^2} + \frac{1}{\Gamma Da_{\mathrm{l}}} \frac{\gamma^2}{(1+\gamma)^2} \tag{98}$$

$$\gamma = \Gamma K = \frac{2}{a} \frac{k_{\mathrm{a}} C_0}{k_{\mathrm{d}}} \tag{99}$$

(*Note*: Since the model is linear for the special case considered, the same equation is also satisfied by the other three variables.) The following observations may be made from Eq. (98) that expresses the dimensionless dispersion coefficient Λ: (i) The first term describes dispersion effects due to velocity gradients when adsorption equilibrium exists at the interface. We note that this expression was first derived by Golay (1958) for capillary chromatography with a retentive layer. (ii) The second term corresponds to dispersion effects due to finite rate of adsorption (since this term vanishes if we assume that adsorption and desorption are very fast so that equilibrium exists at the interface). (iii) The effective dispersion coefficient reduces to the Taylor limit when the adsorption rate constant or the adsorption capacity is zero. (iv) As is well known (Rhee *et al.*, 1986), the effective solute velocity is reduced by a factor $(1 + \gamma)$. (v) For the case of irreversible adsorption ($\gamma \to \infty$ and $Da_{\mathrm{l}} \to \infty$), the dispersion coefficient is equal to 11 times the Taylor value. It is also equal to the reciprocal of the asymptotic Sherwood number for mass transfer in a circular

channel with constant wall flux boundary condition. (vi) When the local Damköhler number is small (adsorption is slow or capacity is low), Λ can be large, leading to long tails in the dispersion curve.

The second limiting case we consider is that of Langmuir adsorption with equilibrium at the interface. This assumption is equivalent to assuming $Da_l \to \infty$ and replacing Eq. (91) by

$$\theta = \frac{KC_w}{1 + KC_w} \tag{100}$$

Combining Eqs. (92) and (93), we get

$$\begin{aligned} C_w &= C_m + \frac{p}{6}\frac{\partial \langle C\rangle}{\partial t} + \frac{11p}{48}\frac{\partial \langle C\rangle}{\partial z} \\ &= C_m + \frac{p}{6}\frac{\partial C_m}{\partial t} + \frac{11p}{48}\frac{\partial C_m}{\partial z} + O(p^2) \end{aligned} \tag{101}$$

Thus, we can obtain the following single evolution equation for the cup-mixing concentration:

$$\begin{aligned} &\frac{\partial C_m}{\partial t} + \frac{\partial C_m}{\partial z} + \frac{p}{24}\frac{\partial^2 C_m}{\partial t^2} + \frac{p}{16}\frac{\partial^2 C_m}{\partial z \partial t} \\ &\quad + \Gamma \frac{\partial}{\partial t}\left(\frac{KC_m + \dfrac{pK}{6}\dfrac{\partial C_m}{\partial t} + \dfrac{11pK}{48}\dfrac{\partial C_m}{\partial z}}{1 + KC_m + \dfrac{pK}{6}\dfrac{\partial C_m}{\partial t} + \dfrac{11pK}{48}\dfrac{\partial C_m}{\partial t}} \right) = 0 \end{aligned} \tag{102}$$

This equation reduces to the zeroth-order hyperbolic model [Eq. (95)] for $p = 0$. It also reduces to the hyperbolic model treated in the previous section for either $\Gamma = 0$ or $K = 0$ (after combining the third and fourth terms using the leading-order approximation). For finite p, Γ, and K, this rigorously derived averaged model is quite different from the intuitively written models in the literature.

The last case we consider is that of a flat velocity profile with linear adsorption and desorption. In this case, the dimensionless model equations are given by

$$\frac{1}{\xi}\frac{\partial}{\partial \xi}\left(\xi \frac{\partial C}{\partial \xi}\right) = p\left[\frac{\partial C}{\partial t} + \frac{\partial C}{\partial z}\right] \tag{103}$$

$$\frac{\partial C}{\partial \xi} = 0 \quad \text{at } \xi = 0 \tag{104}$$

$$\frac{1}{Da_l}\frac{\partial C}{\partial \xi}(\xi = 1, z, t) = -\frac{\Gamma}{2}\left[C_w(1-\theta) - \frac{\theta}{K}\right], \quad C_w = C(\xi = 1, z, t) \tag{105}$$

$$p\frac{\partial\theta}{\partial t} = Da_{\mathrm{I}}\left[C_{\mathrm{w}}(1-\theta) - \frac{\theta}{K}\right] \tag{106}$$

Now, because of flat velocity profile, the distinction between cup-mixing and averaged concentrations disappears and the averaged model to order p is a *three-mode model* given by

$$\frac{\partial\langle C\rangle}{\partial t} + \frac{\partial\langle C\rangle}{\partial z} + \Gamma\frac{\partial\theta}{\partial t} = 0 \tag{107}$$

$$p\frac{\partial\theta}{\partial t} = Da_{\mathrm{I}}\left[C_{\mathrm{w}}(1-\theta) - \frac{\theta}{K}\right] \tag{108}$$

$$C_{\mathrm{w}} - \langle C\rangle = \frac{p}{8}\left(\frac{\partial\langle C\rangle}{\partial t} + \frac{\partial\langle C\rangle}{\partial z}\right) \tag{109}$$

For the case of linear adsorption, we can combine these equations into a single hyperbolic equation:

$$\frac{\partial\langle C\rangle}{\partial t} + \frac{1}{(1+\gamma)}\frac{\partial\langle C\rangle}{\partial z} + p\Lambda\frac{\partial^2\langle C\rangle}{\partial z\partial t} = 0 \tag{110}$$

$$\Lambda = \frac{1}{8}\frac{\gamma^2}{(1+\gamma)^2} + \frac{1}{\Gamma Da_{\mathrm{I}}}\frac{\gamma^2}{(1+\gamma)^2} \tag{111}$$

Comparing Eqs. (97) and (110), we see that the adsorption induced dispersion is independent of the velocity profile. We also note that for the case of flat velocity profile, there is no dispersion when $\gamma = 0$. When equilibrium is assumed at the wall, we can eliminate θ and C_{w} and write the averaged equation as

$$\frac{\partial\langle C\rangle}{\partial t} + \frac{\partial\langle C\rangle}{\partial z} + \Gamma\frac{\partial}{\partial t}\left(\frac{K\langle C\rangle + \dfrac{pK}{8}\dfrac{\partial\langle C\rangle}{\partial t} + \dfrac{pK}{8}\dfrac{\partial\langle C\rangle}{\partial z}}{1 + K\langle C\rangle + \dfrac{pK}{8}\dfrac{\partial\langle C\rangle}{\partial t} + \dfrac{pK}{8}\dfrac{\partial\langle C\rangle}{\partial z}}\right) = 0 \tag{112}$$

As expected, for $p = 0$, this model reduces again to the zeroth-order hyperbolic model, Eq. (95), but for any finite p, it does not simplify to any of the standard models in the literature.

The order p terms that appear in Eqs. (102) and (112) modify the leading-order hyperbolic behavior by introducing dispersion (which is always present in real systems due to velocity gradients and finite rates of adsorption). As is well known in the literature, the leading (zeroth)-order hyperbolic models may have discontinuous solution profiles (Rhee *et al.*, 1986). As stated in the introduction, in the literature, these models are often modified by adding a dispersion term

and transforming them to a parabolic form. The above analysis shows that the parabolic form of the reduced model is not only a poor approximation but also cannot be justified based on physical grounds (and rigorous derivation). The L–S method of averaging modifies the zeroth-order hyperbolic models by adding order p corrections and gives the averaged models in multi-mode (hyperbolic) form. As shown above, in some special cases (e.g. linear adsorption or equilibrium at the wall) it is possible to transform them to a single-mode form which is a hyperbolic equation containing the dispersion effects. When this simplification is not possible, it is best to leave the averaged models in multi-mode form, which is more convenient for numerical solution.

C. A Hyperbolic Model for Describing Dispersion Effects in Monoliths with Diffusion into the Solid Phase

We can extend the hyperbolic model to cases in which the solute diffuses in more than one phase. A common case is that of a monolith channel in which the flow is laminar and the walls are coated with a washcoat layer into which the solute can diffuse (Fig. 4). The complete model for a non-reacting solute here is described by the convection–diffusion equation for the fluid phase coupled with the unsteady-state diffusion equation in the solid phase with continuity of concentration and flux at the fluid–solid interface. Transverse averaging of such a model gives the following hyperbolic model for the cup-mixing concentration in the fluid phase:

$$\frac{\partial C_{\mathrm{fm}}}{\partial t} + \varepsilon \frac{\partial C_{\mathrm{fm}}}{\partial z} + \Lambda_1(\varepsilon, \mu) p \frac{\partial^2 C_{\mathrm{fm}}}{\partial z \partial t} - \Lambda_2(\varepsilon, \mu) p \frac{\partial^2 C_{\mathrm{fm}}}{\partial z^2} = 0 \tag{113}$$

Here, t and z have been scaled with respect to the convection time and length of monolith, respectively. The transverse or local Peclet number p and the radial Peclet number Pe_{r} are defined as in the case of the Taylor problem, ε is the volume fraction of the fluid phase and

$$\Lambda_2(\varepsilon, \mu) = \frac{1}{Pe_{\mathrm{r}}^2}\left(\varepsilon + \frac{1-\varepsilon}{\mu}\right), \quad \mu = \frac{D_{\mathrm{es}}}{D_{\mathrm{m}}} \tag{114}$$

(D_{es} is the effective diffusivity of the solute in the solid phase while D_{m} is the molecular diffusivity in the fluid phase.) The function $\Lambda_1(\varepsilon, \mu)$ depends on the shape of the channel and the washcoat surrounding it. For the case of a circular channel with a uniform washcoat thickness, it can be shown that

$$\Lambda_1(\varepsilon, \mu) = \frac{6\varepsilon^2 - 16\varepsilon + 11}{48} + \frac{\mu}{8}(4\varepsilon - \varepsilon^2 - 2 - 2\ln\varepsilon) \tag{115}$$

We note that when $\varepsilon = 1$, Eq. (113) reduces to the Taylor problem (with axial diffusion included). As ε decreases or μ increases, the magnitude of dispersion

increases leading to long tails in the dispersion curve. Once again, the hyperbolic model describes this solute retaining behavior much better than the traditional parabolic models.

IV. Spatially Averaged Multi-mode (Multi-scale) Models for Homogeneous Reactors

In this section, we present spatially averaged multi-scale models for different types of homogeneous reactors. We consider a single homogeneous reaction involving M species, which is given by

$$\sum_{j=1}^{M} \nu_j A_j = 0 \tag{116}$$

where, ν_j is the stoichiometric coefficient of species A_j, and we use the usual convention of $\nu_j > 0$ if A_j is a product and $\nu_j < 0$ if A_j is a reactant.

A. Isothermal Tubular Reactors

1. Laminar Flows

For a constant density system, the scalar concentration $C_j(\xi', \varphi, x, t')$ of species j in a tubular reactor of uniform cross-section Ω with unidirectional laminar flow (Fig. 1) obeys the CDR equation

$$\begin{aligned} &\frac{\partial C_j}{\partial t'} + u_x(\xi')\frac{\partial C_j}{\partial x} - \nu_j R(C_1, C_2, \ldots, C_M) \\ &\quad = D_{\mathrm{m},j}\left[\frac{1}{\xi'}\frac{\partial}{\partial \xi'}\left(\xi'\frac{\partial C_j}{\partial \xi'}\right) + \frac{1}{\xi'^2}\frac{\partial^2 C_j}{\partial \varphi^2}\frac{\partial^2 C_j}{\partial x^2}\right] \end{aligned} \tag{117}$$

where $u_x(\xi')$ is the fully developed velocity field, $D_{\mathrm{m},j}$ the molecular diffusivity of species j, $R(C_j)$ the intrinsic reaction rate, and x, φ, and ξ' are the axial, azimuthal, and radial coordinates, respectively. In the transverse direction, Eq. (117) is subject to the no-flux boundary condition at the wall,

$$\nabla C_j \cdot \mathbf{n} = 0 \tag{118}$$

where $\mathbf{n}$ is the unit normal to the boundary $\partial\Omega$ and ∇ is the gradient operator in Ω, while the inlet condition is of Danckwerts' type,

$$D_{\mathrm{m},j}\frac{\partial C_j}{\partial x} = u_x(\xi')[C_j(\xi', \varphi, x, t') - C_{j,\mathrm{in}}(\xi', \varphi, t')] \quad \text{at } x = 0 \tag{119}$$

and the exit condition is

$$\frac{\partial C_j}{\partial x} = 0 \quad \text{at } x = L \tag{120}$$

Using a (radius of the pipe) and L (length of the pipe) as the characteristic lengths in the transverse and axial directions, respectively, C_R as the reference concentration, and $D_{m,R}$ as the reference molecular diffusivity, we obtain four time scales in the system associated with convection (τ_C), local/transverse diffusion (t_D), axial diffusion (t_Z), and reaction (t_R),

$$\tau_C = \frac{V}{q_{in}} = \frac{L}{\langle u_x \rangle}, \quad t_D = \frac{a^2}{D_{m,R}}, \quad t_Z = \frac{L^2}{D_{m,R}}, \quad t_R = \frac{C_R}{R(C_R)} \tag{121}$$

where V and q_{in} are the volume of the reactor and the volumetric flow rate of the reactants, respectively. The ratios of these time scales give rise to the dimensionless parameters: p (transverse or local Peclet number), Pe_r (radial Peclet number), Da (reactor scale Damköhler number), and ϕ^2 (local Damköhler number), given by

$$\begin{aligned} p &= \frac{a^2\langle u_x \rangle}{L D_{m,R}} = \frac{t_D}{\tau_C}, \quad Pe_r = \frac{\langle u_x \rangle a}{D_{m,R}}, \quad Pe = \frac{\langle u_x \rangle L}{D_{e,R}} = \frac{t_Z}{\tau_C} = \frac{Pe_r^2}{p} \\ \kappa_j &= \frac{D_{m,R}}{D_{m,j}}, \quad Da = \frac{LR(C_R)}{\langle u_z \rangle C_R} = \frac{\tau_C}{t_R}, \quad \phi^2 = pDa = \frac{a^2 R(C_R)}{D_{m,R} C_R} = \frac{t_D}{t_R} \end{aligned} \tag{122}$$

We use the following dimensionless variables:

$$t = \frac{t'}{\tau_C}, \quad \xi = \frac{\xi'}{a}, \quad z = \frac{x}{L}, \quad u = \frac{u_x}{\langle u_x \rangle}, \quad c_j = \frac{C}{C_R}, \quad r(\boldsymbol{c}) = \frac{R(C_1, C_2, \ldots, C_M)}{R(C_R)}$$

to rewrite Eq. (117) in dimensionless form as

$$\frac{1}{\xi}\frac{\partial}{\partial \xi}\left(\xi \frac{\partial c_j}{\partial \xi}\right) + \frac{1}{\xi^2}\left(\frac{\partial^2 c_j}{\partial \varphi^2}\right) = p\kappa_j \left[\frac{\partial c_j}{\partial t} - \frac{p}{\kappa_j Pe_r^2}\frac{\partial^2 c_j}{\partial z^2} + u(\xi)\frac{\partial c_j}{\partial z} - v_j Da\, r(\boldsymbol{c})\right] \tag{123}$$

$$\underline{\underline{\Delta}} pf(\boldsymbol{c}, p, \boldsymbol{p}^*) \tag{124}$$

As in the previous problems, we assume that $p \ll 1$ while Da, κ_j, and Pe_r are order-one parameters. The boundary and initial conditions on the model are given by

$$\frac{p}{\kappa_j Pe_r^2}\frac{\partial c_j}{\partial z} = u(\xi)[c_j - c_{j,in}(\xi, \varphi, t)] \quad \text{at } z = 0 \tag{125}$$

$$\frac{\partial c_j}{\partial z} = 0 \quad \text{at } z = 1 \tag{126}$$

$$\frac{\partial c_j}{\partial \xi} = 0 \quad \text{at } \xi = 0, 1 \tag{127}$$

$$c_j(\xi, \varphi, z, t) = c_j(\xi, \varphi + 2\pi, z, t) \tag{128}$$

$$c_j(\xi, \varphi, z, t = 0) = c_{j,0}(\xi, \varphi, z) \tag{129}$$

Transverse averaging of the above model using the procedure outlined in the previous section for the case of laminar flow in a tube, i.e. $u(\xi) = 2(1 - \xi^2)$, with azimuthally symmetric feeding gives the following two-mode model for the jth species ($j = 1, 2, \ldots, M$), involving the spatially averaged concentration $\langle c_j \rangle$ and the mixing-cup concentration $c_{j,\mathrm{m}}$ to order p:

$$\frac{\partial \langle c_j \rangle}{\partial t} + \frac{\partial c_{j,\mathrm{m}}}{\partial z} - \frac{p}{\kappa_j Pe_{\mathrm{r}}^2} \frac{\partial^2 \langle c_j \rangle}{\partial z^2} - v_j Da\, r(\langle \mathbf{c} \rangle) + O(p^2) = 0 \tag{130}$$

$$\langle c_j \rangle - c_{j,\mathrm{m}} = \beta_1 p \kappa_j \frac{\partial c_{j,\mathrm{m}}}{\partial z} + O(p^2) \tag{131}$$

with boundary and initial conditions given by

$$\frac{p}{\kappa_j Pe_{\mathrm{r}}^2} \frac{\partial \langle c_j \rangle}{\partial z} = c_{j,\mathrm{m}} - c_{j,\mathrm{m,in}}(t), \quad \text{at } z = 0 \tag{132}$$

$$\frac{\partial \langle c_j \rangle}{\partial z} = 0, \quad \text{at } z = 1 \tag{133}$$

$$\langle c_j \rangle = \langle c_{j,0} \rangle(z), \quad \text{at } t = 0 \tag{134}$$

where $\langle c_j \rangle$ is the transverse-averaged concentration in the reactor and $c_{j,\mathrm{m}}$ is the mixing-cup concentration, which for the tubular geometry are given by

$$\langle c_j \rangle = \frac{1}{2\pi} \int_{\xi=0}^{\xi=1} \int_{\varphi=0}^{\varphi=2\pi} 2\xi c_j(\xi, \varphi, z)\, \mathrm{d}\varphi\, \mathrm{d}\xi \tag{135}$$

$$c_{j,\mathrm{m}} = \frac{\int_{\xi=0}^{\xi=1} \int_{\varphi=0}^{\varphi=2\pi} c_j u(\xi) 2\xi\, \mathrm{d}\varphi\, \mathrm{d}\xi}{2\pi \int_0^1 u(\xi) 2\xi\, \mathrm{d}\xi} \tag{136}$$

respectively. The numerical coefficient $\beta_1 = \frac{1}{48}$ for fully developed laminar flow in a pipe. (*Note*: $\beta_1 = \frac{2}{105}$ for plane Poiseuille flow while it is $\frac{1}{30}$ for Couette

flows.) It may be noted that the low-dimensional model defined by Eqs. (130)–(134) has the same number of parameters as the full CDR equations. For $p = 0$, the model reduces to the zeroth-order plug-flow model, while for any $p > 0$, the plug-flow model is modified by including the effects of local velocity gradients and diffusion (micromixing) as well as reactor scale mixing. In this reduced model, reactor scale mixing (macromixing) is captured by the third term in Eq. (130) while the local mixing (micromixing) is captured through the local equation [Eq. (131)].

We now consider some important limiting cases of this model. First, we note that when axial molecular diffusion is negligible, Eqs. (130)–(131) reduce to hyperbolic model:

$$\frac{\partial c_{j,\mathrm{m}}}{\partial t} + \frac{\partial c_{j,\mathrm{m}}}{\partial z} + \beta_1 p \kappa_j \frac{\partial^2 c_{j,\mathrm{m}}}{\partial z \partial t} - v_j Da\, r(\langle \boldsymbol{c} \rangle) = 0 \tag{137}$$

$$\langle c_j \rangle - c_{j,\mathrm{m}} = \beta_1 p \kappa_j \frac{\partial c_{j,\mathrm{m}}}{\partial z} \tag{138}$$

$$c_{j,\mathrm{m}} = c_{j,\mathrm{m,in}}(t) \quad \text{at } z = 0; \quad \langle c_j \rangle = \langle c_{j,0} \rangle (z), \quad \text{at } t = 0 \tag{139}$$

Under steady-state conditions (and assuming that the inlet condition is independent of time), this two-mode model can be further simplified to

$$\frac{\mathrm{d}c_{j,\mathrm{m}}}{\mathrm{d}z} = v_j Da\, r(\langle \mathbf{c} \rangle) \quad \text{with } c_{j,\mathrm{m}}|_{z=0} = c_{j,\mathrm{m,in}} \tag{140}$$

$$\langle c_j \rangle - c_{j,\mathrm{m}} = \beta_1 p \kappa_j \frac{\mathrm{d}c_{j,\mathrm{m}}}{\mathrm{d}z} = \beta_1 p \kappa_j v_j Da\, r(\langle \mathbf{c} \rangle) \tag{141}$$

which in dimensional form may be written as

$$\langle u_x \rangle \frac{\mathrm{d}C_{j,\mathrm{m}}}{\mathrm{d}x} = v_j R(\langle \mathbf{C} \rangle) \quad \text{with } C_{j,\mathrm{m}}|_{x=0} = C_{j,\mathrm{m,in}} \tag{142}$$

$$\langle C_j \rangle - C_{j,\mathrm{m}} = t_{\mathrm{mix},j} v_j R(\langle \mathbf{C} \rangle) \tag{143}$$

where

$$t_{\mathrm{mix},j} = \beta_1 \frac{a^2}{D_{\mathrm{m},j}} = \frac{t_{\mathrm{mix}}}{\kappa_j} \tag{144}$$

is the local mixing time of the jth species and t_{mix} is the characteristic local mixing time of the system defined in terms of the reference species. The dimensionless form of the characteristic local mixing time of the system (η), is obtained by non-dimensionalizing t_{mix} w.r.t. the residence time in the reactor

and is given by

$$\eta = \frac{t_{\text{mix}}}{\tau_{\text{C}}} = \beta_1 \frac{a^2/D_{\text{m,R}}}{\tau_{\text{C}}} = \beta_1 p \tag{145}$$

The solutions of the steady-state two-model model given by Eq. (140)–(141) should be compared to the parabolic axial dispersion model with Danckwerts boundary conditions (Danckwerts, 1953; Wehner and Wilhelm, 1956):

$$\frac{1}{\kappa_j Pe}\frac{\mathrm{d}^2\langle c_j\rangle}{\mathrm{d}z^2} - \frac{\mathrm{d}\langle c_j\rangle}{\mathrm{d}z} + v_j Da\, r(\langle \mathbf{c}\rangle) = 0, \quad 0 < z < 1 \tag{146}$$

$$\frac{1}{\kappa_j Pe}\frac{\mathrm{d}\langle c_j\rangle}{\mathrm{d}z} = \langle c_j\rangle - \langle c_{j,in}\rangle \ \text{ at } z = 0, \quad \frac{\mathrm{d}\langle c_j\rangle}{\mathrm{d}z} = 0 \ \text{ at } z = 1 \tag{147}$$

The Danckwerts model lumps the combined effect of axial diffusion, velocity gradients, and transverse molecular diffusion into an effective axial dispersion coefficient (axial Peclet number, Pe). However, when $L/a \gg 1$ (or $Pe_{\text{r}} \gg 1$), the two-mode model represents dispersion using the local mixing time and two concentration variables. As in the Taylor problem, the exit concentration predicted by the Danckwerts model is always bounded between the two limiting cases of plug flow ($Pe = \infty$) and CSTR ($Pe = 0$). This is not the case for the two models defined by Eqs. (140)–(141). While for $p \to 0$ (or $\eta \to 0$) the solution approaches the plug-flow limit, as p (or η) increases the conversions can be below those obtained in a CSTR. This is the so-called mixing limited asymptote which is similar to the mass transfer controlled case for the case of catalytic reactions. The single-mode Danckwerts model cannot describe (even qualitatively) this mixing (or more precisely micromixing) limited regime.

This feature is illustrated in Fig. 9, which compares the solution of the ideal PFR, ideal CSTR, and the Danckwerts model [Eqs. (146)–(147)] with the two-mode convection model [Eqs. (140)–(141)] for the case of steady-state and single first-order homogeneous reaction of the form $A \to B$. The solution of the steady-state Danckwerts model is given by

$$X = 1 - \frac{4q\exp(Pe/2)}{(1+q)^2\ \exp\left(\dfrac{Peq}{2}\right) - (1+q)^2\ \exp\left(\dfrac{Peq}{2}\right)} \tag{148}$$

where $q = \sqrt{1 + 4Da/Pe}$ and X is the conversion of A, while the solution of the steady-state two-mode convection model is given by

$$X = 1 - \exp\left(\frac{-Da}{1+\eta Da}\right) \tag{149}$$

and the variances (σ^2) of the models are given by Eqs. (71) and (63),

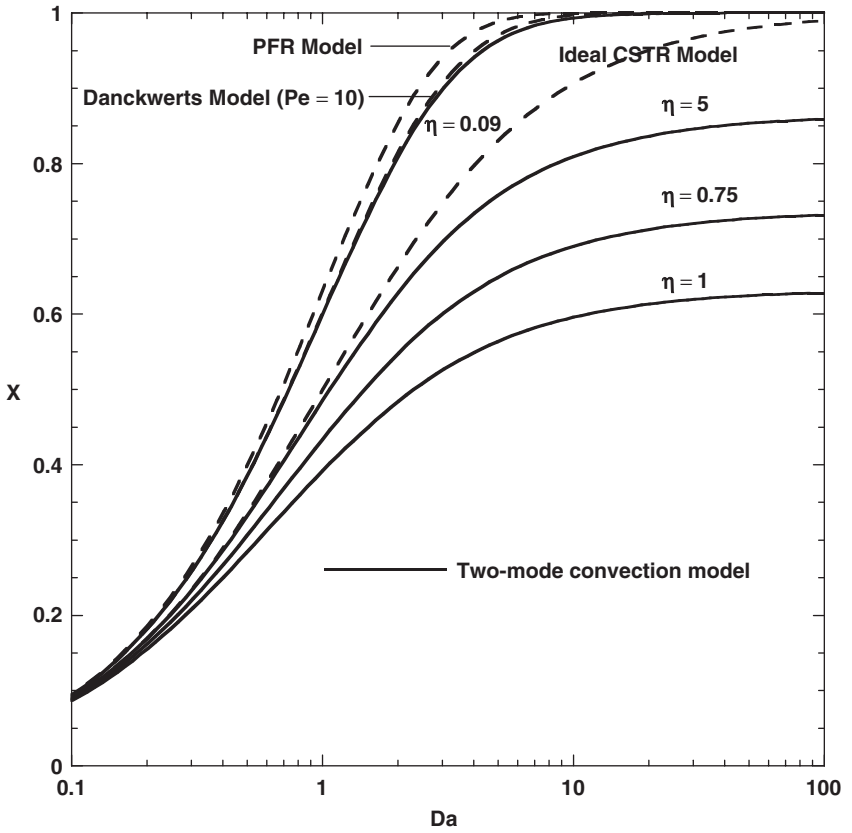

FIG. 9. Comparison of the solutions of ideal PFR, CSTR, and Danckwerts models with that of two-mode convection model for an isothermal first-order homogeneous reaction.

respectively. We note that for small values of σ^2, both models predict

$$1 - X = \exp(-Da)[1 + \sigma^2 Da^2] + O(\eta^2) \tag{150}$$

Needless to mention that the Danckwerts model [Eqs. (146)–(147)] reduces to the ideal PFR and the ideal CSTR models in the limits of $Pe \to \infty$ and $Pe \to 0$, respectively. As seen in Fig. 9, the ideal PFR model and the ideal CSTR model bound the solution of the Danckwerts model [Eqs. (146)–(147)] for the case of any finite Pe number. As shown in Fig. 9 (and from Eq. (150)), for $Pe \geqslant 10$, the two-mode model predicts very close to the Danckwerts model when the variances of the two models are matched using Eqs. (71) and (63). However, the two-mode models can predict conversions in regions in the parameter space which are inaccessible to the Danckwerts models. These are the micromixing limited conversions which are even below conversions predicted by the ideal

CSTR model. As illustrated in Fig. 9, these solutions of the two-mode model attain mixing limited asymptotes for large values of Da.

The second important limiting case of the general model [Eqs. (130)–(134)] we consider is that of the steady-state case in which macro (axial) and micro (transverse) mixing effects are of the same order of magnitude. Assuming that the inlet concentrations are independent of time, the general model simplifies to

$$\frac{\mathrm{d}c_{j,\mathrm{m}}}{\mathrm{d}z} - \frac{p}{\kappa_j Pe_\mathrm{r}^2}\frac{\mathrm{d}^2\langle c_j\rangle}{\mathrm{d}z^2} - \nu_j Da\, r(\langle\mathbf{c}\rangle) + O(p^2) = 0 \tag{151}$$

$$\langle c_j\rangle - c_{j,\mathrm{m}} = \beta_1 p\kappa_j \frac{\mathrm{d}c_{j,\mathrm{m}}}{\mathrm{d}z} + O(p^2) = \beta_1 p\kappa_j \frac{\mathrm{d}\langle c_j\rangle}{\mathrm{d}z} + O(p^2) \tag{152}$$

with boundary conditions given by

$$\frac{p}{\kappa_j Pe_\mathrm{r}^2}\frac{\mathrm{d}\langle c_j\rangle}{\mathrm{d}z} = c_{j,\mathrm{m}} - c_{j,\mathrm{m,in}}, \quad \text{at } z = 0 \tag{153}$$

$$\frac{\mathrm{d}\langle c_j\rangle}{\mathrm{d}z} = 0, \quad \text{at } z = 1 \tag{154}$$

Eqs. (151)–(153) may be combined and written as

$$\frac{\mathrm{d}\langle c_j\rangle}{\mathrm{d}z} - \left(\beta_1 p\kappa_j + \frac{p}{\kappa_j Pe_\mathrm{r}^2}\right)\frac{\mathrm{d}^2\langle c_j\rangle}{\mathrm{d}z^2} - \nu_j Da\, r(\langle\mathbf{c}\rangle) + O(p^2) = 0 \tag{155}$$

$$\left(\beta_1 p\kappa_j + \frac{p}{\kappa_j Pe_\mathrm{r}^2}\right)\frac{\mathrm{d}\langle c_j\rangle}{\mathrm{d}z} = \langle c_j\rangle - c_{j,\mathrm{m,in}}, \quad \text{at } z = 0 \tag{156}$$

Thus, we recover the Danckwerts model only if no distinction is made between the cup-mixing and spatial average concentrations (with this assumption, the effective axial dispersion coefficient is given by the Taylor–Aris theory). This derivation also shows that the concept of an effective axial dispersion coefficient and lumping the macro- and micromixing effects into one parameter is valid only at steady-state, constant inlet conditions and when the deviation from plug flow is small. [*Remark*: Even with all these constraints, the error in the model because of the assumption $\langle c_j\rangle = c_{j,\mathrm{m}}$ is of the same order of magnitude as the dispersion effect!]

The last limiting case of the general model we consider is that of a tubular reactor in which macromixing effect is dominant compared to the micromixing effect. (This could be the case when the tube diameter or length are of the same order of magnitude or when there is physical backmixing). Here, the general model given by Eqs. (130)–(134) is valid again but we replace p/Pe_r^2 by $1/Pe$, where Pe is the axial Peclet number, which is of order unity. Now, we have a

two-parameter two-mode mixing model where the magnitude of Pe is an indication of the macromixing while that of p gives the micromixing effect. For example, for the case of steady state, the model may be written as

$$\frac{1}{\kappa_j Pe}\frac{\mathrm{d}^2\langle c_j\rangle}{\mathrm{d}z^2} - \frac{\mathrm{d}c_{j,\mathrm{m}}}{\mathrm{d}z} + \nu_j Da\, r(\langle \mathbf{c}\rangle) = 0; \quad 0<z<1 \tag{157}$$

$$\langle c_j\rangle - c_{j,\mathrm{m}} = \beta_1 p\kappa_j \frac{\mathrm{d}c_{j,\mathrm{m}}}{\mathrm{d}z} \tag{158}$$

$$\frac{1}{\kappa_j Pe}\frac{\mathrm{d}\langle c_j\rangle}{\mathrm{d}z} = c_{j,\mathrm{m}} - c_{j,\mathrm{m,in}} \text{ at } z=0, \quad \frac{\mathrm{d}\langle c_j\rangle}{\mathrm{d}z} = 0 \text{ at } z=1 \tag{159}$$

For $p = 1/Pe = 0$, this model reduces to the ideal PFR model, for $p = 0$, it reduces to the Danckwerts model, for $1/Pe = 0$, it reduces to the two-mode plug-flow model while for $Pe = 0$, it reduces to the two-mode CSTR model (discussed below). Thus, we have shown that the hyperbolic two-mode model given by Eqs. (130)–(134) has a much larger region of validity than the traditional homogeneous tubular reactor models.

2. *Turbulent Flows*

The extension of the two-mode axial dispersion model to the case of fully developed turbulent flow in a pipe could be achieved by starting with the time-smoothed (Reynolds-averaged) CDR equation, given by Eq. (117), where the reaction rate term $R(C)$ in Eq. (117) is replaced by the Reynolds-averaged reaction rate term $R_{\mathrm{av}}(\mathbf{C})$, and the molecular diffusivity $D_{\mathrm{m},j}$ is replaced by the effective diffusivity $D_{\mathrm{e},j}$ in turbulent flows given by

$$D_{\mathrm{e},j} = D_{\mathrm{m},j} + D_{\mathrm{T}} \tag{160}$$

where D_{T} is the turbulent diffusivity, which could be obtained on the basis of turbulent shear stress and expressed in terms of Reynolds number using one of the correlations presented by Taylor (1954), Sittel *et al.* (1968), or Wen and Fan (1975).

The Reynolds-averaged reaction rate $R_{\mathrm{av}}(c)$ could be evaluated by using simple closure models of Bourne and Toor (1977), Brodkey and Lewalle (1985), Li and Toor (1986), Dutta and Tarbell (1989), etc. It should also be pointed out that the spatial averaging presented here is independent of the methodology using which $R_{\mathrm{av}}(c)$ and D_{T} are evaluated, or in other words, spatial averaging follows time averaging.

We use an universal velocity distribution obtained by Churchill (2001) to approximate the fully developed velocity profile $u(\xi)$ across the turbulent core,

given by

$$u(\xi) = \sqrt{\frac{f_t}{2}}\left(5.5 + 2.5\ln\left[(1-\xi)Re\sqrt{\frac{f_t}{8}}\right] + \frac{15}{4}(1-\xi)^2 - \frac{10}{3}(1-\xi)^3\right) \quad (161)$$

where f_t is the Fanning friction factor and Re is the Reynolds number.

Using the velocity profile given by Eq. (161) to solve the local equations, we obtain the leading-order fluctuations $c_{j,1}$ as

$$c_{j,1} = 0.1647\sqrt{f_t}\,\frac{\partial\langle c_j\rangle}{\partial z}\left[\begin{array}{c} 1 - 2.684\xi - 0.895\xi^2 + 1.79\xi^3 - 3.355\xi^4 + 1.431\xi^5 \\ +0.536\omega(2\xi^2 - 1) + 2.68(\xi^2 - 1)\ln[1-\xi] \end{array}\right] \quad (162)$$

where

$$\omega = 5.5 + 2.5\ln\left(Re\sqrt{\frac{f_t}{8}}\right) - \sqrt{\frac{2}{f_t}} \quad (163)$$

The important result is that the two-mode models for a turbulent flow tubular reactor are the same as those for laminar flow tubular reactors. The two-mode axial dispersion model for turbulent flow tubular reactors is again given by Eqs. (130)–(134), while the two-mode convection model for the same is given by Eqs. (137)–(139), where the reaction rate term $r(\langle\mathbf{c}\rangle)$ is replaced by the Reynolds-averaged reaction rate term $r_{\rm av}(\langle\mathbf{c}\rangle)$. The local mixing time $t_{{\rm mix},j}$ for turbulent flows is given by

$$t_{{\rm mix},j} = \beta_1\frac{a^2}{D_{{\rm m},j} + D_{\rm T}} \quad (164)$$

where β_1 is given by

$$\begin{aligned}\beta_1 &= 0.1f_t(\omega - 3.45)\\ &= 0.1f_t\left(2.05 + 2.5\ln\left[Re\sqrt{\frac{f_t}{8}}\right] - \sqrt{\frac{2}{f_t}}\right)\end{aligned} \quad (165)$$

We note that in turbulent flows, typically $D_{{\rm m},j} \ll D_{\rm T}$ $(j = 1,\ldots,M)$, a result of which, the local mixing time $t_{\rm mix}$ is practically independent of the molecular diffusivity or the molecular Schmidt number, i.e. $t_{{\rm mix},j} \approx t_{{\rm mix,T}}$ $(j = 1,\ldots,M)$, where

$$t_{\rm mix,T} = \beta_1\frac{a^2}{D_{\rm T}} \quad (166)$$

B. Loop and Recycle Reactors

In this section, we present the two-mode models for loop and recycle reactors. In a loop reactor (Fig. 10) of loop length L, a flow rate of q_{in} with an average velocity of $\langle u_{\text{in}} \rangle$ enters and leaves the reactor at points $x = 0$ and $x = l$, respectively (where x is the length coordinate along the loop), and the total flow rate in the loop is $Q + q_{\text{in}}$ between points $x = 0$ and $x = l$, and is Q between points $x = l$ and $x = L$, due to a recycle rate of Q. The recycle ratio Λ is the ratio of the volume of fluid returned to the reactor entrance per unit time to the volume of fluid leaving the system per unit time, and is given by $\Lambda = Q/q_{\text{in}}$.

Neglecting axial diffusion (or assuming $L/a \gg 1$), the three-dimensional CDR equation of a laminar flow loop reactor is given by

$$\frac{\partial C_j}{\partial t'} + u_{\text{in}}(\xi') \frac{\partial C_j}{\partial x} - v_j R(C_1, C_2, \ldots, C_M) = D_{\text{m},j} \left[\frac{1}{\xi'} \frac{\partial}{\partial \xi'} \left(\xi' \frac{\partial C_j}{\partial \xi'} \right) + \frac{1}{\xi'^2} \frac{\partial^2 C_j}{\partial \varphi^2} \right] \tag{167}$$

with boundary and initial conditions being given by

$$C_j(\xi', \varphi, x = 0) = \frac{C_{j,\text{in}} + \Lambda C_j(\xi', \varphi, x = L)}{1 + \Lambda} \tag{168}$$

$$C_j(\xi', \varphi, x = l^+) = C_j(\xi', \varphi, x = l^-) \tag{169}$$

$$\frac{\partial C_j}{\partial \xi'} = 0 \quad \text{at} \quad \xi' = 1 \tag{170}$$

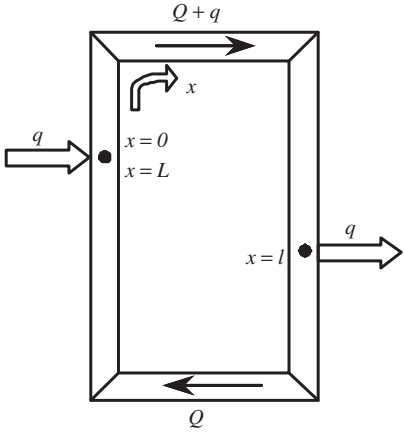

Fig. 10. Schematic diagram of a loop reactor with a single (premixed) feed and product streams.

$$C_j(\xi', \varphi, x) = C_j(\xi', \varphi + 2\pi, x) \tag{171}$$

$$C_j(t' = 0) = C_{j0} \tag{172}$$

Using the spatial averaging procedure illustrated in Section II, we average Eqs. (167)–(171) in the transverse direction to obtain the two-mode model for a loop reactor, which is given by

$$\langle u_{\text{in}} \rangle \frac{\partial C_{j,\text{m}}}{\partial x} = \begin{cases} -\dfrac{1}{1+\Lambda}\left[\dfrac{C_{j,\text{m}} - \langle C_j \rangle}{t_{\text{mix},j}}\right], & 0 \leqslant x < l \\ -\dfrac{1}{\Lambda}\left[\dfrac{C_{j,\text{m}} - \langle C_j \rangle}{t_{\text{mix},j}}\right], & l \leqslant x \leqslant L \end{cases} \tag{173}$$

$$\frac{\partial \langle C_j \rangle}{\partial t'} = \frac{C_{j,\text{m}} - \langle C_j \rangle}{t_{\text{mix},j}} + v_j R(\langle \mathbf{C} \rangle), \quad 0 \leqslant x < L \tag{174}$$

(for $j = 1, 2, \ldots, M$), with the boundary and initial conditions being

$$C_{j,\text{m}}(x = 0) = \frac{C_{j,\text{m,in},} + \Lambda C_{j,\text{m}}(x = L)}{1 + \Lambda} \tag{175}$$

$$\langle C_j \rangle (x = l^-) = \langle C_j \rangle (x = l^+) \tag{176}$$

$$\langle C_j \rangle (t' = 0) = C_{j0} \tag{177}$$

For the special case when no reaction occurs between $x = l$ and $x = L$, i.e. $C_{j,\text{m}}(x = l) = C_{j,\text{m}}(x = L)$, the loop reactor reduces to a recycle reactor of length l, the two-mode model for which is given by

$$\langle u_{\text{in}} \rangle \frac{\partial C_{j,\text{m}}}{\partial x} = -\frac{1}{1+\Lambda}\left[\frac{C_{j,\text{m}} - \langle C_j \rangle}{t_{\text{mix},j}}\right] \tag{178}$$

$$\frac{\partial \langle C_j \rangle}{\partial t'} = \frac{C_{j,\text{m}} - \langle C_j \rangle}{t_{\text{mix},j}} + v_j R(\langle \mathbf{C} \rangle), \quad 0 \leqslant x < l \tag{179}$$

with the boundary condition

$$C_{j,\text{m}}(x = 0) = \frac{C_{j,\text{m,in}} + \Lambda C_{j,\text{m}}(x = l)}{1 + \Lambda} \tag{180}$$

and initial condition being given by Eq. (177).

The two-mode loop and recycle reactor models are two-parameter two-mode models. Here, the two parameters are the recycle ratio Λ, and the dimensionless

local mixing time t_{mix}/τ_c, which describe macro- and micromixing effects in the system, respectively.

C. Tank Reactors (CSTRs)

1. Two-mode Model for Premixed Feed

It is well known that as the recycle ratio Λ of a recycle reactor is increased, the behavior shifts from a PFR at $\Lambda = 0$ (no macromixing) to a CSTR at $\Lambda = \infty$ (perfect macromixing). We use this limit to obtain the two-mode model for a perfectly macromixed CSTR, by integrating Eq. (178) along the length of the reactor x and simplifying the resulting equation for $\Lambda \gg 1$. This gives the two-mode model for a CSTR as

$$\frac{d\langle C_j\rangle}{dt'} = \frac{C_{j,m} - \langle C_j\rangle}{t_{mix,j}} + \nu_j R(\langle \mathbf{C}\rangle), \quad \text{with } \langle C_j\rangle(t' = 0) = C_{j,0} \tag{181}$$

$$\frac{C_{j,m} - \langle C_j\rangle}{t_{mix,j}} = \frac{C_{j,m,in} - C_{j,m}}{\tau_C} \tag{182}$$

where $\tau_C (= V/q_{in})$ is the total residence time in the reactor and t_{mix} is the characteristic local mixing time. Equations (181) and (182) constitute a two-mode one-parameter model for a perfectly macromixed CSTR where feed enters the tank as a single (premixed) stream. Micromixing effects are captured through the local mixing time t_{mix}, and in the limit of complete micromixing (i.e. $t_{mix} \to 0$), it reduces to the ideal one-mode zero-parameter CSTR model.

2. Two-mode Two-mixing Time Model for a General CSTR

In real tanks, both micro- and macromixing effects are important, and are influenced by several factors including the type and speed of impellers, number, and position of baffles, and the manner of feed distribution. Macromixing effects in tanks have often been modeled by using compartment models in the mixing literature (Baldyga and Bourne, 1999). Recently, Bhattacharya *et al.* (2004) used the L–S technique to develop a two-mode two-mixing time CSTR model that in addition to capturing micromixing, accounts for macromixing effects resulting from unmixed feed. Here, we summarize this model for the isothermal case.

Consider a single-phase homogeneous stirred-tank reactor with a time-invariant velocity field $U(x', y', z')$ a single reaction of the form $A \to B$. (This approach can be extended to the case of time-dependent velocity fields. If the flow in the tank is turbulent, then the velocity field is the solution of the Reynolds averaged Navier–Stokes equations). The tank is divided into a three-dimensional network of n spatially fixed volumetric elements, or n-interacting

cells. Theoretically speaking, n can be arbitrarily large but the size of any cell is such that the length scale associated with it is at least one order of magnitude larger than the continuum scale. Here, the continuum scale is the microscale, the length scale of any cell is the mesoscale, and the reactor scale is the macroscale. In practice, the division of the reactor into n cells depends intricately on various design parameters including stirrer and baffle positions, feed distributions, number of circulation zones, etc. Inside each cell, the reactant is transported by diffusion and convection and is consumed by reaction, while interacting with the other cells through the cell boundaries. Depending on the location, the boundary of cell i may be divided into the following types: (i) $\partial\Omega_i^{\text{in}}$ is the boundary through which the reacting fluid enters the tank through cell i with flow rate $q_i^{\text{in}}(C_i^{\text{in}}, T_i^{\text{in}})$, (ii) $\partial\Omega_i^e$ is the boundary through which the reacting fluid leaves the reactor through cell i with flow rate $q_i^e(C_i^e, T_i^e)$, (iii) $\partial\Omega_{ij}^{\text{c}}, j = 1, 2, \ldots, n$ $(j \neq i)$ is the boundary through which cell i interacts with cell j with circulation flow rate $q_{ij}^{\text{c}}(C_{i,\text{m}}^{\text{c}}, T_{i,\text{m}}^{\text{c}})$, (iv) $\partial\Omega_{ji}^{\text{c}}, j = 1, 2, \ldots, n$ $(j \neq i)$ is the boundary through which cell j interacts with cell i with circulation flow rate $q_{ji}^{\text{c}}(C_{j,\text{m}}^{\text{c}}, T_{j,\text{m}}^{\text{c}})$, and (v) $\partial\Omega_i^{\text{b}}$ is the boundary with no mass flux (as shown in Fig. 2), where the quantities in the bracketed terms represent the concentration and temperature of the corresponding streams, respectively. Here, $c_{i,\text{m}}^{\text{c}}(T_{i,\text{m}}^{\text{c}})$ and $c_{j,\text{m}}^{\text{c}}(T_{j,\text{m}}^{\text{c}})$ are the mean cup-mixing concentrations (temperatures) of the circulating stream leaving cell i and j, respectively. [*Remark*: For non-isothermal CSTR with external or internal cooling (or heating), cell i may have boundary $\partial\Omega_i^{\theta}$, through which it exchanges heat with cooling (or heating) fluid $(T_{i,\text{c}})$.] In the first step of the reduction process, the mass and energy balance (CDR) equations in each cell, which describes mixing at the local scale and are infinite-dimensional in nature, are reduced by L–S technique as described in Section II. This is followed by a finite-dimensional reduction on n cells, resulting in the final reduced model for the whole tank containing both micro- as well as macromixing effect (see Bhattacharya *et al.*, 2004, for details). The final reduced model that describes both macro- and micromixing effects in an isothermal CSTR is given by

$$\frac{\mathrm{d}\langle C\rangle}{\mathrm{d}t'} + R(\langle C\rangle) = \frac{1}{\tau_{\text{c}}}(C_{\text{m}}^{\text{in}} - C_{\text{m}}) \tag{183}$$

$$C_{\text{m}} - \langle C\rangle = \frac{1}{\tau_{\text{c}}}(t_{\text{mix},2}\, C_{\text{m}}^{\text{in}} - t_{\text{mix},1}\, C_{\text{m}}) \tag{184}$$

where $t_{\text{mix},1}$ is the overall mixing time of the tank, which depends on the local variables (such as local velocity gradients, local diffusion length, diffusivity) as well as reactor scale variables (such as baffle position, stirrer type, circulation time or stirrer speed, feed pipe locations, etc.), while $t_{\text{mix},2}$ captures the effect of non-uniform feeding. For the case of all feed streams premixed and entering as a

single stream, i.e. uniform feeding:

$$t_{\mathrm{mix},2} = t_{\mathrm{mix},1} = t_{\mathrm{mix}} \tag{185}$$

and Eqs. (183) and (184) reduce to Eqs. (181)–(182). For the general case, both $t_{\mathrm{mix},1}$ and $t_{\mathrm{mix},2}$ have contributions from two terms and can be written as

$$t_{\mathrm{mix},1} = \underbrace{\tau_{\mathrm{d}} v_1}_{\text{micromixing}} + \underbrace{\tau_{\mathrm{E}} v_2}_{\text{macromixing}} = t_{\mathrm{micro},1} + t_{\mathrm{macro},1} \tag{186}$$

$$t_{\mathrm{mix},2} = \underbrace{\tau_{\mathrm{d}} v_3}_{\text{micromixing}} + \underbrace{\tau_{\mathrm{E}} v_4}_{\text{macromixing}} = t_{\mathrm{micro},2} + t_{\mathrm{macro},2} \tag{187}$$

where $\tau_{\mathrm{d}} = l_{\mathrm{d}}^2/D_{\mathrm{e}}$ is the local diffusion time, which is a measure of local scale mixing or micromixing present within the tank and τ_{E} is the exchange or macromixing time of the whole tank. (*Remark*: τ_{E} is inversely proportional to the impeller rpm.) The coefficients v_{i}, $i = 1, 2, 3, 4$, are functions of reactor geometry (including number, design and positions of baffles and stirrers, feed positions, etc.) as well as feed distributions, where the coefficients v_3 and v_4, associated with $t_{\mathrm{mix},2}$, capture the effect of non-uniform or distributed feeding through their additional dependency on feed compositions. For turbulent flow within the tank, the local diffusion length l_{d} depends on kinematic viscosity as well as the power input per unit mass and can be as small as Kolmogorov length scale, while l_{d} for laminar flow is much bigger and can be as large as reactor length scale. On the other hand, the exchange time, which depends on both circulation or exchange flow rate and reactor volume, is in general inversely proportional to the impeller speed. The local diffusion time enters in the expressions for mixing times from the reduction of local CDR equation from micro to meso scale, while the exchange time appears through the second step of reduction from meso scale to reactor scale. The contribution of these two scales of mixing appears in the overall mixing time as a combined function of reactor geometry, feed distribution and composition, etc. and cannot be separated from each other. It should be pointed that the coefficients (v_{i}) can be positive as well as negative.

D. Non-isothermal Reactor Models

In this section, we present the low-dimensional multi-mode models for different types of non-isothermal homogeneous reactors. Here, we skip the details of the averaging process and summarize the results.

1. Tubular Reactors

In obtaining the low-dimensional models for non-isothermal tubular reactors, we start with the full energy balance equations in conjunction with the species balance Eqs. (117)–(119). For the case of a non-isothermal homogeneous reactor the energy balance equations are given by fluid- and solid-state thermal balances which are coupled through the boundary conditions. The fluid temperature $T_f(\xi', \varphi, x, t')$ obeys the following energy balance equation

$$\rho_f C_{pf}\left[\frac{\partial T_f}{\partial t'} + u_x(\xi')\frac{\partial T_f}{\partial x}\right] + (\Delta H_R)R(C_1, C_2, \ldots, C_M, T_f) = k_f\left[\frac{1}{\xi'}\frac{\partial}{\partial \xi'}\left(\xi'\frac{\partial T_f}{\partial \xi'}\right) + \frac{1}{\xi'^2}\frac{\partial^2 T_f}{\partial \varphi^2} + \frac{\partial^2 T_f}{\partial x^2}\right] \tag{188}$$

while the temperature $T_S(\xi', \varphi, x, t')$ in the solid wall (of thickness $a\lambda$) of the channel is given by the equation

$$\rho_f C_{pf}\frac{\partial T_S}{\partial t'} = \nabla_\perp \cdot (k_S \nabla_\perp T_S) + \frac{\partial}{\partial x}\left(k_S\frac{\partial T_S}{\partial x}\right) \tag{189}$$

Equation (188) is subject to the boundary and initial conditions

$$\frac{\partial T_f}{\partial \xi'} = 0 \quad \text{at } \xi' = 0 \tag{190}$$

$$T_f(\xi' = a, \varphi, x, t') = T_S(\xi' = a, \varphi, x, t') \tag{191}$$

$$T_f(\xi', \varphi, x, t') = T_f(\xi', \varphi + 2\pi, x, t') \tag{192}$$

$$\frac{k_f}{\rho_f C_{pf}}\frac{\partial T_f}{\partial x} = u_x(\xi')[T_f(\xi', x) - T_{in}] \text{ at } x = 0; \quad \frac{\partial T_f}{\partial x} = 0 \text{ at } x = L \tag{193}$$

$$T_f(\xi', \varphi, x, t' = 0) = T_{f0} \tag{194}$$

respectively, while the boundary and initial conditions for Eq. (189) describing the solid temperature are

$$-k_S\frac{\partial T_S}{\partial \xi'} = -k_f\frac{\partial T_f}{\partial \xi'} \text{ at } \xi' = a, \qquad -k_S\frac{\partial T_S}{\partial \xi'} = h(T_S - T_C) \quad \text{at } \xi' = a(1+\lambda) \tag{195}$$

$$T_S(\xi', \varphi, x, t') = T_S(\xi', \varphi + 2\pi, x, t') \tag{196}$$

$$\frac{\partial T_S}{\partial x} = 0 \text{ at } x = 0, L \tag{197}$$

$$T_S(\xi', \varphi, x, t' = 0) = T_{S0} \tag{198}$$

respectively, where T_C is the coolant temperature and $a\lambda$ is the thickness of the solid wall. In addition to the dimensionless parameters defined in Eq. (122), we define some new parameters to non-dimensionalize the energy balance equations. These dimensionless parameters are Le_f (fluid Lewis number), St (Stanton number), Bi (Biot number), B (Zeldovich number), γ (dimensionless activation energy), α (coolant capacity), etc., which are given by

$$Le_f = \frac{k_f}{D_{e,R}\rho_f C_{pf}}, \quad St = \frac{2hL}{\rho_f C_{pf} a(1+\lambda)\langle u_x\rangle},$$
$$\alpha = \frac{2hC_R}{\rho_f C_{pf} a(1+\lambda)R(C_R, T_{in})} = \frac{St}{Da}$$

$$Bi = \frac{2ah}{k_f(1+\lambda)} = \frac{p}{Le_f} St, \quad \gamma = \frac{E}{RT_{in}}, \quad \frac{\lambda_f}{\lambda_S} = \frac{k_f}{k_S}\left(\frac{\rho_S C_{pS}}{\rho_f C_{pf}}\right) \tag{199}$$

$$\kappa = \frac{k_f}{k_S}, \quad \sigma_{sf} = \frac{\rho_S C_{pS}}{\rho_f C_{pf}}, \quad Pe_S = \frac{\langle u_x\rangle L \rho_f C_{pf}}{k_S} = \frac{p}{\kappa Le_f Pe_r^2}, \quad B = \frac{\gamma(-\Delta H_R)C_R}{\rho_f C_{pf} T_{in}}$$

The dimensionless temperature variables for the fluid and solid phases (θ_f and θ_S) and the dimensionless reaction rate ($r(\boldsymbol{c}, \theta_f)$) are given by

$$\theta_f = \gamma\frac{T_f - T_{in}}{T_{in}}, \quad \theta_S = \gamma\frac{T_S - T_{in}}{T_{in}}, \quad r(\boldsymbol{c}, \theta_f) = \frac{R(C_1, C_2, \ldots, C_M, T_f)}{R(C_R, T_{in})} \tag{200}$$

Using the above dimensionless parameters and variables, Eqs. (188)–(198) are written in dimensionless form and spatially averaged over transverse dimensions to obtain the low-dimensional model for non-isothermal homogeneous tubular reactors, which is given to order p by Eqs. (130)–(134) with $r(\langle c\rangle)$ being replaced by $r(\langle c\rangle, \langle\theta_f\rangle)$ and

$$\varepsilon\frac{\partial\langle\theta_f\rangle}{\partial t} + \sigma_{sf}(1-\varepsilon)\frac{\partial\langle\theta_S\rangle}{\partial t} + \varepsilon\frac{\partial\theta_{fm}}{\partial z} = \left(\begin{array}{l} \dfrac{p}{Pe_r^2 Le_f}\left\{\varepsilon\dfrac{\partial^2\langle\theta_f\rangle}{\partial z^2} + \left(\dfrac{1-\varepsilon}{\kappa}\right)\dfrac{\partial^2\langle\theta_S\rangle}{\partial z^2}\right\} \\ +\varepsilon BDa\, r(\langle c\rangle, \langle\theta_f\rangle) - St(\langle\theta_S\rangle - \theta_C) \end{array}\right) \tag{201}$$

$$\frac{\theta_{fm} - \langle\theta_f\rangle}{\eta_H} = -\frac{\partial\theta_{fm}}{\partial z} + \beta_2\frac{1}{\varepsilon}\left[\sigma_{sf}(1-\varepsilon)\frac{\partial\langle\theta_S\rangle}{\partial t} + St(\langle\theta_S\rangle - \theta_C)\right] \tag{202}$$

$$\frac{\langle\theta_S\rangle - \langle\theta_f\rangle}{\eta_H} = \beta_3 \frac{\partial\theta_{fm}}{\partial z} - \frac{\beta_4}{\beta_1}\frac{1}{\varepsilon}\left[\sigma_{sf}(1-\varepsilon)\frac{\partial\langle\theta_S\rangle}{\partial t} + St(\langle\theta_S\rangle - \theta_C)\right] \tag{203}$$

with the boundary and initial conditions being given by

$$\frac{p}{Le_f Pe_r^2}\frac{\partial\langle\theta_f\rangle}{\partial z} = \theta_{fm} - \theta_{fm,in}, \text{ at } z = 0; \quad \frac{\partial\theta_{fm}}{\partial z} = 0 \text{ at } z = 1,$$
$$\frac{\partial\langle\theta_S\rangle}{\partial z} = 0, \text{ at } z = 0, 1 \tag{204}$$

$$\langle\theta_f\rangle = \langle\theta_{f0}\rangle, \quad \text{and } \langle\theta_S\rangle = \langle\theta_{S0}\rangle \quad \text{at } t = 0 \tag{205}$$

where, ε is the volume fraction of the fluid phase in the system, $\langle\theta_f\rangle$ and $\langle\theta_S\rangle$ are the transverse averaged temperatures of the fluid- and solid phases, respectively, and θ_{fm} is the mixing-cup temperature of the fluid phase, which are given by

$$\varepsilon = -\frac{1}{(1+\lambda)^2} \tag{206}$$

$$\langle\theta_f\rangle = \frac{\int_{\xi=0}^{\xi=1}\int_{\varphi=0}^{\varphi=2\pi}\xi\theta_f(\xi,\varphi,z,t)\,d\varphi\,d\xi}{\int_{\xi=0}^{\xi=1}\int_{\varphi=0}^{\varphi=2\pi}\xi\,d\varphi\,d\xi} \tag{207}$$

$$\theta_{fm} = \frac{\int_{\xi=0}^{\xi=1}\int_{\varphi=0}^{\varphi=2\pi}\xi u(\xi)\theta_f\,d\varphi\,d\xi}{\int_{\xi=0}^{\xi=1}\int_{\varphi=0}^{\varphi=2\pi}\xi u(\xi)\,d\varphi\,d\xi} = \langle\theta_f\rangle + \langle u'\theta_f'\rangle \tag{208}$$

$$\langle\theta_S\rangle = \frac{\int_{\xi=1}^{\xi=1+\lambda}\int_{\varphi=0}^{\varphi=2\pi}\xi\theta_S(\xi,\varphi,z,t)\,d\varphi\,d\xi}{\int_{\xi=1}^{\xi=1+\lambda}\int_{\varphi=0}^{\varphi=2\pi}\xi\,d\varphi\,d\xi} \tag{209}$$

In Eqs. (202)–(203), η_H is the characteristic dimensionless local thermal mixing time, which is given by

$$\eta_H = \frac{t_{mix,H}}{\tau_C} = \beta_1\frac{a^2/\lambda_f}{\tau_C} = \beta_1\frac{p}{Le_f} \tag{210}$$

The coefficients β_1, β_2, and β_3 depend on the flow profile and the local shear rates of the system, and β_4 depends on the reactor geometry and for a tubular geometry,

$$\beta_4 = \tfrac{1}{8} \tag{211}$$

For the case of laminar flow in a tube,

$$\beta_1 = \tfrac{1}{48} \tag{212}$$

$$\beta_2 = 2 \tag{213}$$

$$\beta_3 = 2 \tag{214}$$

while for the case of fully-developed turbulent flows in tubes,

$$\beta_1 = 0.1 f_t(\omega - 3.45) \tag{215}$$

$$\beta_2 = \frac{1.41}{\sqrt{f_t}(\omega - 3.45)} \tag{216}$$

$$\beta_3 = \frac{0.89}{\sqrt{f_t}}\left(1 - \frac{1.55}{\omega - 3.45}\right) \tag{217}$$

where ω is given by Eq. (163).

In the above model [Eqs. (201)–(203)], thermal micromixing is captured through the dimensionless local thermal mixing times of the system, η_{H}, as an exchange of energy between the two temperature modes $\theta_{\mathrm{f,m}}$ and $\langle\theta_{\mathrm{f}}\rangle$ by the local equation (202). The other local equation [Eq. (203)] captures the energy transfer between the fluid- and solid phases as an exchange between the average fluid ($\langle\theta_{\mathrm{f}}\rangle$) and solid ($\langle\theta_{\mathrm{S}}\rangle$) temperatures. It should also be pointed out that our low-dimensional model retains all the parameters ($p, Pe_{\mathrm{r}}, Le_{\mathrm{f}}, B, Da, St, \kappa, \sigma_{\mathrm{sf}}$) present in the full CDR model, and in the limit of complete mass and thermal micromixing ($\eta \to 0$, $\eta_{\mathrm{H}} \to 0$), our model reduces to the plug-flow model for tubular reactors with wall cooling.

Low-dimensional models for loop, recycle, and tank reactors could similarly be derived starting from the coupled mass and thermal balances. Here, we present the reduced models and refer to a previous publication (Chakraborty and Balakotaiah, 2004) for the derivation of these models.

2. *Loop and Recycle Reactors*

a. Loop reactors. The low-dimensional model for non-isothermal homogeneous loop reactor (as shown in Fig. 10) is given by

$$\frac{\partial\langle c_j\rangle}{\partial t} = \frac{c_{j,\mathrm{m}} - \langle c_j\rangle}{\eta\kappa_j} + v_j Da\, r(\langle\mathbf{c}\rangle, \langle\theta_{\mathrm{f}}\rangle), \quad 0 < z < 1 \tag{218}$$

$$\frac{\partial c_{j,\mathrm{m}}}{\partial z} = \begin{cases} -\dfrac{1}{1+\Lambda}\left[\dfrac{c_{j,\mathrm{m}} - \langle c_j\rangle}{\eta\kappa_j}\right], & 0<z<\hat{l}, \text{ where } \hat{l} = \dfrac{l}{L} \\ -\dfrac{1}{\Lambda}\left[\dfrac{c_{j,\mathrm{m}} - \langle c_j\rangle}{\eta\kappa_j}\right], & \hat{l}<z<1 \end{cases} \qquad (j = 1, 2, \ldots, M) \tag{219}$$

$$\frac{\partial\langle\theta_\mathrm{f}\rangle}{\partial t} = \zeta\left[\left(\beta_3 + \frac{\beta_4}{\beta_1}\right)\frac{\theta_\mathrm{fm} - \langle\theta_\mathrm{f}\rangle}{\eta_\mathrm{H}} + (1+\beta_2)\frac{\langle\theta_\mathrm{S}\rangle - \langle\theta_\mathrm{f}\rangle}{\eta_\mathrm{H}}\right] + BDa\, r(\langle\mathbf{c}\rangle, \langle\theta_\mathrm{f}\rangle), \quad 0<z<1 \tag{220}$$

$$\frac{\partial\theta_\mathrm{fm}}{\partial z} = \begin{cases} -\dfrac{\zeta}{1+\Lambda}\left[\dfrac{\beta_4}{\beta_1}\dfrac{\theta_\mathrm{fm} - \langle\theta_\mathrm{f}\rangle}{\eta_\mathrm{H}} + \beta_2\dfrac{\langle\theta_\mathrm{S}\rangle - \langle\theta_\mathrm{f}\rangle}{\eta_\mathrm{H}}\right], & 0<z<\hat{l} \\ -\dfrac{\zeta}{\Lambda}\left[\dfrac{\beta_4}{\beta_1}\dfrac{\theta_\mathrm{fm} - \langle\theta_\mathrm{f}\rangle}{\eta_\mathrm{H}} + \beta_2\dfrac{\langle\theta_\mathrm{S}\rangle - \langle\theta_\mathrm{f}\rangle}{\eta_\mathrm{H}}\right], & \hat{l}<z<1 \end{cases} \tag{221}$$

for the fluid-phase mass and thermal balances, respectively, with boundary and initial conditions being given by

$$c_{j,\mathrm{m}}|_{z=0} = \frac{c_{j,\mathrm{m,in}} + \Lambda c_{j,\mathrm{m}}|_{z=1}}{1+\Lambda}; \quad \langle c_j\rangle|_{z=\hat{l}^-} = \langle c_j\rangle|_{z=\hat{l}^+} \tag{222}$$

$$\langle c_j\rangle = c_{j,0} \quad \text{at } t = 0 \tag{223}$$

$$\theta_\mathrm{fm}|_{z=0} = \frac{\theta_\mathrm{fm,in} + \Lambda\theta_\mathrm{fm}|_{z=1}}{1+\Lambda}; \quad \langle\theta_\mathrm{f}\rangle|_{z=\hat{l}^-} = \langle\theta_\mathrm{f}\rangle|_{z=\hat{l}^+} \tag{224}$$

$$\langle\theta_\mathrm{f}\rangle = \theta_{\mathrm{f}0} \quad \text{at } t = 0 \tag{225}$$

The solid-phase thermal balance is given by

$$\sigma_\mathrm{sf}(1-\varepsilon)\frac{\partial\langle\theta_\mathrm{S}\rangle}{\partial t} = -\zeta\varepsilon\left[\beta_3\frac{\theta_\mathrm{fm} - \langle\theta_\mathrm{f}\rangle}{\eta_\mathrm{H}} + \frac{\langle\theta_\mathrm{S}\rangle - \langle\theta_\mathrm{f}\rangle}{\eta_\mathrm{H}}\right] - St(\langle\theta_\mathrm{S}\rangle - \theta_\mathrm{C}) \tag{226}$$

for $0 \leqslant z \leqslant 1$, with the initial condition being given by $\langle\theta_\mathrm{S}\rangle = \theta_{\mathrm{S}0}$ at $t = 0$, and where $\zeta = \beta_1/(\beta_4 - \beta_1\beta_2\beta_3)$.

b. Recycle reactors. For the special case when no reaction occurs between $z = \hat{l}$ and $z = 1$, i.e. $c_{j,\mathrm{m}}|_{z=\hat{l}} = c_{j,\mathrm{m}}|_{z=1}$, the loop reactor reduces to a recycle reactor ($0<z<1$), the low-dimensional model for which is given by

$$\frac{\partial\langle c_j\rangle}{\partial t} = \frac{c_{j,\mathrm{m}} - \langle c_j\rangle}{\eta\kappa_j} + v_j Da\, r(\langle\mathbf{c}\rangle, \langle\theta_\mathrm{f}\rangle) \tag{227}$$

$$\frac{\partial c_{j,\mathrm{m}}}{\partial z} = -\frac{1}{1+\Lambda}\left[\frac{c_{j,\mathrm{m}} - \langle c_j\rangle}{\eta\kappa_j}\right] \tag{228}$$

$$\frac{\partial\langle\theta_\mathrm{f}\rangle}{\partial t} = \zeta\left[\left(\beta_3 + \frac{\beta_4}{\beta_1}\right)\frac{\theta_\mathrm{fm} - \langle\theta_\mathrm{f}\rangle}{\eta_\mathrm{H}} + (1+\beta_2)\frac{\langle\theta_\mathrm{S}\rangle - \langle\theta_\mathrm{f}\rangle}{\eta_\mathrm{H}}\right] + BDa\, r(\langle c\rangle, \langle\theta_\mathrm{f}\rangle) \tag{229}$$

$$\frac{\partial\theta_\mathrm{fm}}{\partial z} = -\frac{\zeta}{1+\Lambda}\left[\frac{\beta_4}{\beta_1}\frac{\theta_\mathrm{fm} - \langle\theta_\mathrm{f}\rangle}{\eta_\mathrm{H}} + \beta_2\frac{\langle\theta_\mathrm{S}\rangle - \langle\theta_\mathrm{f}\rangle}{\eta_\mathrm{H}}\right] \tag{230}$$

with boundary conditions given by

$$c_{j,\mathrm{m}}|_{z=0} = \frac{c_{j,\mathrm{m,in}} + \Lambda c_{j,\mathrm{m}}|_{z=1}}{1+\Lambda} \tag{231}$$

$$\theta_\mathrm{fm}|_{z=0} = \frac{\theta_\mathrm{fm,in} + \Lambda\theta_\mathrm{fm}|_{z=1}}{1+\Lambda} \tag{232}$$

The solid-phase balance [Eq. (226)] with accompanying boundary and initial conditions remain unaltered.

3. Tank Reactors

The low-dimensional model for a non-isothermal homogeneous tank reactor with premixed feed is given by

$$\frac{\mathrm{d}\langle c_j\rangle}{\mathrm{d}t} + (c_{j,\mathrm{m}} - c_{j,\mathrm{m,in}}) = \nu_j Da\, r(\langle\boldsymbol{c}\rangle, \langle\theta_\mathrm{f}\rangle) \tag{233}$$

$$c_{j,\mathrm{m}} - c_{j,\mathrm{m,in}} = \frac{\langle c\rangle - c_{j,\mathrm{m}}}{\eta\kappa_j} \tag{234}$$

as the fluid-phase species balance equation,

$$\frac{\mathrm{d}\langle\theta_\mathrm{f}\rangle}{\mathrm{d}t} = \zeta\left[\left(\beta_3 + \frac{\beta_4}{\beta_1}\right)\frac{\theta_\mathrm{fm} - \langle\theta_\mathrm{f}\rangle}{\eta_\mathrm{H}} + (1+\beta_2)\frac{\langle\theta_\mathrm{S}\rangle - \langle\theta_\mathrm{f}\rangle}{\eta_\mathrm{H}}\right] + BDa\, r(\langle\boldsymbol{c}\rangle, \langle\theta_\mathrm{f}\rangle) \tag{235}$$

$$\langle\theta_\mathrm{f}\rangle = -\zeta\left[\frac{\beta_4}{\beta_1}\frac{\theta_\mathrm{fm} - \langle\theta_\mathrm{f}\rangle}{\eta_\mathrm{H}} + \beta_2\frac{\langle\theta_\mathrm{S}\rangle - \langle\theta_\mathrm{f}\rangle}{\eta_\mathrm{H}}\right] \tag{236}$$

as the fluid-phase thermal balance equation, and

$$\sigma_\mathrm{sf}(1-\varepsilon)\frac{\mathrm{d}\langle\theta_\mathrm{S}\rangle}{\mathrm{d}t} = -\zeta\varepsilon\left[\beta_3\frac{\theta_\mathrm{fm} - \langle\theta_\mathrm{f}\rangle}{\eta_\mathrm{H}} + \frac{\langle\theta_\mathrm{S}\rangle - \langle\theta_\mathrm{f}\rangle}{\eta_\mathrm{H}}\right] - St(\langle\theta_\mathrm{S}\rangle - \theta_\mathrm{C}) \tag{237}$$

as the solid-phase thermal balance, where $\zeta = \beta_1/(\beta_4 - \beta_1\beta_2\beta_3)$, and the initial

conditions are given by $\langle c\rangle = c_0$, $\langle\theta_f\rangle = \theta_{f0}$, and $\langle\theta_S\rangle = \theta_{S0}$ at $t = 0$. The β_j's and ζ are the five independent constants that could be obtained for each tank depending on the local flow profile and the shape of the tank.

For the special case of a simple reaction A $\rightarrow$ B, the low-dimensional model for a CSTR with premixed feed consists of three differential equations and two algebraic equations. When the mass and thermal micromixing effects are ignored ($\eta = \eta_H = 0$), $c_m = \langle c\rangle$, $\langle\theta_f\rangle = \theta_{fm} = \langle\theta_S\rangle$, and we get the classical pseudohomogeneous CSTR model

$$\frac{d\langle c\rangle}{dt} = (c_{in} - \langle c\rangle) - Da\, r(\langle c\rangle, \langle\theta_f\rangle) \tag{238}$$

$$Le^* \frac{d\langle\theta_f\rangle}{dt} = \langle\theta_{f,in}\rangle - \langle\theta_f\rangle + BDa\, r(\langle c\rangle, \langle\theta_f\rangle) - \frac{St}{\varepsilon}(\langle\theta_f\rangle - \theta_C) \tag{239}$$

where

$$Le^* = 1 + \frac{1-\varepsilon}{\varepsilon}\sigma_{sf} \tag{240}$$

E. Multiple Reactions

Here, we extend the low-dimensional models derived for the case of a single reaction to the case of multiple homogeneous reactions represented by

$$\sum_{j=1}^{M} \nu_{ij} A_j = 0, \quad i = 1, 2, \ldots, N_H \tag{241}$$

involving M species in N_H homogeneous reactions occurring in a constant density system, in which the species obey the laws of binary diffusion. We use the usual convention of $\nu_{ij} > 0$ if A_j is a product and $\nu_{ij} < 0$ if A_j is a reactant. Here, we use the same notations as in the single reaction case, with the exception of Da_i (Damköhler number), B_i (Zeldovich number), and r_i (reaction rate) of the ith reaction, which are defined as

$$Da_i = \frac{LR_i(C_R, T_{in})}{\langle u_x\rangle C_R}, \quad B_i = \frac{\gamma_i(-\Delta H_R)_i C_R}{\rho_f C_{pf} T_{in}}, \quad r_i(\langle\mathbf{c}\rangle, \theta_f) = \frac{R_i(C_1, C_2, \ldots, C_M, T_f)}{R_i(C_R, T_{in})}$$

where $R_i(C_1, C_2, \ldots, C_M, T_f)$ is the intrinsic rate of the ith reaction, and γ_i and $(\Delta H_R)_i$ are the dimensionless activation energy and the heat of reaction of the ith reaction, respectively.

The low-dimensional models obtained for the case of multiple reactions are the same as that obtained for the case of the single reactions in the previous examples, with the term $v_j r(\langle c\rangle, \langle\theta_f\rangle)$ in the species balance equation for the jth species being replaced by $\sum_{i=1}^{N_H} v_{ij} r_i(\langle \mathbf{c}\rangle, \langle\theta_f\rangle)$, and the term $BDa\, r(\langle \mathbf{c}\rangle, \langle\theta_f\rangle)$ in the energy balance equation being replaced by $\sum_{i=1}^{N_H} B_i Da_i r_i(\langle \mathbf{c}\rangle, \langle\theta_f\rangle)$. For example, the steady state averaged model for a tubular reactor with negligible axial dispersion ($Pe_r \gg 1$) in which multiple reactions [given by Eq. (241)] occur, is given by the following global equations:

$$\frac{dc_{j,m}}{dz} = \sum_{i=1}^{N_H} v_{ij} Da_i r_i(\langle \mathbf{c}\rangle, \langle\theta_f\rangle) \tag{242}$$

$$\frac{d\theta_{fm}}{dz} = \sum_{i=1}^{N_H} B_i Da_i r_i(\langle \mathbf{c}\rangle, \langle\theta_f\rangle) - \frac{St}{\varepsilon}(\langle\theta_S\rangle - \theta_C) \tag{243}$$

while the local equations are given by

$$\frac{\langle c_j\rangle - c_{j,m}}{\eta\kappa_j} = -\frac{dc_{j,m}}{dz} \tag{244}$$

$$\frac{\theta_{fm} - \langle\theta_f\rangle}{\eta_H} = -\frac{d\theta_{fm}}{dz} + \beta_2 \frac{St(\langle\theta_S\rangle - \theta_C)}{\varepsilon} \tag{245}$$

$$\frac{\langle\theta_S\rangle - \langle\theta_f\rangle}{\eta_H} = \beta_3 \frac{d\theta_{fm}}{dz} - \frac{\beta_4}{\beta_1}\frac{St(\langle\theta_S\rangle - \theta_C)}{\varepsilon} \tag{246}$$

with $c_{j,m}|_{z=0} = c_{j,m,in}$, and $\theta_{fm}|_{z=0} = \theta_{fm,in}$. The low-dimensional models for other types of homogeneous reactors for the multiple reaction case are similarly obtained.

F. Examples Illustrating Use of Multi-mode Homogeneous Reactor Models

In this section, we present examples to illustrate the usefulness of multi-mode homogeneous reactor models in predicting micromixing effects on yield and selectivity, reactor runaway, etc.

1. Single Bimolecular Reaction in a Tubular Reactor: Mixing Effects on Conversion

Here, we consider the case of a bimolecular reaction of the type $A + B \xrightarrow{k}$ Products, with $R(\langle C_A\rangle, \langle C_B\rangle) = k\langle C_A\rangle\langle C_B\rangle$, for the case of premixed feed as well as unmixed feed.

a. Premixed feed. Our two-mode model equations are given by

$$\frac{\mathrm{d}C_{A,\mathrm{m}}}{\mathrm{d}z} = -\frac{Da}{C_{A,\mathrm{in}}}\langle C_A\rangle\langle C_B\rangle \tag{247}$$

$$\frac{\mathrm{d}C_{B,\mathrm{m}}}{\mathrm{d}z} = -\frac{Da}{C_{A,\mathrm{in}}}\langle C_A\rangle\langle C_B\rangle \tag{248}$$

$$C_{A,\mathrm{m}} - \langle C_A\rangle = \eta_A \frac{Da}{C_{A,\mathrm{in}}}\langle C_A\rangle\langle C_B\rangle \tag{249}$$

$$C_{B,\mathrm{m}} - \langle C_B\rangle = \eta_B \frac{Da}{C_{A,\mathrm{in}}}\langle C_A\rangle\langle C_B\rangle \tag{250}$$

with the boundary conditions $C_{A,\mathrm{m}} = C_{B,\mathrm{m}} = C_{A,\mathrm{in}}$ at $z = 0$ (i.e. for the case of uniform and stoichiometric feeding of reactants). In the above Eqs. (247)–(250), η_A and η_B are the dimensionless mixing times of A and B, respectively, given by $\eta_A = t_{A,\mathrm{mix}}/\tau_\mathrm{C}$, $\eta_B = t_{B,\mathrm{mix}}/\tau_\mathrm{C}$, where $\tau_\mathrm{C}(= L/\langle u_x\rangle)$ is the total residence time in the reactor, $t_{A,\mathrm{mix}} = \beta_1 a^2/D_{A\mathrm{m}}$ and $t_{B,\mathrm{mix}} = \beta_1 a^2/D_{B\mathrm{m}}$, and the Damköhler number $Da = kC_{A,\mathrm{in}}\tau_\mathrm{C}$.

We first analyze the case where the mixing times of A and B are equal, i.e. $\eta_A = \eta_B = \eta$. Figure 11 illustrates how the conversion $X(= 1 - C_{A,\mathrm{m}}(z = 0)/C_{A,\mathrm{m,in}})$ varies with the Damköhler number Da for different values of the dimensionless mixing time η, for the case of stoichiometric feeding of reactants.

In order to examine the effects of differences in mixing times on conversion, we solve Eqs. (247)–(250) for a wide range of values of κ, where $\kappa = \eta_A/\eta_B(= D_{B\mathrm{m}}/D_{A\mathrm{m}})$ is the ratio of the mixing times of A and B. The results, which have been plotted in Fig. 12, enable us to capture solely the effects of differences in transport properties (i.e. species diffusivities) on product formation. It may be noted from Fig. 12, that conversion attains a maximum at $\kappa = 1$ because for the case of premixed feed, the two species A and B are interchangeable and the curves are therefore symmetric about $\kappa = 1$.

b. Unmixed feed. In this example, we show how the two-mode models, unlike the traditional tubular reactor models, can capture the effects of non-uniform reactant feeding on reactor performance.

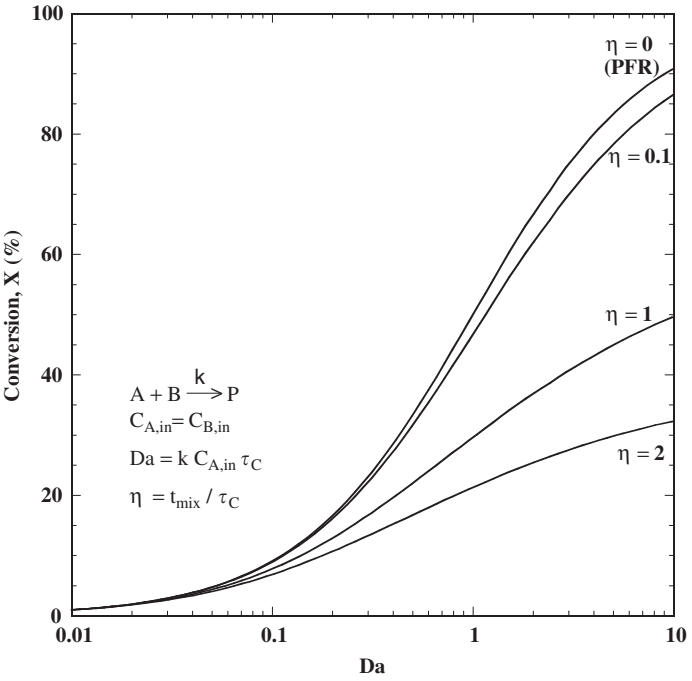

FIG. 11. Plot of conversion vs. *Da* for a bimolecular second-order reaction in a tubular reactor, for different values of the dimensionless mixing time η.

In order to capture the effects of non-uniform reactant feeding at the reactor entrance, we rederive our two-mode models by introducing a delta function source in the species balance equation for the *j*th species [Eq. (123)]

$$\frac{1}{\xi'}\frac{\partial}{\partial \xi'}\left(D_{\mathrm{m},j}\xi'\frac{\partial C_j}{\partial \xi'}\right) + \nu_j R(\mathbf{C}) = \frac{\partial C_j}{\partial t} + u_x(\xi')\frac{\partial C_j}{\partial x} - u_x(\xi')C_{j,\mathrm{in}}(\xi')\delta(x) \tag{251}$$

with boundary conditions given by

$$\frac{\partial C_j}{\partial \xi'} = 0 \quad \text{at } \xi' = 0, a \tag{252}$$

$$C_j(\xi', x) = 0 \quad \text{at } x = 0 \tag{253}$$

Transverse averaging of Eqs. (251)–(253) leads to the following global evolution and local equations, respectively:

$$\frac{\partial \langle C_j \rangle}{\partial t} + \langle u_x \rangle \frac{\partial C_{j,\mathrm{m}}}{\partial x} = -R(\langle \mathbf{C} \rangle) + C_{j,\mathrm{m,in}}\delta(x) \tag{254}$$

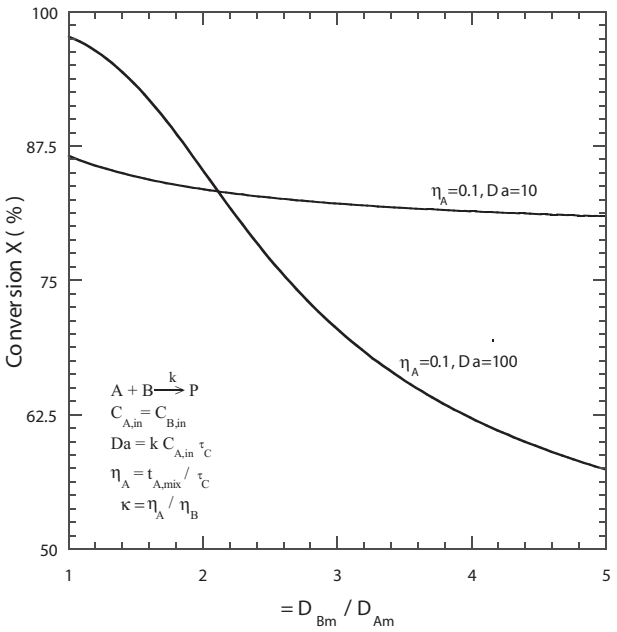

FIG. 12. Influence of the difference in local mixing times of species A and B on conversion in a second-order bimolecular reaction in a tubular reactor.

$$\langle C_j \rangle - C_{j,\mathrm{m}} = t_{\mathrm{mix},j} \left[\langle u_x \rangle \frac{\partial C_{j,\mathrm{m}}}{\partial x} - \chi_{1,j} \delta(x) \right] \tag{255}$$

where

$$C_{j,\mathrm{m,in}} = \langle u_x(\xi') C_{j,\mathrm{in}}(\xi') \rangle / \langle u_x \rangle \tag{256}$$

$$\chi_{1,j} = \langle u_x(\xi') f_j(\xi') \rangle / (\beta_1 \langle u_x \rangle) \tag{257}$$

$$f_j(\xi') = \int_0^{\xi'} \frac{1}{\kappa} \int_0^{\kappa} \zeta u(\zeta) J_j(\zeta)\, \mathrm{d}\zeta\, \mathrm{d}\kappa - \left\langle \int_0^{\xi'} \frac{1}{\kappa} \int_0^{\kappa} \zeta u(\zeta) J_j(\zeta)\, \mathrm{d}\zeta\, \mathrm{d}\kappa \right\rangle \tag{258}$$

$$J_j(\xi') = C_{j,\mathrm{m,in}} - C_{j,\mathrm{in}}(\xi')$$

In order to illustrate how this formulation can capture mixing effects resulting from non-uniform reactant feeding at the reactor inlet, we apply the steady-state version of our model [Eqs. (254)–(258)] to the simple case of bimolecular

second-order reaction of the type $A + B \xrightarrow{k}$ Products, with $R(\langle C_A\rangle, \langle C_B\rangle) = k\langle C_A\rangle\langle C_B\rangle$, where the reactants are fed as

$$C_{A,\mathrm{in}}(\xi') = 2\left(\frac{\xi'}{a}\right)^2 \langle C_{\mathrm{in}}\rangle$$

$$C_{B,\mathrm{in}}(\xi') = 2\left[1 - \left(\frac{\xi'}{a}\right)^2\right] \langle C_{\mathrm{in}}\rangle$$

such that $\langle C_{A,\mathrm{in}}(\xi)\rangle = \langle C_{B,\mathrm{in}}(\xi)\rangle = \langle C_{\mathrm{in}}\rangle$ but $C_{A,\mathrm{m,in}} \neq C_{B,\mathrm{m,in}}$. Here $C_{A,\mathrm{m,in}} = \frac{2}{3}\langle C_{\mathrm{in}}\rangle$, $C_{B,\mathrm{m,in}} = \frac{4}{3}\langle C_{\mathrm{in}}\rangle$, $\chi_{1,A} = -\frac{1}{60}\langle C_{\mathrm{in}}\rangle$, and $\chi_{1,B} = \frac{1}{60}\langle C_{\mathrm{in}}\rangle$.

Figure 13 shows how the steady-state exit conversion $X[= 1 - C_{B,\mathrm{m}}(z = 1)/C_{B,\mathrm{m,in}}]$ varies with the Damköhler number Da for different values of the dimensionless mixing time $\eta(= t_{\mathrm{mix}}/\tau)$. The figure shows how non-uniform feeding could significantly reduce the conversion as compared to premixed feed for the case of a bimolecular second-order reaction (e.g. by a factor of 2 for the case of $\eta = 0.1$), when mixing limitations are present in the system.

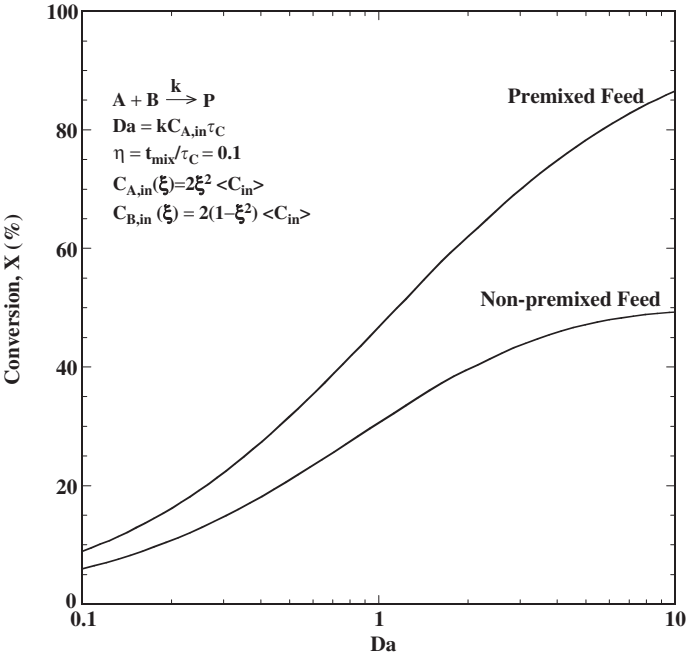

FIG. 13. Comparison of conversion for a bimolecular second-order reaction in a homogeneous tubular reactor for premixed and unmixed reactant feeding.

2. Single Non-isothermal Reaction in a Tubular Reactor: Mixing Effects on Multiplicity Features

It is well known that a tubular reactor model with no macromixing (i.e. $Pe_r \gg 1$) and perfect micromixing ($\eta = 0$) exhibits no multiple solutions, even in the presence of autocatalytic (e.g. non-isothermal) kinetics. However, even in the presence of small micromixing limitations (i.e. $\eta > 0$), the reaction–diffusion problem at the local scale starts generating multiple solutions (if the kinetics is autocatalytic), leading to multiplicity in the solution of the full CDR equation at the global scale. While this feature could be captured by the full CDR equations, it is completely missed by the traditional low-dimensional models, such as the plug-flow model.

The multi-mode model for a tubular reactor, even in its simplest form (steady state, $Pe_r \gg 1$), is an index–infinity differential algebraic system. The local equation of the multi-mode model, which captures the reaction–diffusion phenomena at the local scale, is algebraic in nature, and produces multiple solutions in the presence of autocatalysis, which, in turn, generates multiplicity in the solution of the global evolution equation. We illustrate this feature of the multi-mode models by considering the example of an adiabatic ($\alpha = 0$) tubular reactor under steady-state operation. We consider the simple case of a non-isothermal first order reaction

$$\mathrm{A} \xrightarrow{k} \text{Products}$$

with Arrhenius kinetics, where the rate of consumption of A, $r(\langle c\rangle$, and $\langle\theta_f\rangle)$ is given by

$$r(\langle c\rangle, \langle\theta_f\rangle) = \langle c\rangle \exp\left[\frac{\langle\theta_f\rangle}{1 + \langle\theta_f\rangle/\gamma}\right] \tag{259}$$

and the multi-mode model is given by

$$\frac{\mathrm{d}c_m}{\mathrm{d}Da} = -\langle c\rangle \exp\left[\frac{\langle\theta_f\rangle}{1 + \langle\theta_f\rangle/\gamma}\right] \tag{260}$$

$$c_m - \langle c\rangle = Da_{loc}\langle c\rangle \exp\left[\frac{\langle\theta_f\rangle}{1 + \langle\theta_f\rangle/\gamma}\right] \tag{261}$$

$$\frac{\mathrm{d}\theta_{fm}}{\mathrm{d}Da} = B\langle c\rangle \exp\left[\frac{\langle\theta_f\rangle}{1 + \langle\theta_f\rangle/\gamma}\right] \tag{262}$$

$$\theta_{fm} - \langle\theta_f\rangle = -Da_{loc}\frac{B}{Le_f}\langle c\rangle \exp\left[\frac{\langle\theta_f\rangle}{1 + \langle\theta_f\rangle/\gamma}\right] \tag{263}$$

with the initial conditions $c_m = 1$ and $\theta_{fm} = 0$ at $Da = 0$, where Da_{loc} is the local Damköhler number, given by

$$Da_{loc} = \frac{t_{mix}}{t_R} = kt_{mix} = \eta Da$$

and B is the Zeldovich number (dimensionless adiabatic temperature rise).

Equations (260)–(263) form a set of differential-algebraic equations which has a unique solution when the two algebraic equations [(261) and (263)] themselves have unique solution of $\langle c \rangle$ (and $\langle \theta_f \rangle$) for any fixed c_m (and θ_{fm}). Equivalently, the above system has multiple solutions only when Eqs. (261) and (263) evaluated at the reactor exit conditions begin to have multiple solutions. For $Le_f \geqslant 1$ (typical fluid Lewis numbers vary between 1 and 100), and for $\gamma \to \infty$, the hysteresis variety for the above set of equations is given by

$$F = \frac{\partial F}{\partial \langle \theta_f \rangle} = \frac{\partial^2 F}{\partial \langle \theta_f \rangle^2} = 0 \tag{264}$$

where

$$F = \langle \theta_f \rangle - \theta_{fm} - \frac{Da_{loc}}{Le_f} \frac{(B - \theta_{fm}) \exp(\langle \theta_f \rangle)}{1 + Da_{loc} \exp(\langle \theta_f \rangle)} \tag{265}$$

Solving Eq. (264), the hysteresis locus is obtained in parametric form as

$$\theta_{fm,exit} = \frac{(4 - s) \exp[s - 2] - s}{1 + \left(1 - \frac{1}{Le_f}\right) \exp[s - 2]}, \quad -\infty < s < 2 \tag{266}$$

$$\langle \theta_f \rangle_{exit} = \theta_{fm,exit} + 2 \tag{267}$$

$$B = \theta_{fm,exit} + 4Le_f \tag{268}$$

$$Da_{loc} = \eta Da = \exp[-2 - \theta_{fm,exit}] \tag{269}$$

$$Da = \int_{s + \theta_{fm,exit}}^{2 + \theta_{fm,exit}} \frac{\exp[-y] - (3 + \theta_{fm,exit} - y) \exp[-2 - \theta_{fm,exit}]}{[4Le_f + \theta_{fm,exit} - y]} \, dy \tag{270}$$

For very small values of the micromixing time, η and for $Le_f = 1$ (turbulent flows), Eqs. (266)–(270) may be simplified to

$$\theta_{fm,exit} = B - 4 \tag{271}$$

$$\langle \theta_f \rangle_{exit} = B - 2 \tag{272}$$

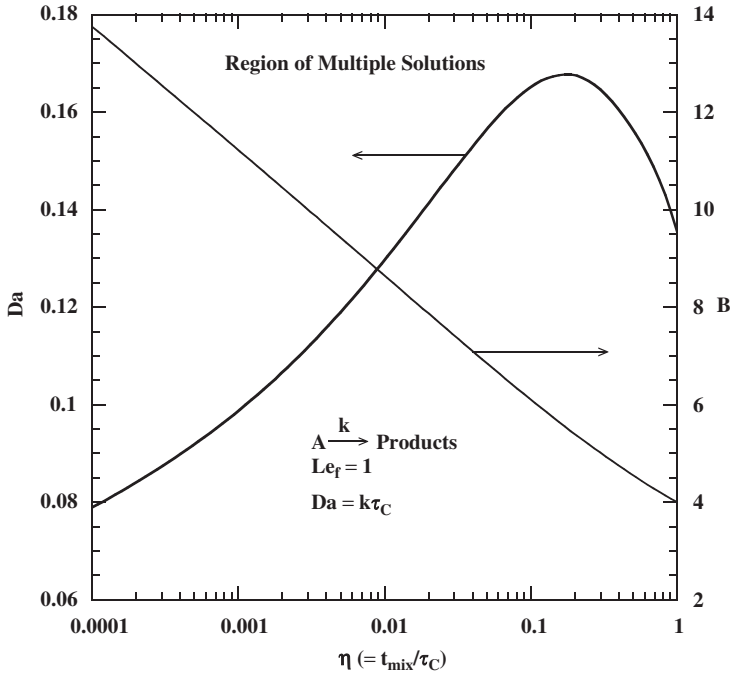

FIG. 14. Hysteresis loci in (Da, η) and (B, η) planes for a first-order non-isothermal reaction in an adiabatic tubular reactor.

$$B\,Da \approx 1 + \frac{1}{B} \tag{273}$$

$$\eta \approx (B-1)\exp[2-B] \tag{274}$$

Figure 14 presents the hysteresis loci [given by Eqs. (266)–(270)] in the (Da, η) and the (B,η) planes, for the case of $Le_f = 1$. For any finite value of the micromixing time, η, the hysteresis locus gives the minimum value of B required to produce multiplicity. It could be observed from Fig. 14 that as η increases, the critical value of B required to produce multiple solutions, decreases, finally reaching the asymptotic limit of 4. It could also be noticed that for even for very small values of η, the critical value of B is reasonably low (e.g. for gas-phase reactions $\eta \approx 0.05$, $B_{\text{critical}} = 6.74$; for liquid-phase reactions $\eta \approx 1$, $B_{\text{critical}} = 4$), indicating that in practice, multiple solutions resulting from micromixing limitations and autocatalytic kinetics are present in all tubular reactors. Thus, the above results clearly contradict the traditional belief that an adiabatic laminar flow reactor (with no axial dispersion) has only one possible steady state, even in the presence of autocatalytic kinetics.

Numerical computations and experiments have revealed that a small change in the operating variables leads to a very large change in the behavior of adiabatic tubular reactors. This phenomenon has been referred to as "parametric sensitivity" in the prior literature (Bilous and Amundson, 1955; Morbidelli and Varma, 1982). The reason for "parametric sensitivity" could be attributed to the presence of multiple steady states in tubular reactors with mixing limitations (at the local scale). As shown above, if the local mixing limitations exceed η_{crit} [given by Eq. (274)], the local equation can have multiple solutions and the reactor might ignite locally. Under such conditions (i.e. $\eta \geqslant \eta_{\text{crit}}$), when one of the operating variables is changed slightly, the local temperature jumps from the stable extinguished steady-state branch to the stable ignited steady-state branch, resulting in local hot spots. Thermal micromixing limitations prevent these local hot spots from being extinguished immediately, and they are carried downstream, where they are eventually stabilized due to transverse diffusion and depletion of the reactant.

The most important observation that follows from the above analysis of the multi-mode model is that in almost all practical cases, tubular reactor instabilities arise due to mixing/diffusional limitations at the small scales and spread over the reactor. In contrast, pseudohomogeneous models predict (erroneously) that reactor instabilities (ignition, multiple solutions, etc.) arise due to macromixing limitations at the reactor scale.

3. *Single Bimolecular Reaction in a CSTR: Micromixing Effects on Conversion*

Second-order reactions provide the simplest example of nonlinear kinetics, where micromixing limitations have significant effects on reactant conversion. We use the two-mode model to determine the same for a typical bimolecular second-order reaction of the type

$$A + B \xrightarrow{k} P \quad \text{with } rate = kC_A C_B$$

occurring in a CSTR. We consider the case of species A and B being fed in stoichiometric amounts, but use two different feeding strategies, namely uniform (premixed) and distributed feeding. In uniform feeding, the reactants are mixed completely before entering the tank and fed as a single stream, while in distributed feeding species A and B are fed separately as two different feed streams of different concentrations (but in stoichiometric amount). Defining $q_A^{\text{in}}(c_A^{\text{in}})$ and $q_B^{\text{in}}(c_B^{\text{in}})$ to be the flow rates (concentrations) of entering feed streams containing pure A and B, respectively, with $q_A^{\text{in}} c_A^{\text{in}} = q_B^{\text{in}} c_B^{\text{in}}$, the mean inlet concentration becomes $c_{\text{m}}^{\text{in}} = q_A^{\text{in}} c_A^{\text{in}}/(q_A^{\text{in}} + q_B^{\text{in}}) = q_B^{\text{in}} c_B^{\text{in}}/(q_A^{\text{in}} + q_B^{\text{in}})$. Therefore, by changing $q_A^{\text{in}} : q_B^{\text{in}}$ from 1:2 to 1:19 [curve (a)–(d) in Fig. 15] with corresponding change of c_A^{in} and c_B^{in} keeping c_{m}^{in} constant, the feed stream containing B becomes more diluted, while A feed stream becomes more concentrated. This corresponds to more mixing limitations within tank and changes mixing times

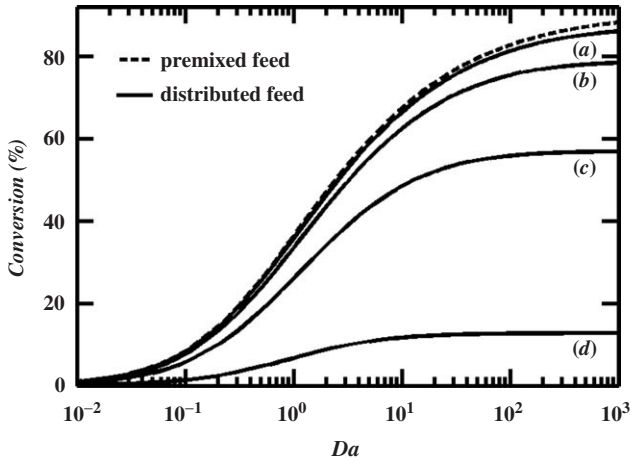

FIG. 15. Variation of conversion with Damköhler number for a bimolecular second-order reaction for uniform and distributed feeding in a CSTR.

TABLE I
MIXING TIMES FOR FIG. 15

	$t^{A}_{\mathrm{mix},1}/\tau_c$	$t^{A}_{\mathrm{mix},2}/\tau_c$	$t^{B}_{\mathrm{mix},1}/\tau_c$	$t^{B}_{\mathrm{mix},2}/\tau_c$
Premixed	0.1	0.1	0.1	0.1
Unmixed (a)	0.1028	0.1417	0.1028	0.0833
Unmixed (b)	0.1090	0.2350	0.1090	0.0775
Unmixed (c)	0.1160	0.4800	0.1160	0.0756
Unmixed (d)	0.1203	0.9775	0.1203	0.0751

as shown in Table I (cases a, b, c, and d corresponding to $q_A^{\mathrm{in}}/q_B^{\mathrm{in}} = \frac{1}{2}, \frac{1}{4}, \frac{1}{9}$, and $\frac{1}{19}$, respectively). The mixing times are calculated by considering a two-zone tank (see Bhattacharya *et al.* (2004), for details). The results are shown in Fig. 15, where the conversion is plotted as a function of reactor Damköhler number (Da). As expected intuitively, the unmixed feed can significantly affect the reactor conversion compared to the premixed feed, as the difference between the concentrations (mixing times) of the two entering streams increases.

4. Competitive–Consecutive Reaction in a CSTR: Micromixing Effects on Selectivity

Next we consider the competitive–consecutive reaction between species A and B of the type

$$A + B \xrightarrow{k_1} R \tag{275}$$

$$B + R \xrightarrow{k_2} S \tag{276}$$

which is encountered very often in many multi-step homogeneous reactions including diazo coupling between 1-napthanol and diazotized sulfanilic acid, where $k_1/k_2 \gg 1$. The latter has been studied extensively, both theoretically (Angst *et al.*, 1982a, b) and experimentally (Angst *et al.*, 1982a, b; Bourne *et al.*, 1981; Zlokarnik, 2002), where it has been shown that the selectivity or yield of the products (R or S) is extremely sensitive to mixing and can differ significantly depending on the absolute value of $q_A^{\text{in}}/q_B^{\text{in}}$, where q_A^{in} and q_B^{in} are the flow rates of entering streams containing pure A and B, respectively with $q_A^{\text{in}} C_A^{\text{in}} = q_B^{\text{in}} C_B^{\text{in}}$ (as considered in the previous example). The selectivity is in general expressed as the fraction of B converting to S and can be defined as $X_S = 2C_{\text{S}}/(2C_{\text{s}} + C_{\text{R}})$. In the literature, two opposing facts of X_S increasing and decreasing with increasing $q_A^{\text{in}}/q_B^{\text{in}}$ have been reported under different reaction conditions. In order to validate these experimental observations, Bhattacharya *et al.* (2004) changed the ratio of the flow rates $q_A^{\text{in}}/q_B^{\text{in}}$ keeping total number of moles of A and B entering the CSTR constant ($q_A^{\text{in}} C_A^{\text{in}} = q_B^{\text{in}} C_B^{\text{in}}$). Following the same procedure as illustrated in previous example (two-zone tank), the mixing times for species A, B, R, and S are calculated with the assumption of τ_{d} being same for all species. Then, the exit cup-mixing concentrations are calculated for $k_1 = 100k_2$ and plotted $X_S = 2C_{\text{mS}}/(2C_{\text{mS}} + C_{\text{mR}})$ as a function of $Da = k_2 C_{\text{m}}^{\text{in}} \tau_{\text{c}}$ in Fig. 16. In Fig. 16(A), the results are calculated for a case where micromixing time is of same order as macromixing time, whereas in Fig. 16(B), the results are calculated for a case where micromixing effect is negligible compared to macromixing. In both the figures, curves (a), (b), (c), and (d) correspond to $q_A^{\text{in}}/q_B^{\text{in}} = \frac{1}{1}, \frac{1}{4}, \frac{1}{9}$, and $\frac{1}{19}$, respectively. As can be observed, the yield of S decreases with increasing $q_A^{\text{in}}/q_B^{\text{in}}$ for micromixing dominated situations, while it increases with increasing $q_A^{\text{in}}/q_B^{\text{in}}$ for macromixing dominated reactor. Another point to be mentioned is that for the first case all mixing times are positive, while the second mixing time of concentrated species is negative for macromixing dominated case.

5. *Prediction of Micromixing Effects on Polymer MWD in Tank Reactors*

It is well known that in polymerization reactions, mixing affects monomer conversion, copolymer distribution, and molecular weight distribution (MWD) (Villermaux, 1991). In linear polymerization systems, imperfect mixing is found to broaden the MWD, while in nonlinear polymerization with significant branching, depending on reaction conditions, imperfect mixing can broaden or narrow the MWD (Zhang and Ray, 1997). Here, we verify the first of the two above-mentioned observations by examining the case of an anionic polymerization using the two-mode model for a CSTR. Anionic polymerization, often used industrially to produce polymers of narrow MWD, is typically characterized by

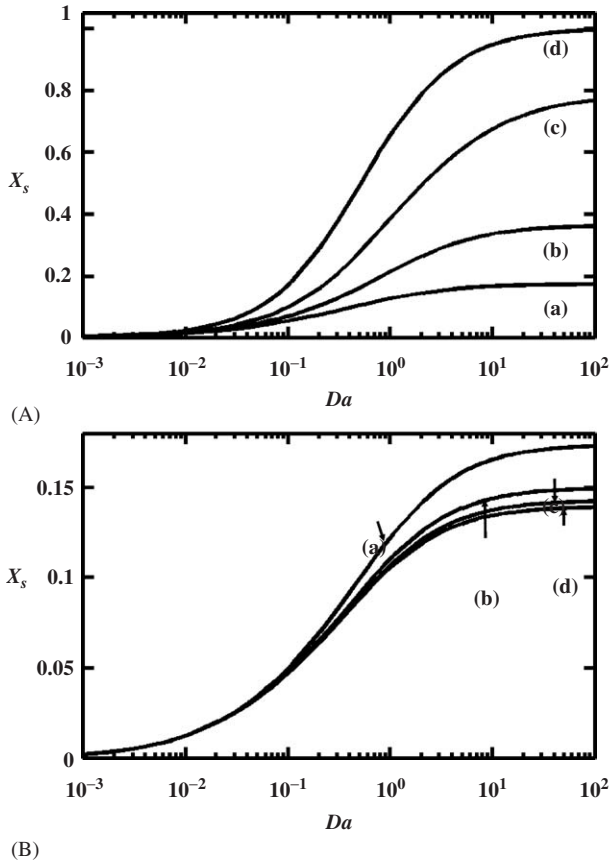

FIG. 16. Variations of selectivity (X_S) with Damköhler number (Da) for $q_A^{\text{in}}/q_B^{\text{in}} = \frac{1}{1}, \frac{1}{4}, \frac{1}{9}$ and $\frac{1}{19}$ corresponding to curves (a), (b), (c), and (d), respectively. (A) $t_{\text{micro}} = t_{\text{macro}} = 0.1\tau_c$ and (B) $t_{\text{micro}} = 0$, $t_{\text{macro}} = 0.1\tau_c$ (Bhattacharya *et al.*, 2004).

the lack of a termination step. The kinetics is

$$I + M \xrightarrow{k_1} P_1$$

$$P_j + M \xrightarrow{k_1} P_{j+1}$$

where the rate of the initiation (assuming a constant initiator concentration) is given by

$$R_1 = k_1 M$$

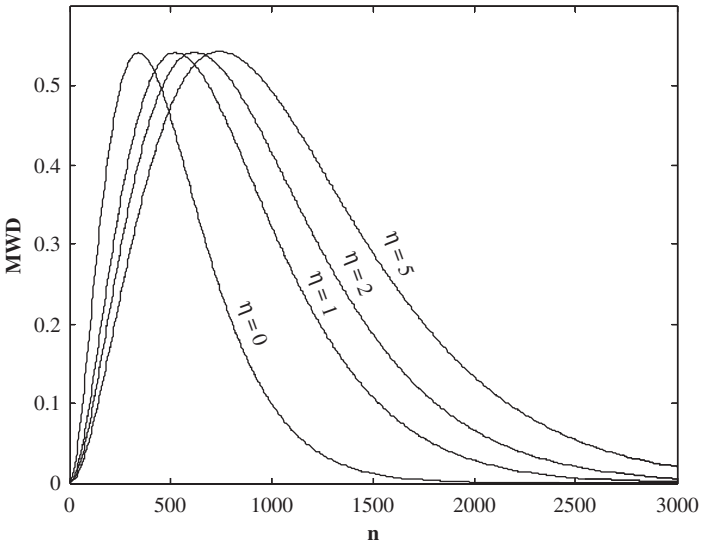

FIG. 17. Effects of mixing on polymer properties: variation of MWD with chain length n, for different values of the dimensionless mixing time, η.

while the rate of propagation is given by

$$R_P = k_P M P_j$$

where k_I and k_P are the initiation and propagation rate constants, respectively.

Application of the two-mode models for a CSTR to the above kinetics results in a set of nonlinear algebraic equations, which when solved gives the MWD and the polydispersity index (PDI). For the case of premixed feed, Fig. 17 shows the variation of the MWD with n, where MWD is defined as

$$\text{MWD} = \frac{n^2 P_n}{\sum_{n=1}^{\infty} n P_n} \tag{277}$$

and n is the chain length of a polymer chain P_n. The MWDs shown in Fig. 17 correspond to the parameter values of $Da = k_I \tau_C = 10^{-3}$ and $k_P/k_I = 2 \times 10^5$, where Da is the Damköhler number and τ_C is the residence time of the tank. While the $\eta = 0$ case shows that the MWD for a perfectly mixed CSTR is fairly narrow, a significant broadening of the MWD is observed as the dimensionless mixing time of the system, $\eta (= t_{mix}/\tau_C)$, is increased.

V. Spatially Averaged Multi-mode (Multi-scale) Models for Catalytic Reactors

A. Wall-catalyzed Reactions

We consider the case of a single heterogeneous wall-catalyzed reaction involving M species given by

$$\sum_{j=1}^{M} \mu_j A_j = 0$$

where μ_j is the stoichiometric coefficient of species j, with $\mu_j > 0$ if A_j is a product and $\mu_j < 0$ if A_j is a reactant. The governing CDR equation for the jth species ($j = 1, 2, \ldots, M$) in the above reaction occurring in a tubular reactor with fully developed laminar flow is given in dimensionless form by

$$\frac{1}{\xi}\frac{\partial}{\partial \xi}\left(\xi \frac{\partial c_j}{\partial \xi}\right) + \frac{1}{\xi^2}\left(\frac{\partial^2 c_j}{\partial \varphi^2}\right) = p\,\kappa_j\left[\frac{\partial c_j}{\partial t} - \frac{p}{k_j Pe_r^2}\frac{\partial^2 c_j}{\partial z^2} + u(\xi)\frac{\partial c_j}{\partial z}\right] \triangleq pf(c_j, p, \mathbf{p}^*) \tag{278}$$

with initial and boundary conditions given by

$$\left.\frac{\partial c_j}{\partial \xi}\right|_{\xi=1} = p\frac{Da_s}{2}\kappa_j \mu_j r_w(c_{1,s}, c_{2,s}, \ldots, c_{M,s}) \tag{279}$$

$$c_j(\xi, \varphi, z, t) = c_j(\xi, \varphi + 2\pi, z, t) \tag{280}$$

$$\frac{p}{\kappa_j\, Pe_r^2}\frac{\partial c_j}{\partial z} = u(\xi)[c_j - c_{j,\text{in}}] \text{ at } z = 0; \quad \frac{\partial c_j}{\partial z} = 0 \text{ at } z = 1 \tag{281}$$

$$c_j(\xi, \varphi, z, t = 0) = c_{j0} \tag{282}$$

In the above equations, $c_{j,s}$ is the surface/wall concentration of species j, r_w ($c_{1,s}$, $c_{2,s}, \ldots, c_{M,s}$) is the dimensionless intrinsic rate of surface reaction, Da_s is the reactor scale Damköhler number, which are given by

$$c_{j,s} = c_j|_{\xi=1} = \langle c_j \rangle + c_j'|_{\xi=1}$$

$$r_w(c_{1,s}, c_{2,s}, \ldots, c_{M,s}) = \frac{R_w(C_{1,s}, C_{2,s}, \ldots, C_{M,s})}{R_w(C_R)}$$

$$Da_s = \frac{2LR_w(C_R)}{\langle u_x \rangle a C_R}$$

while the other symbols retain their usual meanings. As in the single homogeneous reaction case, we represent $r_w(c_{1,s},c_{2,s},\ldots,c_{M,s})$ by $r_w(\mathbf{c}_s)$ and $R_w(C_{1,s},C_{2,s},\ldots,C_{M,s})$ by $R_w(\mathbf{C}_s)$ for the sake of simplicity.

It may be noted that the above set of equations has a zero eigenvalue and a corresponding constant eigenfunction for $p = 0$, making spatial averaging by L–S technique possible. Using the averaging theory outlined in Section II, the spatially averaged low-dimensional model for heterogeneous wall-catalyzed reactors to $O(p)$ is obtained as

$$\frac{\partial \langle c_j \rangle}{\partial t} + \frac{\partial c_{j,m}}{\partial z} - \frac{p}{\kappa_j Pe_r^2} \frac{\partial^2 \langle c_j \rangle}{\partial z^2} - \mu_j Da_s r_w(\mathbf{c}_s) = 0 \tag{283}$$

$$\frac{c_{j,m} - \langle c_j \rangle}{\eta\, \kappa_j} = -\frac{\partial c_{j,m}}{\partial z} - \beta_2 \mu_j Da_s r_w(\mathbf{c}_s) \tag{284}$$

$$\frac{c_{j,s} - \langle c_j \rangle}{\eta\, \kappa_j} = \beta_3 \frac{\partial c_{j,m}}{\partial z} + \frac{\beta_4}{\beta_1} \mu_j Da_s r_w(\mathbf{c}_s) \tag{285}$$

where β_4 is given by Eq. (211) for tubular geometry and $\beta_1 - \beta_3$ are given as by Eqs. (212)–(214). The boundary and initial conditions for this averaged model are same as those in the case of homogeneous tubular reactor [Eqs. (132)–(134)].

It may be noticed that unlike in the isothermal homogeneous tubular reactor models, which were "two-mode models", the catalytic reactor models are "three-mode models", the three modes being the spatially averaged ($\langle c_j \rangle$), mixing-cup ($c_{j,m}$), and surface or wall ($c_{j,s}$) concentrations. The cup-mixing and wall concentrations are necessary to describe the mass transfer between the bulk and the wall [Eq. (285)] while the two-modes $c_{j,m}$ and $\langle c_j \rangle$ describe micromixing that occurs in the fluid phase [Eq. (284)] due to transverse velocity gradients and transverse molecular diffusion. Traditional two-phase models of catalytic reactors that use only the wall and the cup-mixing concentrations ignore this term which can be important in transient operation of the reactor.

It should be noted that it is possible to eliminate $\langle c \rangle$ from Eq. (283) and write the model in two-mode form using c_m and c_s. For the simple case of single reaction $A \rightarrow B$, the two-mode model for a wall-catalyzed reactor is given by

$$\left[1 - \frac{p}{24} Da_s \frac{\partial r_w}{\partial c}(c_s)\right] \frac{\partial c_m}{\partial t} + \frac{\partial c_m}{\partial z} + \frac{p}{48} \frac{\partial^2 c_m}{\partial z \partial t} - \frac{p}{Pe_r^2} \frac{\partial^2 c_m}{\partial z^2} + Da_s r_w(c_s) = 0 \tag{286}$$

$$c_s - c_m = \frac{p}{16} \frac{\partial c_m}{\partial z} - \frac{p}{6} Da_s r_w(c_s) \tag{287}$$

where the symbol c now represents the concentration of the reactant A. In this form, the applicability of the model is limited to the parameter range in which the term in square bracket does not vanish.

1. Limiting Cases

We now consider various limiting cases using the example of a single reaction $A \to B$.

The first limiting case we consider is that of steady-state limit with negligible axial dispersion ($Pe_r \gg 1$). For this case, Eqs. (286) and (287) reduce to the two-mode form given by

$$\frac{c_s - c_m}{\frac{11}{48}p} = \frac{dc_m}{dz} = -Da_s r_w(c_s), \quad \text{with } c_m|_{z=0} = c_{m,in} \tag{288}$$

In this form, the two-mode model is identical to the classical steady-state two-phase model of a tubular catalytic reactor with negligible axial dispersion. There is also a striking structural similarity between the two-mode models for homogeneous reactions and two-phase models for catalytic reactions in the practical limit of $Pe_r \gg 1$. This could be seen more clearly when Eqs. (137) and (138) are rewritten as

$$\frac{dc_m}{dz} = \frac{\langle c\rangle - c_m}{\beta_1 p} = -Dar(\langle c\rangle) \quad \text{with } c_m|_{z=0} = c_{m,in} \tag{289}$$

and Eq. (288) is written as

$$\frac{dc_m}{dz} = \frac{c_s - c_m}{\beta_5 p} = -Da_s r_w(\langle c\rangle) \quad \text{with } c_m|_{z=0} = c_{m,in} \tag{290}$$

where $\beta_1 = \frac{1}{48}$ and $\beta_5 = \frac{11}{48}$ for laminar flow tubular reactors, and

$$\eta_{TP} = \beta_5 p \tag{291}$$

is the dimensionless two-phase transfer time. The reciprocals of β_1 and β_5 are the asymptotic Sherwood numbers or dimensionless mass transfer coefficients for exchange between the two modes. There is an exact one to one correspondence between the two-mode models of homogeneous reactions and the two-phase models of catalytic reactions. For example, just as the reaction rate in the two-phase model is not evaluated at the mixing-cup concentration c_m but at the wall concentration c_s, similarly the reaction rate term in the two-mode homogeneous reactor model is evaluated at the spatially averaged concentration $\langle c\rangle$. Also analogous to the dimensionless two phase transfer time, $\eta_{TP}(= \beta_5 p)$, in the two-phase model is the dimensionless local mixing time, $\eta(= \beta_1 p)$, in the two-mode model.

The second limiting case we consider is that of linear kinetics with negligible axial diffusion ($Pe_r \gg 1$). For this case, the averaged model can be written in

terms of the mixing-cup concentration as

$$\left[\frac{2}{3}+\frac{1}{3}\frac{1+\phi_s^2/24}{1+\phi_s^2/6}\right]\frac{\partial c_m}{\partial t}+\left[1+\frac{\phi_s^2/16}{1+\phi_s^2/6}\right]\frac{\partial c_m}{\partial z}+\frac{p}{48}\left[\frac{1+\phi_s^2/24}{1+\phi_s^2/6}\right]\frac{\partial^2 c_m}{\partial z\partial t}+\frac{Da_s}{1+\phi_s^2/6}c_m=0 \tag{292}$$

where

$$\phi_s^2 = pDa_s \tag{293}$$

is the local Damköhler number. For the case of $\phi_s^2 \to 0$ (slow wall reaction), Eq. (292) reduces to

$$\frac{\partial c_m}{\partial t}+\frac{\partial c_m}{\partial z}+\frac{p}{48}\frac{\partial^2 c_m}{\partial z\partial t}+Da_s c_m=0 \tag{294}$$

while for the case of $\phi_s^2 \to \infty$ (infinitely fast wall reaction or the mass-transfer-controlled limit), it may be written as

$$\frac{\partial c_m}{\partial t}+\frac{11}{6}\frac{\partial c_m}{\partial z}+\frac{p}{144}\frac{\partial^2 c_m}{\partial z\partial t}+\frac{8}{p}c_m=0 \tag{295}$$

Comparing this with the slow reaction case, we note that the effective velocity has increased (by a factor 1.83), the dispersion coefficient is reduced by a factor 3 while the apparent reactor scale Damköhler number changed from Da_s to $8/p$.

The last limiting case we consider is the practical case of long tubes where the axial dispersion term may be neglected. For this case, it is more convenient to write the three-mode model given by Eqs. (283)–(285) in the following form:

$$\begin{pmatrix} \frac{p}{24}\frac{\partial\langle c\rangle}{\partial t} \\ \frac{p}{24}\frac{\partial c_m}{\partial z} \\ Da_s r_w(c_s) \end{pmatrix} = \begin{pmatrix} -11 & 8 & 3 \\ 8 & -6 & -2 \\ 3 & -2 & -1 \end{pmatrix} \begin{pmatrix} \langle c\rangle \\ c_m \\ c_s \end{pmatrix} \tag{296}$$

with initial and boundary conditions

$$\langle c\rangle(z, t=0) = c_0(z), \quad c_m(z, t=0) = c_{m0}(z), \quad c_m(z=0, t) = c_{m,in}(t) \tag{297}$$

This model reduces to the two-phase model given by Eq. (288) under steady-state conditions. However, for the general case of time-varying inlet conditions this model retains all the qualitative features of the full partial differential equation model and while the traditional two-phase model which does not distinguish between c_m and $\langle c\rangle$ ignores the dispersion effect in the fluid phase.

B. Coupled Homogeneous and Wall-catalyzed Reactions

We now consider the case of coupled homogeneous and wall-catalyzed reactions involving M species occurring in a tubular reactor. The homogeneous reaction is of the form

$$\sum_{j=1}^{M} \nu_j A_j = 0$$

while the wall-catalyzed reaction is of the form

$$\sum_{j=1}^{M} \mu_j A_j = 0$$

where ν_j and μ_j are the stoichiometric coefficient of species j in the homogeneous and the wall-catalyzed reactions, respectively, with $\nu_j > 0$ if A_j is a product in the homogeneous reaction and $\mu_j > 0$ if A_j is a product in the wall-catalyzed reaction. If species A_j does not participate in the homogeneous (wall-catalyzed) reaction, then $\nu_j(\mu_j)$ is zero.

The governing CDR equation for the jth species is given by Eq. (123), with initial and boundary conditions being given by Eqs. (279)–(282). As in the case of wall-catalyzed reactions, the local/transverse diffusion operator has a zero eigenvalue and a corresponding constant eigenfunction, thus enabling spatial averaging by L–S technique. In this case, the low-dimensional model is described by three modes, namely, the spatially averaged concentration $\langle c_j \rangle$, the cup-mixing concentration $c_{j,\mathrm{m}}$, and the wall (or surface) concentration $c_{j,\mathrm{s}}$, and is given for the jth species ($j = 1, 2, \ldots, M$) by

$$\frac{\partial \langle c_j \rangle}{\partial t} + \frac{\partial c_{j,\mathrm{m}}}{\partial z} - \frac{p}{\kappa_j Pe_{\mathrm{r}}^2} \frac{\partial^2 \langle c_j \rangle}{\partial z^2} = \nu_j Da\, r(\langle \mathbf{c} \rangle) + \mu_j Da_{\mathrm{s}} r_{\mathrm{w}}(\mathbf{c}_{\mathrm{s}}) \tag{298}$$

along with Eqs. (284)–(285), with Eqs. (132)–(134) as boundary and initial conditions. The coefficients $\beta_1 - \beta_4$ are given by Eqs. (211)–(217).

It is interesting to note the above equations that mixing in the fluid phase (which is described by the exchange between $c_{j,\mathrm{m}}$ and $\langle c_j \rangle$), and transfer between phases (which is described by the exchange between $c_{j,\mathrm{m}}$ and $c_{j,\mathrm{s}}$) are both influenced not only by the rate of the homogeneous reaction and the local mixing time but also by the rate of the wall reaction and the two-phase transfer time. These rigorously derived low-dimensional models thus illustrate that for the case of coupled homogeneous–heterogeneous reactions, the system cannot be described by a single transfer/exchange time, as has been traditionally done.

C. Non-isothermal Reactor Models

1. Wall-catalyzed Reactions

The low-dimensional model for non-isothermal wall-catalyzed reaction in a tubular reactor is given by Eqs. (283)–(285) and

$$\varepsilon\frac{\partial\langle\theta_{\mathrm{f}}\rangle}{\partial t}+\sigma_{\mathrm{sf}}(1-\varepsilon)\frac{\partial\langle\theta_{\mathrm{s}}\rangle}{\partial t}+\varepsilon\frac{\partial\theta_{\mathrm{fm}}}{\partial z}=\begin{pmatrix}\dfrac{p}{Pe_{\mathrm{r}}^{2}Le_{\mathrm{f}}}\left[\varepsilon\dfrac{\partial^{2}\langle\theta_{\mathrm{f}}\rangle}{\partial z^{2}}\right]+\left(\dfrac{1-\varepsilon}{\kappa}\right)\dfrac{\partial^{2}\langle\theta_{\mathrm{s}}\rangle}{\partial z^{2}}\\ +\varepsilon B_{\mathrm{s}}Da_{\mathrm{s}}r_{\mathrm{w}}(\langle\mathbf{c}\rangle,\langle\theta_{\mathrm{f}}\rangle)-St(\langle\theta_{\mathrm{s}}\rangle-\theta_{\mathrm{C}})\end{pmatrix} \tag{299}$$

$$\frac{\theta_{\mathrm{fm}}-\langle\theta_{\mathrm{f}}\rangle}{\eta_{\mathrm{H}}}=-\frac{\partial\theta_{\mathrm{fm}}}{\partial z}+\beta_{2}\frac{1}{\varepsilon}\begin{bmatrix}\sigma_{\mathrm{sf}}(1-\varepsilon)\frac{\partial\langle\theta_{\mathrm{s}}\rangle}{\partial t}\\ -\varepsilon B_{\mathrm{s}}Da_{\mathrm{s}}r_{\mathrm{w}}(\langle\mathbf{c}\rangle,\langle\theta_{\mathrm{f}}\rangle)+St(\langle\theta_{\mathrm{s}}\rangle-\theta_{\mathrm{C}})\end{bmatrix} \tag{300}$$

$$\frac{\langle\theta_{\mathrm{s}}\rangle-\langle\theta_{\mathrm{f}}\rangle}{\eta_{\mathrm{H}}}=\beta_{3}\frac{\partial\theta_{\mathrm{fm}}}{\partial z}-\frac{\beta_{4}}{\beta_{1}}\frac{1}{\varepsilon}\begin{bmatrix}\sigma_{\mathrm{sf}}(1-\varepsilon)\frac{\partial\langle\theta_{\mathrm{s}}\rangle}{\partial t}\\ -\varepsilon B_{\mathrm{s}}Da_{\mathrm{s}}r_{\mathrm{w}}(\langle\mathbf{c}\rangle,\langle\theta_{\mathrm{f}}\rangle)+St(\langle\theta_{\mathrm{s}}\rangle-\theta_{\mathrm{C}})\end{bmatrix} \tag{301}$$

with boundary and initial conditions being given by Eqs. (132)–(134), (204), and (205), where B_{s} is the Zeldovich number for the wall-catalyzed reaction and all other symbols retain their usual meanings.

2. Coupled Homogeneous and Wall-catalyzed Reactions

The low-dimensional model for coupled non-isothermal homogeneous and wall-catalyzed reactions in a tubular reactor is given by Eqs. (284), (285), (298), (300), and (301) and

$$\varepsilon\frac{\partial\langle\theta_{\mathrm{f}}\rangle}{\partial t}+\sigma_{\mathrm{sf}}(1-\varepsilon)\frac{\partial\langle\theta_{\mathrm{s}}\rangle}{\partial t}+\varepsilon\frac{\partial\theta_{\mathrm{fm}}}{\partial z}=\begin{pmatrix}\dfrac{p}{Pe^{2}Le_{\mathrm{f}}}\left[\varepsilon\dfrac{\partial^{2}\langle\theta_{\mathrm{f}}\rangle}{\partial z^{2}}+\left(\dfrac{1-\varepsilon}{\kappa}\right)\dfrac{\partial^{2}\langle\theta_{\mathrm{s}}\rangle}{\partial z^{2}}\right]\\ +\varepsilon[BDa\,r(\langle\mathbf{c}\rangle,\langle\theta_{\mathrm{f}}\rangle)+B_{\mathrm{s}}Da_{\mathrm{s}}r_{\mathrm{w}}(\mathbf{c}_{S},\theta_{\mathrm{s}})]\\ -St(\langle\theta_{\mathrm{s}}\rangle-\theta_{\mathrm{C}})\end{pmatrix} \tag{302}$$

with boundary and initial conditions being given by Eqs. (132)–(134), (204), and (205).

D. Examples Illustrating Use of Multi-mode Catalytic Reactor Models

1. Wall-catalyzed Reactions

We apply the low-dimensional convection model [Eq. (288)] to the simple case of a isothermal bimolecular wall-catalyzed reaction occurring in a tubular reactor. For the reaction

$$A + B \xrightarrow{k_s} P, \quad \text{with rate} = k_s C_A C_B$$

where k_s is the second-order surface rate constant, and for the case in which the molecular diffusivities of A and B are assumed to be equal, the balance equations in dimensionless form are given by

$$\frac{dc_{A,m}}{dz} = -Da_s \langle c_A \rangle \langle c_B \rangle = \frac{dc_{B,m}}{dz} \quad \text{with } c_{A,m}|_{z=0} = c_{A,in}, \ \ c_{B,m}|_{z=0} = c_{B,in} \tag{303}$$

$$c_{A,m} - \langle c_A \rangle = \eta_{TP} Da_s \langle c_A \rangle \langle c_B \rangle = c_{B,m} - \langle c_B \rangle \tag{304}$$

where

$$Da_s = \frac{2k_s C_{A,in} \tau_C}{a}, \quad \eta_{TP} = \beta_5 p \tag{305}$$

Figure 18 shows the variation of conversion

$$X = 1 - \frac{c_{A,m}|_{z=1}}{c_{A,in}} \tag{306}$$

with reactor-scale Damköhler number Da_s for different values of dimensionless two-phase transfer time η_{TP}, for the case of stoichiometric feeding ($c_{A,in} = C_{B,in}$). The case of $\eta_{TP} = 0$ corresponds to the case of an ideal PFR, where conversion X is given by $X = Da_s/(1 + Da_s)$. In the limit of mass transfer control, i.e. $\eta_{TP} > 0$, $Da_s \to \infty$ (but $\eta_{TP} Da_s$ is finite), $c_{A,s} \to 0$, $c_{B,s} \to 0$, and conversion is given by

$$X_\infty = 1 - \exp\left[-\frac{1}{\eta_{TP}}\right] \tag{307}$$

Figure 18 illustrates these asymptotic limits.

2. Coupled Homogeneous and Wall-catalyzed Reactions

In this example, we examine the effects of mixing and mass transfer limitations on the yields of competitive–consecutive reactions of the type

$$A + B \xrightarrow{k_1} R \quad \text{(homogeneous)} \tag{308}$$

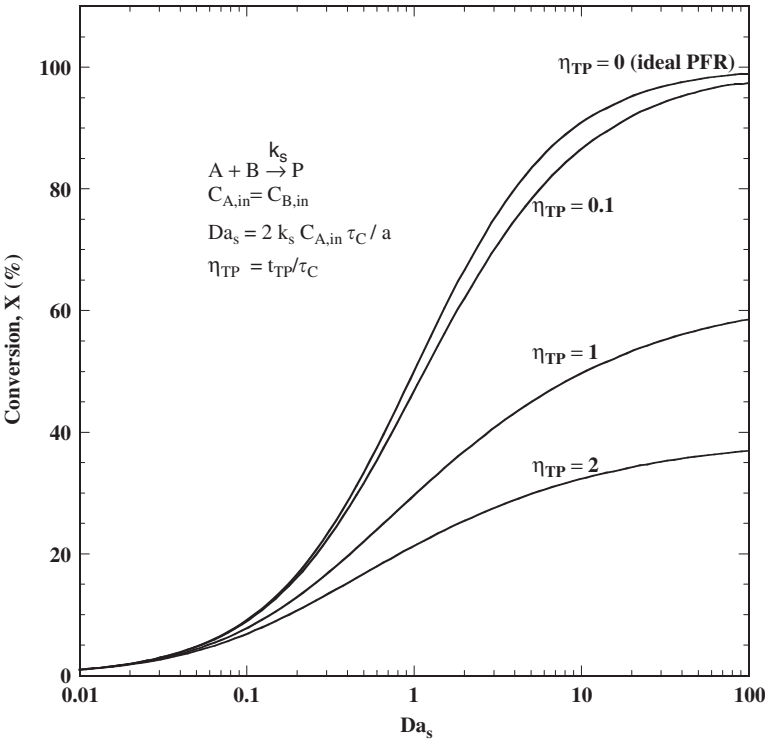

FIG. 18. Variation of conversion (X) with the Damköhler number, Da_s, for a bimolecular second-order wall-catalyzed reaction occurring in a tubular reactor.

$$B + R \xrightarrow{k_{2S}} S \quad \text{(catalytic)} \tag{309}$$

occurring in an isothermal tubular reactor in which the first reaction [Eq. (308)] is a homogeneous one, which occurs in the bulk fluid phase, and the second reaction [Eq. (309)] is catalytic. As in the homogeneous case, if the first reaction is infinitely fast as compared to the second one (i.e. $k_1/k_2 s \to \infty$), and A and B are fed in stoichiometric ratio, under perfectly micromixed conditions, B is completely consumed in the homogeneous reaction and the catalytic reaction does not occur. However, if micromixing limitations are present in the fluid phase, the homogeneous reaction attains a mixing limited asymptote resulting in a local excess of B, which can take part in the catalytic reaction. We use the multi-mode steady convection model for coupled homogeneous–heterogeneous reactors to quantify the yield of S (Y_S) under such conditions, where

$$Y_S = \frac{2c_{S,\mathrm{m}}|_{z=1}}{2c_{S,\mathrm{m}}|_{z=1} + c_{R,\mathrm{m}}|_{z=1}} \tag{310}$$

The multi-mode model for the above reaction scheme in an isothermal tank reactor is given by

$$\frac{\mathrm{d}c_{A,\mathrm{m}}}{\mathrm{d}z} = -Da\langle c_A\rangle\langle c_B\rangle \tag{311}$$

$$\frac{\mathrm{d}c_{B,\mathrm{m}}}{\mathrm{d}z} = -[Da\langle c_A\rangle\langle c_B\rangle + Da_{\mathrm{s}}c_{B,\mathrm{s}}c_{R,\mathrm{s}}] \tag{312}$$

$$\frac{\mathrm{d}c_{R,\mathrm{m}}}{\mathrm{d}z} = Da\langle c_A\rangle\langle c_B\rangle - Da_{\mathrm{s}}c_{B,\mathrm{s}}c_{R,\mathrm{s}} \tag{313}$$

$$\frac{c_{A,\mathrm{m}} - \langle c_A\rangle}{\eta} = Da\langle c_A\rangle\langle c_B\rangle \tag{314}$$

$$\frac{c_{B,\mathrm{m}} - \langle c_B\rangle}{\eta} = Da\langle c_A\rangle\langle c_B\rangle + (1+\beta_2)Da_{\mathrm{s}}c_{B,\mathrm{s}}c_{R,\mathrm{s}} \tag{315}$$

$$\frac{c_{C,\mathrm{m}} - \langle c_{\mathrm{R}}\rangle}{\eta} = -Da\langle c_A\rangle\langle c_B\rangle + (1+\beta_2)Da_{\mathrm{s}}c_{B,\mathrm{s}}c_{R,\mathrm{s}} \tag{316}$$

$$\frac{c_{A,\mathrm{s}} - \langle c_A\rangle}{\eta} = -\beta_3 Da\langle c_A\rangle\langle c_B\rangle \tag{317}$$

$$\frac{c_{B,\mathrm{s}} - \langle c_B\rangle}{\eta} = -\beta_3 Da\langle c_A\rangle\langle c_B\rangle - \left(\beta_3 + \frac{\beta_4}{\beta_1}\right)Da_{\mathrm{s}}c_{B,\mathrm{s}}c_{R,\mathrm{s}} \tag{318}$$

$$\frac{c_{R,\mathrm{s}} - \langle c_R\rangle}{\eta} = \beta_3 Da\langle c_A\rangle\langle c_B\rangle + \left(\beta_3 + \frac{\beta_4}{\beta_1}\right)Da_{\mathrm{s}}c_{B,\mathrm{s}}c_{R,\mathrm{s}} \tag{319}$$

where $Da(= k_1 C_{A,\mathrm{in}}\tau_{\mathrm{C}})$ is the Damköhler number of the homogeneous reaction, $Da_{\mathrm{s}}(= 2k_{2\mathrm{s}}C_{A,\mathrm{in}}\tau_{\mathrm{C}}/a)$ is the Damköhler number of the catalytic reaction, and $\eta(= t_{\mathrm{mix}}/\tau_{\mathrm{C}})$ is the dimensionless local mass micromixing time, which is assumed to same and equal for all species. For the case of a laminar flow reactor considered here, $\beta_1 = \frac{1}{48}$, $\beta_2 = 2$, $\beta_3 = 2$, $\beta_4 = \frac{1}{8}$. In this example, we consider the case, where the first reaction is infinitely fast as compared to the second one, i.e. $Da = k_1 C_{A,\mathrm{in}}\tau_{\mathrm{C}} \to \infty$, and attains a mixing limited asymptote within a very short residence time in the reactor. Using the formula for mixing limited conversion in a tubular reactor (Chakraborty and Balakotaiah, 2002a), the local excess of B that remains after the first reaction attains its mixing-limited asymptote is obtained as

$$\frac{c^{1}_{B,\mathrm{m}}}{c_{\mathrm{in}}} = \exp\left(-\frac{1}{\eta}\right) \tag{320}$$

the amount of R formed from the first reaction is given by

$$\frac{c^{1}_{R,\mathrm{m}}}{c_{\mathrm{in}}} = 1 - \exp\left(-\frac{1}{\eta}\right) \tag{321}$$

The catalytic reaction is simply a bimolecular reaction between B and R, with boundary conditions given by $c_{B,\mathrm{m}}|_{z=0^+} = c^{1}_{B,\mathrm{m}}$, $c_{R,\mathrm{m}}|_{z=0^+} = c^{1}_{R,\mathrm{m}}$. The yield of S increases monotonically as the Damköhler number of the catalytic reaction, Da_{s}, increases, and finally attains an asymptotic value when the catalytic reaction reaches its mass transfer limited asymptote. This feature is illustrated in Fig. 19, where the variation of Y_S with Da_{s} is shown. It is interesting to note from Fig. 19, that the value of the mass transfer limited asymptote depends on the micromixing limitation of the homogeneous reaction. Larger is the micromixing limitation (η) of the homogeneous reaction, more is the local

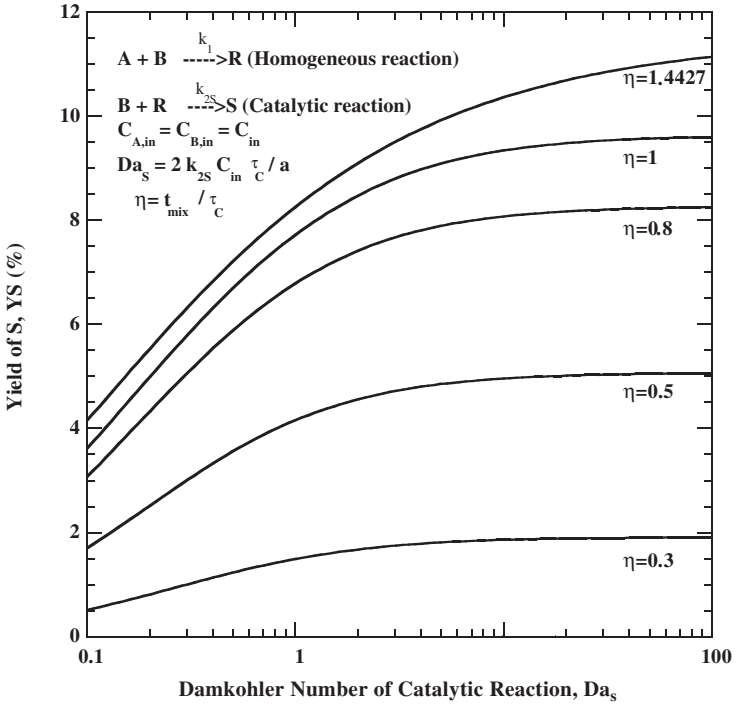

FIG. 19. Influence of micromixing and mass transfer limitations on the yield of competitive-consecutive reactions (of which one reaction is homogeneous and the other is wall-catalyzed) in a tubular reactor.

excess of (unreacted) B that can participate in the catalytic reaction. However, as could be seen from Fig. 19, the maximum yield of $S(Y_S)$ is obtained when $c^1_{B,\mathrm{m}} = c^1_{R,\mathrm{m}}$, i.e. when $\eta = -1/\ln 0.5 = 1.4427$. If $\eta > 1.4427$, R becomes the limiting reactant in the catalytic reaction (instead of B), leading to decrease in the yield of S.

VI. Accuracy, Convergence and Region of Validity of Multi-mode/ Multi-scale Averaged Models

In this section, we consider briefly the accuracy and convergence aspects of the multi-mode models derived by the L–S method. We also illustrate the regularization procedure used for the local equation(s) to increase the region of convergence of the multi-mode models.

A. Accuracy

It follows from the procedure explained in Section II that the global equation is a Taylor series expansion of the nonlinear operator around some base point, while the local equation is a perturbation series in p. Thus, the accuracy and convergence properties of the averaged equation depend on the parameter p, the specific nonlinear operator $f(c)$, and the initial and boundary conditions. For example, the global equation converges iff the Taylor series expansion of $f(c)$ around the base point $c = \langle c \rangle$ converges. Similarly, if the perturbation expansion for c' does not converge, then the local equation and hence the averaged model does not exist.

The accuracy of the averaged model truncated at order $p^q (q \geqslant 0)$ thus depends on the truncation of the Taylor series as well as on the truncation of the perturbation expansion used in the local equation. The first error may be determined from the order p^{q+1} term in Eq. (23) and may be zero in many practical cases [e.g. linear or second-order kinetics, wall reaction case, or thermal and solutal dispersion problems in which f and $r_{\mathrm{w}}(c)$ are linear in c] and the averaged equation may be closed exactly, i.e. higher order Fréchet derivatives are zero and the Taylor expansion given by Eq. (23) terminates at some finite order (usually after the linear and quadratic terms in most applications). In such cases, the only error is the second error due to the perturbation expansion of the local equation. This error ε for the local Eq. (20) truncated at $O(p^q)$ may be expressed as

$$\varepsilon(z, t, p, \mathbf{p}^*) = \sum_{i=q}^{\infty} p^{i+1} E_{i+1}(z, t, \mathbf{p}^*) \tag{322}$$

where the function $E_{i+1}(z,t,\mathbf{p}^*)$ depends on the specific nature of the nonlinear operators f and $r_w(c)$. The magnitude of the truncation error of the local equation depends on the convergence properties of the series given by Eq. (322), which could only be evaluated on a case to case basis.

It should also be noted that this "model accuracy" is distinct from the "solution accuracy" (or error), which is defined by

$$\hat{\varepsilon}(z,t,p) = \|\langle c\rangle(z,t,p) - \langle c\rangle_e(z,t,p)\| \tag{323}$$

where $\langle c\rangle(z,t,p)$ is the solution of the truncated (at order p^q) averaged model, while $\langle c\rangle_e(z,t,p)$ is the exact solution of the CDR equation and $||\cdot||$ is a norm in the appropriate Banach space. For example, for steady-state problems, the quantity of practical interest is the exit concentration. In this case, we simply take

$$\hat{\varepsilon}(p) = |\langle c\rangle(z=1,p) - \langle c\rangle_e(z=1,p)| \tag{324}$$

In general, it is not possible to obtain exact expressions for $\hat{\varepsilon}$ as it requires knowledge of the exact solution of $\langle c\rangle_e$ as well as the solution of the truncated model. However, an estimate of the order of magnitude of the error may be obtained by simply expanding it in a Taylor series around $p=0$. For example, for $p \to 0$, we have

$$\hat{\varepsilon}(z,t,p) = p^{q+1}E_1(z,t,p) \tag{325}$$

where the function E_1 (with $E_1(z,t,0)\neq 0$) depends on the specific nonlinear operator f. Thus, for the common case of $q=1$ and $p \ll 1$, $\hat{\varepsilon} = O(p^2)$.

The accuracy of low-dimensional models derived using the L–S method has been tested for isothermal tubular reactors for specific kinetics by comparing the solution of the full CDR equation [Eq. (117)] with that of the averaged models (Chakraborty and Balakotaiah, 2002a). For example, for the case of a single second order reaction, the two-mode model predicts the exit conversion to three decimal accuracy when for $\phi^2(=pDa) \leqslant 1$, and the maximum error is below 6% for $\phi^2 \approx 20$, where $\phi^2(=pDa)$ is the local Damköhler number of the reaction. Such accuracy tests have also been performed for competitive–consecutive reaction schemes and the truncated two-mode models have been found to be very accurate within their region of convergence (discussed below).

B. Convergence

We now consider the convergence aspects of the averaged models by considering some specific cases.

1. Homogeneous Reactions

As our first example, we consider the case of a first-order homogeneous reaction $A \rightarrow B$ in a laminar flow tubular reactor for which the global equation is linear in c (i.e. $r(\langle c\rangle) = \langle c\rangle$) and is therefore completely closed. To obtain the range of convergence of the two-mode model, we need to consider only the local equation. In this specific case, the reduced model equations to all orders of p are then given by

$$\frac{\mathrm{d}c_{\mathrm{m}}}{\mathrm{d}z} = -Da\langle c\rangle \tag{326}$$

$$c_{\mathrm{m}} = \langle c\rangle \left[1 + \sum_{i=1}^{\infty} \beta_i (pDa)^i\right] \tag{327}$$

where $\beta_1 = \frac{1}{48}$, $\beta_2 = -\frac{1}{11{,}520}$, $\beta_3 = \frac{59}{77{,}41{,}440}$, etc. Substituting $\langle c\rangle$ from Eq. (138) to Eq. (137), we get

$$\frac{\mathrm{d}c_{\mathrm{m}}}{\mathrm{d}z} = -Da\,\frac{c_{\mathrm{m}}}{\left[1 + \sum_{i=1}^{\infty} \beta_i (pDa)^i\right]} \tag{328}$$

The averaged model given by Eq. (328) can be expanded in a convergent power series expansion in $\phi^2 (= pDa)$ provided the infinite series in the denominator of Eq. (328) is convergent. The series $(1 + \sum_{i=1}^{\infty} \beta_i \phi^{2i})$ is convergent if $\rho < 1$, where ρ is defined by

$$\lim_{n\to\infty} \frac{\beta_{n+1}}{\beta_n} \phi^2 = \rho \tag{329}$$

The first 20 of the coefficients β_i have been calculated and from these, the convergence criterion for the above series is obtained as (Chakraborty and Balakotaiah, 2002a)

$$pDa < 41.17$$

that is

$$Da_{\mathrm{loc}} < 0.858 \tag{330}$$

where Da_{loc} is the local Damköhler number, given by $Da_{\mathrm{loc}} = t_{\mathrm{mix}}/t_{\mathrm{R}} = \eta\, Da = \beta_1 \phi^2$, where η is the dimensionless local mixing time, given by

$$\eta = t_{\mathrm{mix}}/\tau_{\mathrm{C}}$$

Criterion (330) specifies the range of validity of the two-mode models for the case of uniform inlet feeding.

A similar convergence test for the case loop and recycle reactors (with large recycle ratio) shows that the terms in the local equation when arranged in ascending order of p change sign alternately (with a finite ratio), thus significantly increasing the radius of convergence, and guarantees convergence for most cases of practical interest. As a result, the two-mode models for homogeneous reactors remain accurate as long as the local Damköhler number, Da_{loc} does not exceed a critical value, which is of order unity. When this is not the case (i.e. $Da_{\mathrm{loc}} \gg 1$) the two-mode models do not converge indicating that the scale separation breaks down. In this case of fast reactions, the reaction length scale becomes smaller than the meso length scale (e.g. tube diameter) so that diffusion is no longer the dominant mechanism at the local scale. In such cases, it is possible to have solutions of the CDR equation (e.g. for autocatalytic kinetics) with length scales smaller than the meso scale, i.e. patterned solutions (Balakotaiah and Chakraborty, 2003; Balakotaiah *et al.*, 2002).

2. *Catalytic Reactors*

For the case of the wall-catalyzed reaction $A \rightarrow B$, the global equation is closed for any type of kinetic expression $r_{\mathrm{w}}(c)$. [Unlike the homogeneous reaction case, here the reaction rate r is evaluated at the surface concentration c_{s}, which contains all the fluctuation modes (c') about the mean $\langle c \rangle$.] Thus, convergence of the model depends only on the local equation. For the special case of linear kinetics, flat velocity, and $Pe_{\mathrm{r}} \rightarrow \infty$, the local equation was determined to be

$$c_{\mathrm{m}} - c_{\mathrm{s}} = c_{\mathrm{s}} \left[\sum_{i=1}^{\infty} \beta_i \phi_{\mathrm{s}}^{2i} \right] \tag{331}$$

where $\beta_1 = \frac{1}{8}$, $\beta_2 = -\frac{1}{96}$, $\beta_3 = \frac{1}{1024}$, $\beta_4 = \frac{1}{11{,}520}$, etc. This series in Eq. (331) has alternating signs and converges absolutely if

$$\phi_{\mathrm{s}}^2 < 10.67 \tag{332}$$

We note that the local equation (331) may be rearranged as

$$c_{\mathrm{m}} - c_{\mathrm{s}} = \frac{\phi_{\mathrm{s}}^2 c_{\mathrm{s}}}{Sh(\phi_{\mathrm{s}}^2)} \tag{333}$$

where

$$Sh(\phi_{\mathrm{s}}^2) = \left(\sum_{i=1}^{\infty} \beta_i \phi_{\mathrm{s}}^{2i-2} \right)^{-1} = \frac{1}{\beta_1 + \beta_2 \phi_{\mathrm{s}}^2 + \cdots} \tag{334}$$

is the Sherwood number or dimensionless mass transfer coefficient. It may be shown that (Gupta and Balakotaiah, 2001) $Sh(\phi_{\mathrm{s}}^2)$ decreases monotonically

from 8 to 5.78 as ϕ_s^2 increases from 0 to ∞. Thus, the rearranged form of the local equation (334) converges for all values of ϕ_s^2.

The special case of linear kinetics with the axial Peclet number, $Pe = 0$ and flat velocity may be examined analytically. This case corresponds to the so-called *short monolith model*, which is given by

$$\frac{1}{\xi}\frac{d}{d\xi}\left(\xi\frac{dc}{d\xi}\right) + p(1-c) = 0; \quad 0 < \xi < 1$$

$$\frac{dc}{d\xi} = 0 \quad \text{at } \xi = 0$$

$$\frac{dc}{d\xi} = -\frac{\phi_s^2}{2}c \quad \text{at } \xi = 1, \quad \phi_s^2 = pDa$$

The exact solution of the model is given by

$$c_m = 1 - \frac{\phi_s^2 I_1(\sqrt{p})}{\sqrt{p}[\sqrt{p}I_1(\sqrt{p}) + (\phi_s^2/2)I_0(\sqrt{p})]} \tag{335}$$

$$c_s = \frac{\sqrt{p}I_1(\sqrt{p})}{\sqrt{p}I_1(\sqrt{p}) + (\phi_s^2/2)I_0(\sqrt{p})} \tag{336}$$

$$c_m - c_s = \frac{\phi_s^2 c_s}{Sh(p)} \tag{337}$$

where the exact Sherwood number as a function of p is given by

$$\frac{1}{Sh(p)} = \frac{I_o(\sqrt{p})}{2\sqrt{p}I_1(\sqrt{p})} - \frac{1}{p} \tag{338}$$

The L–S procedure gives the global and the local equations as

$$c_{m,in} - c_m = Da\, c_s \tag{339}$$

$$c_m - c_s = \phi_s^2 c_s\left[\frac{1}{8} - \frac{p}{192} + \frac{p^2}{3072} - \frac{p^3}{46,080} + \cdots\right] \tag{340}$$

Comparison of Eqs. (337) and (340) shows that the term in the brackets in Eq. (340) is just the Taylor series expansion of $1/Sh(p)$ around $p = 0$. Thus, the local equation converges for all values of ϕ_s^2 and p. For this special case, we can also estimate the error in the solution when the local equation is truncated at

order p as

$$\varepsilon = \frac{p^2}{192}\left(\frac{Da}{1+Da}\right)^2 + \cdots \tag{341}$$

Thus, for the practical case of $p<1$ (high conversion branch), the averaged model gives at least two decimal accuracy for the mass transfer-limited case ($Da \to \infty$) and higher accuracy in the kinetic regime.

C. Regularization of the Local Equation

Here, we illustrate a mathematical technique called "regularization", that we use to increase the region of convergence of the low-dimensional multi-mode models.

When a function is defined by an infinite power series in terms of a parameter p, the traditional approach is to truncate the power series, retaining terms up to p^q. However, if the power series fails to converge (i.e. outside the region of convergence of the local equation), including higher order terms does not save the truncated series from failure, and the truncated series may lead to non-physical results in the limit of $p \to \infty$.

Fortunately, there is an remedy for a poorly convergent power series, known as Padé approximation. Consider a function $\psi(k)$, given in terms of the power series, as

$$\psi = c_0 + c_1 k + c_2 k^2 + \cdots \tag{342}$$

The power series may be only poorly convergent or even non-convergent, in which case the truncated series becomes a poor approximation to ψ. Unlike the power series, which tries to express ψ in terms of a single polynomial, the Padé approximation expresses ψ as a ratio of two polynomials. The procedure to determine the two polynomials involves converting the power series [Eq. (342)] into another power series

$$f = g\,\psi = a_0 + a_1 k + a_2 k^2 + \cdots \tag{343}$$

such that $\psi = f/g$, where

$$g = 1 + b_1 k + b_2 k^2 + \cdots + b_n k^n \tag{344}$$

It is expected that a suitable choice of g will improve the convergence of the power series as the singularity of ψ may be cancelled by the zero of g. In most cases, the Padé approximation f/g provides with a better approximation than the corresponding power series truncated at any order q, especially when $|k|$ is comparable to (or even greater than) the convergence radius of the power series [Eq. (342)] (Takeshi, 1999).

Here, we use the example of the Taylor dispersion problem discussed Section III to illustrate the regularization procedure. For simplicity, we illustrate this only for the case of $Pe_r \to \infty$ (negligible axial diffusion). In this case, the global equation is given by

$$\frac{\partial \langle C \rangle}{\partial t} + \frac{\partial C_m}{\partial z} = 0 \tag{345}$$

while the local equation is given by

$$C_m = \langle C \rangle + \langle u(\xi) C' \rangle \tag{346}$$

where C' is determined from

$$\frac{1}{\xi}\frac{\partial}{\partial \xi}\left(\xi \frac{\partial C'}{\partial \xi}\right) = p f(\langle C \rangle + C') \tag{347}$$

with

$$f(C) = \frac{\partial C}{\partial t} + u(\xi)\frac{\partial C}{\partial z}, \quad u(\xi) = 2(1 - \xi^2)$$

Writing

$$C' = \sum_{i=1}^{\infty} p^i c_i \tag{348}$$

the functions c_i satisfy the boundary and solvability conditions

$$\frac{\partial c_i}{\partial \xi} = 0 \quad \text{at } \xi = 0, 1 \tag{349}$$

$$\langle c_i \rangle = 0, \quad i \geqslant 1 \tag{350}$$

Following the procedure outlined in Section II, c_1 and c_i ($i \geqslant 2$) are obtained by solving

$$\frac{1}{\xi}\frac{\partial}{\partial \xi}\left(\xi \frac{\partial c_1}{\partial \xi}\right) = (u - 1)\frac{\partial \langle C \rangle}{\partial z} \tag{351}$$

$$\frac{1}{\xi}\frac{\partial}{\partial \xi}\left(\xi \frac{\partial c_i}{\partial \xi}\right) = \frac{\partial c_{i-1}}{\partial t} + u\frac{\partial c_{i-1}}{\partial z}; \quad i \geqslant 2 \tag{352}$$

along with the above boundary and solvability conditions [Eqs. (349) and (350)]. Solving Eq. (351), c_1 is obtained as

$$c_1 = h_1(\xi)\frac{\partial \langle C \rangle}{\partial z} \tag{353}$$

where

$$h_1(\xi) = -\left[\frac{1}{12} - \frac{\xi^2}{4} + \frac{\xi^4}{8}\right] \tag{354}$$

and

$$\langle uc_1 \rangle = -\frac{1}{48}\frac{\partial \langle C \rangle}{\partial z} \tag{355}$$

Substituting for c_1 and using the leading-order approximation

$$\frac{\partial \langle C \rangle}{\partial t} = -\frac{\partial \langle C \rangle}{\partial z} + O(p)$$

the equation for $c_2(\xi)$ may be written as

$$\frac{1}{\xi}\frac{\partial}{\partial \xi}\left(\xi \frac{\partial c_2}{\partial \xi}\right) = (u-1)h_1(\xi)\frac{\partial^2 \langle C \rangle}{\partial z^2} \tag{356}$$

which when solved along with Eqs. (349) and (350) gives

$$c_2 = h_2(\xi)\frac{\partial^2 \langle C \rangle}{\partial z^2} \tag{357}$$

where

$$h_2(\xi) = \frac{1}{11,520}[45\xi^8 - 200\xi^6 + 300\xi^4 - 180\xi^2 + 31] \tag{358}$$

and

$$\langle uc_2 \rangle = \frac{1}{2880}\frac{\partial^2 \langle C \rangle}{\partial z^2} \tag{359}$$

Therefore, the local equation to $O(p^2)$ is

$$C_m - \langle C \rangle = -\frac{p}{48}\frac{\partial \langle C \rangle}{\partial z} + \frac{p^2}{2880}\frac{\partial^2 \langle C \rangle}{\partial z^2} - \cdots \tag{360}$$

Similarly, it is easily seen that

$$c_i = h_i(\xi)\frac{\partial^i \langle C \rangle}{\partial z^i}, \quad i \geqslant 1 \tag{361}$$

The local equation that relates $\langle C \rangle$ to C_m could now be written as

$$\begin{aligned} C_m - \langle C \rangle &= \langle u(\xi) C' \rangle \\ &= \sum_{i=1}^{\infty} p^i \langle u(\xi) c_i \rangle \\ &= \sum_{i=1}^{\infty} p^i \frac{\partial^i \langle C \rangle}{\partial z^i} \langle u(\xi) h_i \rangle \\ &= \sum_{i=1}^{\infty} \mu_i k^i \langle C \rangle \end{aligned} \tag{362}$$

where

$$\mu_i = \langle u(\xi) h_i \rangle, \quad i \geqslant 1$$

$$k = p \frac{\partial}{\partial z} \tag{363}$$

The parameters μ_i's can be calculated using a symbolic manipulation package. The first 20 of these are listed in Table II. We note that these coefficients have alternate positive and negative signs (with approximate periodicity of 2), indicating that the series given by Eq. (362) is convergent. Using the method outlined by Mercer and Roberts (1990), the radius of convergence of this series may be estimated to be 13.8. The physical meaning of this result is that the local equation is meaningful only for wavelengths

TABLE II
COEFFICIENTS IN THE LOCAL EQUATION FOR THE TAYLOR DISPERSION PROBLEM

i	μ_I	I	μ_i
1	2.0833×10^{-2}	11	3.2220×10^{-15}
2	-3.4722×10^{-4}	12	-7.5088×10^{-17}
3	-1.5889×10^{-5}	13	-1.0632×10^{-17}
4	1.1755×10^{-6}	14	7.0908×10^{-19}
5	4.9257×10^{-9}	15	1.9357×10^{-20}
6	-3.6895×10^{-9}	16	-3.8083×10^{-21}
7	1.0715×10^{-10}	17	5.7558×10^{-23}
8	9.3087×10^{-12}	18	1.4781×10^{-23}
9	-7.2057×10^{-13}	19	-8.1784×10^{-25}
10	-1.0244×10^{-14}	20	-3.5907×10^{-26}

exceeding the critical value

$$L_c = \frac{2\pi a^2 \langle u \rangle}{13.8 D_m} = \frac{a^2 \langle u \rangle}{2.2 D_m} \tag{364}$$

or equivalently, for $p > 2.2$ (where the p value is based on the minimum wavelength contained in the initial conditions).

Regularization of the local equation may be used to increase the region of validity of the truncated local equation. In fact, the regularized local equation may be written such that it gives a physically meaningful solution even in the limit of large p.

Using Eq. (362), we write

$$C_m = \mu_0 \langle C \rangle + \mu_1 k \langle C \rangle + \mu_2 k^2 \langle C \rangle + \cdots \tag{365}$$

where $\mu_0 = 1$. Following the regularization principle outlined above [Eqs. (342)–(344)], we express C_m as a ratio of two series:

$$C_m = \frac{[\mu_0 + (b_1 \mu_0 + \mu_1)k]}{1 + b_1 k} \langle C \rangle$$

that is

$$(1 + b_1 k) C_m = [\mu_0 + (b_1 \mu_0 + \mu_1)k] \langle C \rangle \tag{366}$$

We choose $b_1 = -\mu_1$, and Eq. (367) simplifies to

$$\langle C \rangle = (1 - \mu_1 k) C_m \tag{367}$$

and the regularized form of the local equation [Eq. (362)] is obtained from Eq. (367) as

$$C_m - \langle C \rangle = \mu_1 p \frac{\partial C_m}{\partial z} \tag{368}$$

$$= -\beta_1 p \frac{\partial C_m}{\partial z} \tag{369}$$

The regularized form of the two-mode model is now given by

$$\frac{\partial \langle C \rangle}{\partial t} + \frac{\partial C_m}{\partial z} = 0 \tag{370}$$

$$C_m - \langle C \rangle = -\beta_1 p \frac{\partial C_m}{\partial z} \tag{371}$$

This regularized form [Eqs. (370) and (371)] has a much larger region of validity than the original low-dimensional model and gives qualitatively correct results for any $p>0$. As discussed in Section III, we can combine the above two equations to get a single hyperbolic regularized equation for C_m.

VII. Summary, Conclusions, and Recommendations for Future Work

The classical ideal reactor models such as the PFR and CSTR, obtained by applying the conservation laws at the meso or macroscale ignore the small-scale physics that is very important in determining the behavior of real reactors. While these models are very simple to analyze and may be easily incorporated in the design and control schemes, they are not realistic as they do not retain the qualitative features of the full CDR equations. However, accurate low-dimensional models that retain most of the qualitative features can be derived by rigorous averaging of the CDR equations using the L–S method. In this chapter, we have demonstrated this for the case of well-defined flow fields for dispersion problems, homogeneous and wall-catalyzed reactors. We have also illustrated the accuracy, convergence, and application of the low-dimensional multi-mode/multi-scale models with commonly used examples from chemical reaction engineering.

Generally speaking, the averaged models exist only when the local diffusion time is much smaller compared to the convection and characteristic reaction times ($p \ll 1$, $Da_{loc} \ll 1$), i.e. physical length scale separation also corresponds to separation of time scales. The accuracy of the averaged model depends on the order of truncation in the small parameter p as well as the magnitude of the other parameters $\mathbf{p}^*$ (e.g. the reactor scale Damköhler number). An averaged model derived to order p^q ($q \geqslant 1$) retains all the parameters of the original CDR equations and the error in the solution is of the order p^{q+1}. While pseudohomogeneous ideal reactor models (corresponding to $q = 0$) do not retain the qualitative features of the full CDR equations, the next order truncation (at $q = 1$) retains all the important features such as the mass transfer or mixing limited asymptote and multiplicity of solutions for autocatalytic kinetics.

It should be noted that for non-isothermal case (and also for isothermal case with autocatalytic kinetics) the local equation may have multiple solutions. When this occurs, the averaged model obtained by the L–S method captures the complete set of solutions of the full CDR equations only within the region of convergence of the local equation. For example, for the wall-catalyzed non-isothermal reaction case, we have shown that the averaged two-mode model can capture only the three azimuthally symmetric solutions of the full CDR equation. The latter has three symmetric solutions (of which two are stable) as

well as an arbitrarily large number of asymmetrical solutions (Balakotaiah *et al*., 2002). These asymmetrical solutions with length scales smaller than the tube radius exist only in the region of parameter space in which the local equation derived by L–S technique does not converge. For the case of fast homogeneous or heterogeneous reaction ($Da_{\mathrm{loc}} \gg 1$), averaged models do not exist as the local time scale can go to zero for $Da_{\mathrm{loc}} \to \infty$. In this limit, the spectrum of the local diffusion operator (with source/sink term either in the equation or boundary condition) becomes continuous and time scale separation breaks down. Thus, for the fast reaction case, it is not possible for any averaged model to capture all the solutions of the full CDR equations.

A major limitation of the present work is that it deals only with well-defined (and mostly unidirectional) flow fields and simple homogeneous and catalytic reactor models. In addition, it ignores the coupling between the flow field and the species and energy balances which may be due to physical property variations or dependence of transport coefficients on state variables. Thus, a major and useful extension of the present work is to consider two- or three-dimensional flow fields (through simplified Navier–Stokes or Reynolds averaged equations), include physical property variations and derive low-dimensional models for various types of multi-phase reactors such as gas–liquid, fluid–solid (with diffusion and reaction in the solid phase) and gas–liquid–solid reactors.

ACKNOWLEDGMENTS

This work was supported by the Robert A. Welch Foundation.

NOMENCLATURE

Roman Letters

a	radius of the tube
B	Zeldovich number (or dimensionless adiabatic temperature rise)
Bi	Biot number
C_j (c_j)	reactant (dimensionless) concentration of the jth species
Da	reactor scale Damköhler number (homogeneous reaction)
Da_{s}	reactor scale Damköhler number (catalytic reaction)
Da_{loc}	local Damköhler number
$D_{\mathrm{e},j}$	effective diffusion coefficient of jth species
$D_{\mathrm{m},j}$	molecular diffusivity of jth species
D_{T}	turbulent diffusivity
f_{t}	friction factor in turbulent flow

ΔH_R heat of reaction
L length of the reactor
Le_f fluid Lewis Number
M number of species
N_H number of homogeneous reactions
N_W number of heterogeneous wall-catalyzed reactions
p transverse Peclet number
Pe axial Peclet number
Pe_r radial Peclet number
Q volumetric flow rate of recycle
q_{in} volumetric flow rate of reactants
R_i intrinsic rate of ith homogeneous reaction (dimensional)
$R_{w,i}$ intrinsic rate of ith wall reaction (dimensional)
St Stanton number
Sh Sherwood number
t dimensionless time
t_{mix} mass micromixing time of the reference species
$t_{mix,j}$ mass micromixing time of the jth species
$t_{mix,H}$ thermal micromixing time
T temperature
u_x velocity in the axial direction
X conversion
x coordinate along the length of the reactor (dimensional)
z dimensionless coordinate along the length of the reactor

Greek Letters

α cooling parameter
β exchange coefficient
γ dimensionless activation energy
ε volume fraction of fluid phase in the reactor
η dimensionless mass micromixing time based on the reference species (t_{mix}/τ_C)
η_j dimensionless mass micromixing time of the jth species ($t_{mix,j}/\tau_C$)
η_H dimensionless thermal micromixing time
θ temperature (dimensionless)
Λ recycle ratio
κ_j ratio of the diffusivities of the reference species to that of the jth species
μ_{ij} stoichiometric coefficient of species A_j in the ith wall reaction
ν_{ij} stoichiometric coefficient of species A_j in the ith homogeneous reaction
ξ dimensionless radial coordinate
τ_C total residence time on the reactor
ϕ^2 Thiele modulus
ϕ_s^2 surface Damköhler number
φ azimuthal coordinate

REFERENCES

Angst, W., Bourne, J. R., and Sharma, R. N. *Chem. Eng. Sci.* **37**(4), 585–590 (1982a).

Angst, W., Bourne, J. R., and Sharma, R. N. *Chem. Eng. Sci.* **37**(8), 1259–1264 (1982b).

Aris, R. *Proc. Roy. Soc. Lond. A* **235**, 67 (1956).

Balakotaiah, V. *Korean J. Chem. Eng.* **21**(2), 318–328 (2004).

Balakotaiah, V., and Chakraborty, S. *Chem. Eng. Sci.* **58**(21), 4769–4786 (2003).

Balakotaiah, V., and Chang, H. -C. *Phil. Trans. Roy. Soc. Lond. A* **351**, 39–75 (1995).

Balakotaiah, V., and Chang, H. -C. *SIAM. J. Appl. Math.* **63**(4), 1231–1258 (2003).

Balakotaiah, V., and Dommeti, S. M. S. *Chem. Eng. Sci.* **54**, 1621–1638 (1999).

Balakotaiah, V., Gupta, N., and West, D. *Chem. Eng. Sci.* **57**, 435 (2002).

Balakotaiah, V., Luss, D., and Keyfitz, B. L. *Chem. Eng. Commun.* **36**, 121 (1985).

Baldyga, J., and Bourne, J. R. *Chem. Eng. Sci.* **39**, 329 (1984).

Baldyga, J., and Bourne, J. R., "Turbulent Mixing and Chemical Reactions". Wiley, New York (1999).

Bhattacharya, M., Harold, M. P., and Balakotaiah, V. *Chem. Eng. Sci.* **59**, 5587 (2004).

Bilous, O., and Amundson, N. R. *AIChE J.* **1**, 513–521 (1955).

Bodenstein, M., and Wolgast, K. *Ztschr. Phys. Chem.* **61**, 422 (1908).

Bourne, J. R., Kozicki, F., and Rys, P. *Chem. Eng. Sci.* **36**(10), 1643–1648 (1981).

Bourne, J. R., and Toor, H. L. *AIChE J.* **23**, 602 (1977).

Brodkey, R. S., and Lewalle, J. *AIChE J.* **31**, 111 (1985).

Carr, J., "Applications of Center Manifold Theory". Springer, Berlin (1981).

Chakraborty, S., and Balakotaiah, V. *Chem. Eng. Sci.* **57**, 2545 (2002a).

Chakraborty, S., and Balakotaiah, V. *AIChE J* **48**, 2571 (2002b).

Chakraborty, S., and Balakotaiah, V. *Chem. Eng. Sci.* **58**, 1053 (2003).

Chakraborty, S., and Balakotaiah, V. *Chem. Eng. Sci.* **59**(17), 3495–3736 (2004).

Churchill, S. W., Turbulent Flow and Convection: The Prediction of Turbulent Flow and Convection in a Round Tube, *in* "Advances in Heat Transfer" Academic Press, New York (J. P. Hartnett, T. F. Irvine, Y. I. Cho, and G. A. Greene, Eds.), (2001).

Curl, R. L. *AIChE J.* **9**, 175 (1963).

Damköhler, G. *Z. Elektrochem.* **43**, 1 (1937).

Danckwerts, P. V. *Chem. Eng. Sci.* **2**, 1 (1953).

Danckwerts, P. V. *Chem. Eng. Sci.* **8**, 93 (1958).

Dommeti, S. M. S., and Balakotaiah, V. *Chem. Eng. Sci.* **55**, 6169 (2000).

Dutta, A., and Tarbell, J. M. *AIChE J.* **35**, 2013 (1989).

Förster, V. T., and Geib, K. H. *Ann. Phys.* **5**, 250 (1934).

Fox, R. O. *Chem. Eng. Sci.* **47**, 2853 (1992).

Froment, G. F., and Bishchoff, K. B., "Chemical Reactor Analysis and Design". Wiley, New York (1990).

Golay, M. J. E., Theory of Chromatography in Open and Coated Tubular Columns with Round and Rectangular Cross-sections, *in* "Gas Chromatography" (D. H. Desty Ed.), pp. 36–49. Butterworth, London (1958).

Golubitsky, M., and Schaeffer, D. G. "Singularities and Groups in Bifurcation Theory". Vol. 1. Springer, Berlin (1984).

Gupta, N., and Balakotaiah, V. *Chem. Eng. Sci.* **56**, 4771 (2001).

Harada, M. *Mem. Facul. Eng., Kyoto Univ.* **24**, 431 (1962).

Hatta, S. *Technol. Rep., Tohoku Univ.* **10**, 119 (1932).

Hiby, J. W. Longitudinal and Transverse Mixing During Single-phase Flow Through Granular Beds, *in* "Proceedings of the Symposium on Interaction between Fluids and Particles" pp. 312–320. Institution of Chemical Engineers, London (1962).

Langmuir, I. *J. Am. Ceram. Soc.* **30**, 656 (1908).

Levenspiel, O., "Chemical Reaction Engineering". Wiley, New York (1999).

Li, K. T., and Toor, H. L. *AIChE J.* **32**, 1312 (1986).
Liu, S. -L., and Amundson, N. R. *I&EC Fund.* **1**, 200 (1962).
Mercer, G. N., and Roberts, A. J. *SIAM. J. Appl. Math.* **50**, 1547–1565 (1990).
Miyawaki, O., Tsujikawa, H., and Uraguchi, Y. *J. Chem. Eng. Japan* **8**, 63 (1975).
Morbidelli, M., and Varma, A. *AIChE J.* **28**, 705 (1982).
Ng, D. Y. C., and Rippin, D. W. T. *Chem. Eng. Sci.* **22**, 65 (1965).
Ottino, J. M., Ranz, W. E., and Macosko, C. W. *Chem. Eng. Sci.* **34**, 877 (1979).
Ranade, V. V., "Computational Flow Modeling for Chemical Reactor Engineering". Academic Press, New York (2002).
Rhee, H. -K., Amundson, N. R., and Aris, R., "First-order Partial Differential Equations: Volume 1: Theory and Application of Single Equations". Prentice-Hall, New York (1986).
Schmitz, R. A., and Amundson, N. R. *Chem. Eng. Sci.* **18**, 415 (1963).
Sittel, C. N., Threadgill, W. D., and Schnelle, K. B. *I&EC Fund.* **7**, 39–43 (1968).
Takeshi, O. *Phys. Fluids* **11**, 3247–3269 (1999).
Taylor, G. I. *Proc. Roy. Soc. Lond. A* **219**, 186 (1953).
Taylor, G. I. *Proc. Roy. Soc. Lond. A* **223**, 446 (1954).
Theile, E. W. *Ind. Eng. Chem.* **31**, 916 (1939).
Trambouze, P. J., and Piret, E. L. *AIChE J.* **6**, 574 (1960).
Vatistas, N., and Marconi, P. F. *Chem. Eng. Sci.* **47**, 1727 (1992).
Villermaux, J. *Rev. Chem. Eng.* **7**(1), 51 (1991).
Villermaux, J., and Devillon, J. C. Représentation de la coalescence et de la redispersion des domaines de ségrégation dans un fluide per modèle d'interaction phénoménologique, Proceedings of the Second Industrial Symposium on Chemical Reactors Engineering, Amsterdam, B1 (1972).
Wehner, J. F., and Wilhelm, R. H. *Chem. Eng. Sci.* **6**, 89 (1956).
Wen, C. Y., and Fan, L. T., "Models for Flow Systems and Chemical Reactors". Marcel Dekker, New York (1975).
Westerterp, K. R., Dilman, V. V., and Kronberg, A. E. *AIChE J.* **41**, 2013 (1995).
Westerterp, K. R., van Swaaij, W. P. M., and Beenackers, A. A. C. M., "Chemical Reactor Design and Operation". Wiley, New York (1984).
Wicke, E. Z. *Elektrochem.* **65**, 267 (1961).
Zeldovich, Ya. B. *Zhur. Fiz. Khim.* **13**, 163 (1939).
Zhang, S. X., and Ray, W. H. *AIChE J.* **43**, 1265 (1997).
Zlokarnik, M., "Scale-Up in Chemical Engineering". Wiley, New York (2002).
Zweitering, T. N. *Chem. Eng. Sci.* **11**, 1 (1959).